

AD-A131 983

EFFECTS OF MICROSTRUCTURE AND PORE FLUIDS ON THE
ACOUSTIC PROPERTIES OF GRANULAR MATERIALS(U) STANFORD
UNIV CALIF DEPT OF GEOPHYSICS A NUR 08 AUG 83

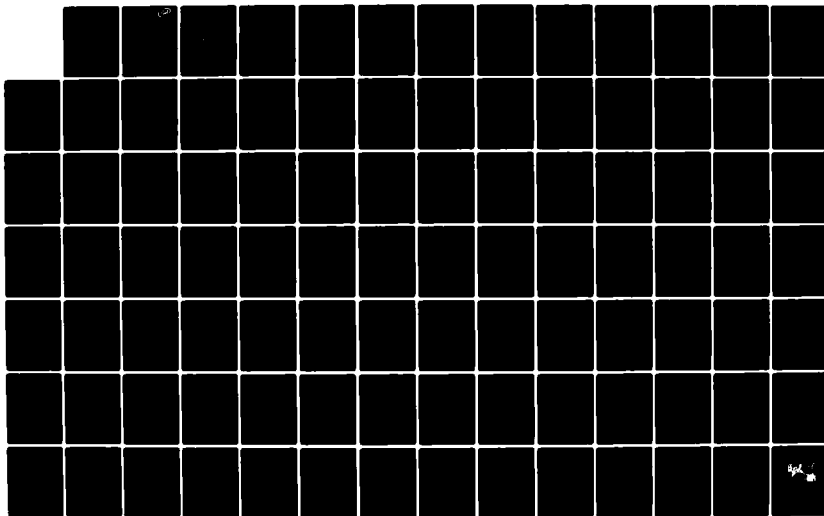
1/2

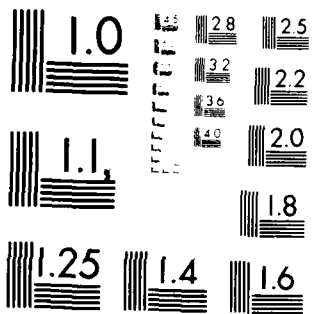
UNCLASSIFIED

N00014-77-C-0390

F/G 8/7

NL





MICROCOPY RESOLUTION TEST CHART
NATIONAL BUREAU OF STANDARDS-1963-A

AD A 131983

12

Final Report

EFFECTS OF MICROSTRUCTURE AND PORE FLUIDS ON THE
ACCOUSTIC PROPERTIES OF GRANULAR MATERIALS

Principal Investigator Amos Nur
Contract No. N00014-77-C-0390
Period covered by the report February 1982 - January 1983

Submitted by:
Amos Nur
Department of Geophysics
Stanford, CA 94305

August 8, 1983

DTIC
1983
E

DTIC FILE COPY

83 08 12 007

This document has been approved
for public release and sale; its
distribution is unlimited.

INTRODUCTION

This report consists of two papers which resulted from the work supported by Contract N00014-77-C-0390 from the Office of Naval Research.

- (1) Grain contacts, disordered microstructure, and dynamic frame moduli in granular sediments.
- (2) Micromechanics of acoustic dissipation in fully and partially water saturated granular sedimentary materials.

Accession For	
NOVA	X
DTIC	
U.S.	
<i>th on file</i>	
Dist	
A	



Grain Contacts, Disordered Microstructure, and Dynamic Frame Moduli in Granular Sediments*

Contents

1. Introduction	9
2. The Problem	13
3. Hertz-Mindlin Theory of Smooth Elastic Spheres in Contact	20
4. Predicted Velocities in Ordered Packings	25
5. Grain Size Effects	32
6. Adhesion of Grain Contacts	39
7. Grain Roughness	47
8. Disordered Packings of Uniform Spheres	51
9. Effects of Grain Angularity	59
10. Natural Grain Size Distributions and Porosity	65
11. Velocities versus Depth	73
12. Conclusions	78

1. INTRODUCTION

Hamilton's pioneering work in geoacoustics (1970, 1971, 1974a,b, 1976a, 1978, 1979a,b, 1980a) has shown the velocities of marine sediments to be strongly dependent on porosity, granular fabric, and depth.

Particularly sensitive to stress conditions and grain size appears to be the shear velocity, V_s . Predictive estimates, laboratory experiments, and in situ measurements exhibit an order of magnitude scatter. The depth dependence of V_s in water saturated sands and silts has been measured anywhere from a 1/3 to a 1/8 power of pressure. Reliable predictive knowledge of V_s is important because the rigidity has been

*Parts to be submitted to the Journal of Geophysical Research and Journal of the Acoustical Society of America in July, 1982.

shown to contribute significantly to the sediment-water reflection coefficient (Hamilton 1971, 1974, 1978). Its depth gradient, $\frac{\partial v_s}{\partial h}$, is an important factor in the refraction of low frequency sound through the ocean floor (Christensen et al., 1975; Hamilton, 1976, 1978, 1980; Fryer, 1981). Shear velocity also holds interest as a possible measure of the nonlinear response and liquefaction potential of coastal and offshore foundations to earthquakes and storm waves (Bea, 1978; Woods, 1978; Hardin, 1978; Stokoe, 1978; Anderson et al., 1978).

The compressional velocity V_p in marine sediments appears to vary quite simply with porosity. Yet attempts thus far to convert interval velocities to formation porosities on the basis of simple averaging models (eg. the time average equation (Wyllie et al., 1956, 1958)) have been unsatisfactory (Geertsma and Smit, 1961; Telford et al., 1976; Watt et al., 1976). V_p in water saturated sands is dependent on the effective pressure (Domenico, 1977) and the depth gradient, $\frac{\partial p}{\partial h}$, has been studied extensively in situ. However, no theory has been proposed which has satisfactorily explained the measurements (Brandt, 1960; White, 1965; Walton, 1975; Stoll, 1980; Digby, 1982).

Gassmann (1951a), Biot (1956), and Brown and Korringa (1975) have shown theoretically that in a macroscopically homogeneous porous media at low acoustic (<500 Hz) and seismic frequencies (figure 1), the dependence of V_p and V_s on microstructure is contained solely within the porosity and the dynamic frame moduli.

Biot's (1956) theory is frequency dependent, attempting to cover the entire range of interest (figure 1). It requires an additional parameter, the so-called structure factor, $\bar{\alpha}$. The structure factor, $\bar{\alpha}$, is a measure of the pore geometry similar to a tortuosity or an

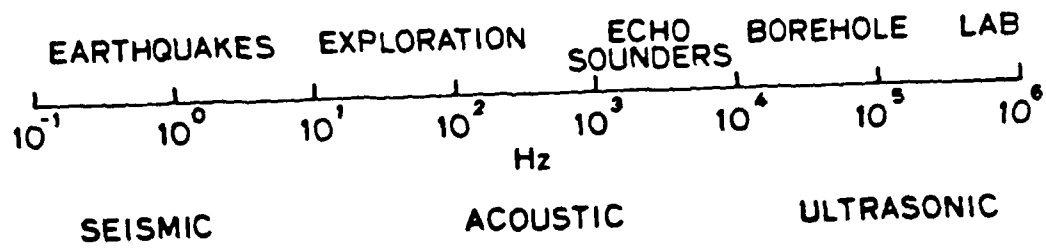


Fig. 1. Spectrum of geoacoustic interest.

index of refraction (Johnson, 1980; Johnson and Sen, 1982). $\bar{\alpha}$ enters Biot's theory in the inertial coupling of the pore fluid to the solid frame and drops out in the low frequency limit, the Biot-Gassmann relations. $\bar{\alpha}$'s significance in the ultrasonic range is under extensive study elsewhere (D.L. Johnson, personal communication).

The porosity, ϕ , is the ratio of the pore volume to the total of the material and is a function of the packing.

The dynamic frame moduli represent the macroscopic or effective stiffness of the granular frame. Neglecting clays and other compositional impurities, we may say that in granular sediments, these stiffnesses result from the tangential contact of elastic quartz grains embedded in a disordered packing. The porosity is related to the frame moduli through the coordination number, i.e. the number of contacts per grain. Understanding how grain contacts and disordered packing determine the dynamic frame moduli is an important step in predicting the acoustic velocities of marine sediments on the one hand, and deciphering the microstructural information contained in measured velocities on the other.

The purpose of this paper is to explain the effects of granular microstructure and effective pressure on low frequency velocities in water saturated granular materials. Micromechanical models are developed for the dry frame moduli. Unambiguous predictions are stated explicitly for V_p' , V_s' , and V_p'/V_s' as a function of grain characteristics, porosity, and effective pressure. The predictions of each step are systematically tested by laboratory measurements of V_p' and V_s' in glass beads and quartz sands. Signal velocities were measured by an ultrasonic pulse transmission technique (similar to that of Elliott

and Wiley, 1975) at frequencies ~200 kHz. All measurements were obtained in vacuum dry (<10 μ m) samples. Although signal velocities are generally equivalent to group velocities in dissipative media (Morse and Ingard, 1968), we are aware of no evidence for dispersion in vacuum dry samples of similar composition. Errors in the moduli are expected to be less than 5%. These moduli are in fact frequency-independent, dry frame moduli and as such are expected to apply across seismic, acoustic, and ultrasonic frequency ranges.

We find that the low frequency, dynamic frame moduli in granular sediments are determined by the grain contact area. At low pressures, the increase in contact area is dominated by the increase in actual contacts per grain. A compaction model is proposed based on the transformation of a Gaussian radial distribution function with pressure. In the high pressure limit where coordination number is constant, granular sediments are well described as a disordered, Hertz-Mindlin granular material. When input into the Biot-Gassmann relations, predictions fit a set of compiled in situ data remarkably well.

2. THE PROBLEM

In situ measurements of V_p versus porosity in ocean bottom sediments are shown in figure 2. The data are taken from Hamilton (1971, 1974b) and Smith (1974). V_p declines gradually with increasing porosity. Scatter is generally less than 5% reaching a maximum of 12% at $\phi = 0.45$. Figure 3 gives in situ V_s versus porosity. It is important to note that Hamilton's data are actually calculated from V_p assuming a hypothetical bulk frame modulus (1971), yet this methodological fact is omitted from Anderson and Hampton's recent (1980) replot of the

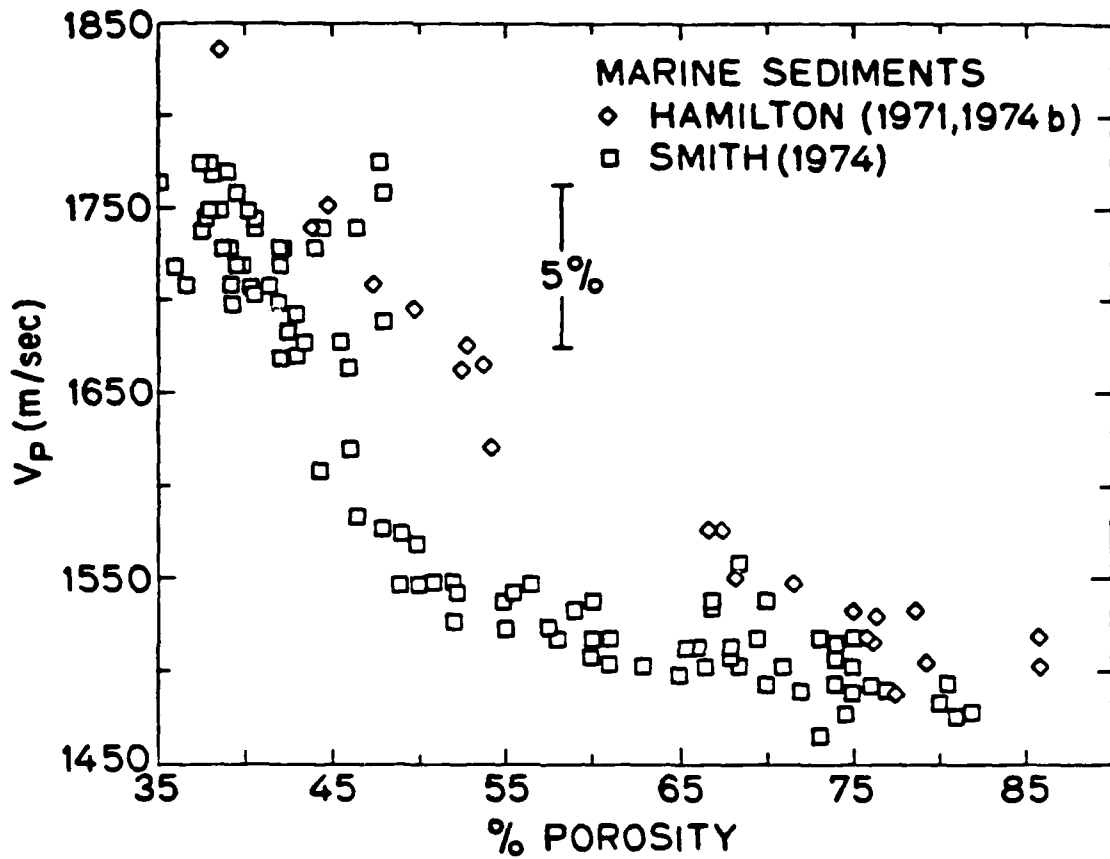


Fig. 2. Compiled measurements of V_p vs. porosity in marine sediments. Hamilton's (1971, 1974b) data is from North Pacific sediments, while Smith's (1974) data is from the North Atlantic sediments.

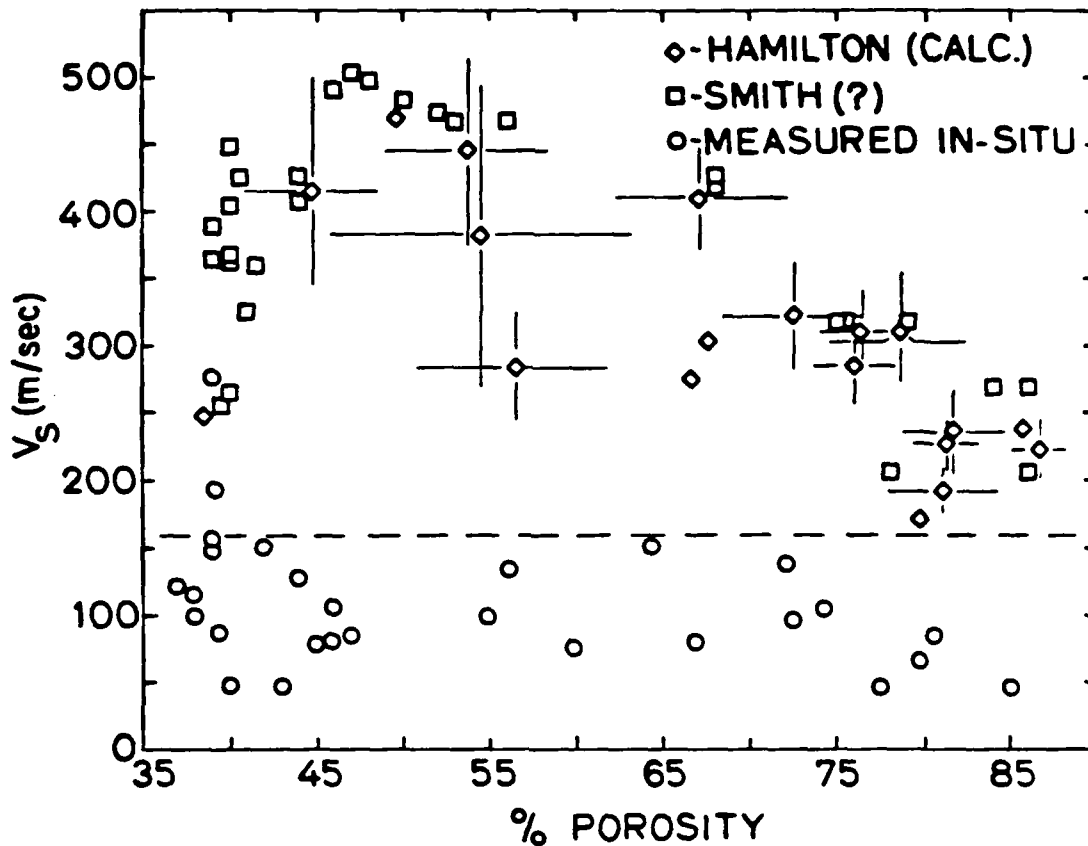


Fig. 3. Compiled data for V_s vs. porosity in in situ sediments. Hamilton's (1971, 1974b) data was calculated from V_p assuming a hypothetical bulk frame modulus. Smith's (1974) techniques were unspecified. Well documented in situ geotechnical measurements (O) are from Anderson et al. (1978), Arango et al. (1978), Kudo and Shima (1970), Hamilton (1976), Barker (1962), Stokoe and Woods (1973), Cunny and Fry (1976), Warrick (1974), and Wilson et al. (1978).

data (their figure 3). Smith's data was first presented in 1974 without description of the measurement techniques. Smith's data has also been replotted in the same figure 3 of Anderson and Hampton (1980). In figure 3 of this paper the "compiled" in situ measurements are taken from the geotechnical literature for water saturated sediments, in which the measurement techniques are fully and explicitly documented. Figure 4 gives the measured porosity in marine sediments versus grain size in microns. The grain size scale is based on a negative logarithm to the base 2, which is equivalent to the phi grain size scale used in sedimentology. The roughly linear plot implies that if the data presented in figures 2 and 3 were plotted against grain size (log to the base 2), homologous effects would be observed.

At low frequency, V_p and V_s are governed by the Biot-Gassmann relations in which

$$V_p = \left(\frac{M_r}{\rho_c} \right)^{1/2}, \quad V_s = \left(\frac{N_r}{\rho_c} \right)^{1/2} \quad (1)$$

where M_r is the low frequency or relaxed compressional wave modulus given by

$$M_r = \frac{(K_s - K_{wr})^2}{K_s \left(1 - \phi - \frac{K_{wr}}{K_s} + \phi \frac{K_s}{K_f} \right)} + K_{wr} + \frac{4}{3} \mu_{wr} \quad (2)$$

when N_r is the low frequency or relaxed shear wave modulus given by

$$N_r = \mu_{wr} \quad (3)$$

and ρ_c is the composite density given by

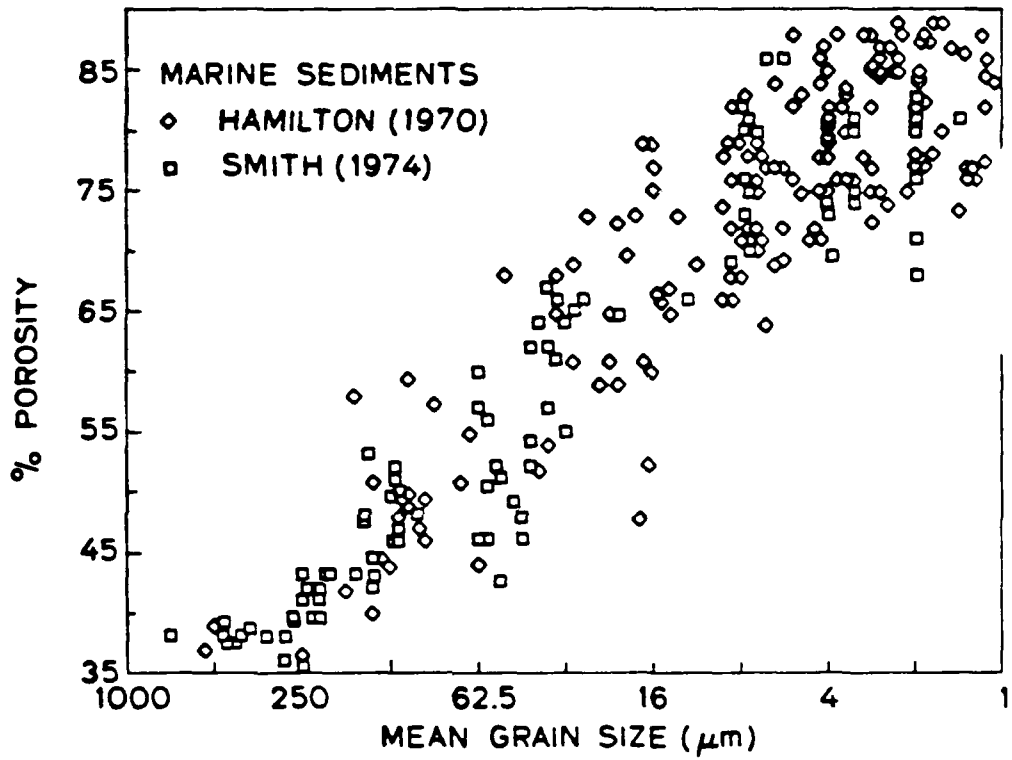


Fig. 4. Porosity vs. grain size in natural sediments.

$$\rho_c = (1 - \phi)\rho_s + \phi S_w \rho_w \quad (4)$$

K_s is the bulk modulus of the solid grains, ρ_s is the density of the solid grains, ρ_w is the density of the water, and S_w is the water saturation which is equal to 1.0 in a fully saturated material. K_f is the bulk modulus of the pore fluid given by

$$\frac{1}{K_f} = \beta_g (1 - S_w) + \beta_w S_w \quad (5)$$

where β_g is the compressibility of the gas and β_w is the compressibility of the water.

K_{wr} and μ_{wr} are the real parts of the relaxed bulk and shear water-wetted frame moduli, respectively. They replace the more ambiguous "frame moduli of the bulk material" of say, Geertsma and Smit (1961). We have observed (e.g. Hardin and Richart, 1963; Spencer, 1981; Murphy, 1982a) a strong modulus defect in sands and sandstones at low acoustic frequencies with the addition of small amounts of moisture. In general, the bulk and shear frame moduli, \bar{K} and \bar{G} , respectively, are complex and strongly frequency dependent on water saturation and frequency as shown in figure 5. These effects of water saturation and frequency are the subject of the related papers (Murphy, 1982a; Murphy, 1982b, Murphy and Nur, 1982a).

In this paper, we focus on i) the dry bulk and shear frame moduli, K_d and μ_d , respectively, which are independent of frequency, and ii) the softening of K_d and μ_d to K_{wr} and μ_{wr} . While it is necessary to predict the low frequency softening in order to test agreement with in situ data, our primary objective is to understand how grain characteristics and granular microstructure determine K_d and μ_d .

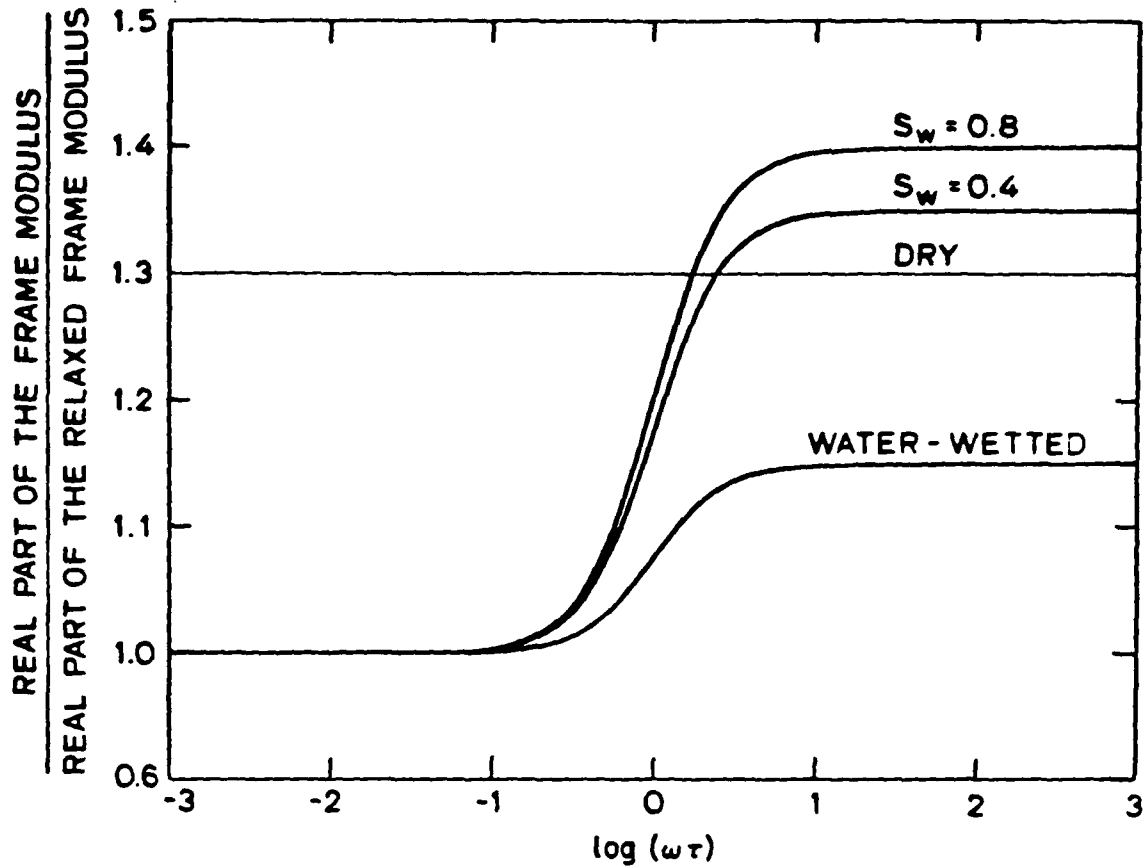


Fig. 5. Theoretical dispersion, as a function of water saturation, of the real part of the frame modulus normalized to the real part of the relaxed frame modulus. In granular sedimentary materials, $\tau = 10^{-3} - 10^{-4}$ sec. In this paper, we focus on the dry frame moduli, and the relaxed wetted frame moduli. Dispersion is neglected.

Microstructure may be decomposed into two categories of relations. The relations between two adjacent individual grains in contact or near contact are called contact theory. The relations between an individual grain and the aggregate of grains are called packing theory. Development of these theories leads to unambiguous predictions for the effects of grain size, shape, and size distribution, as well as for the effects of porosity and effective pressure. All of which are directly testable by simple experiment.

Digression

This problem is intimately related to the nature of the seismic properties of the shallow lunar crust which have been studied by Warren and Anderson (1973), Talwani et al. (1973), Gangi (1981), Johnson et al. (1982), and most notably by Tittmann et al. (1972, 1976, 1977, 1978, 1979). The results of this work are applied to lunar problems in a subsequent article (Murphy and Nur, 1982b).

3. HERTZ-MINDLIN THEORY OF SMOOTH ELASTIC SPHERES IN CONTACT

Consider two identical smooth elastic spheres in tangential contact at a point (fig. 6a). The application of a finite force normal to the plane of contact results in a circular area of contact (fig. 6b). We assume that the radius of the contact is small compared to the radii of the spheres. The classical theory of Hertz (Timoshenko and Goodier, 1951) shows the relation between the normal contact force, n , and the radius of the area of contact, a , to be

$$a = \left[\frac{3(1-\nu)nR}{8\mu} \right]^{1/3} \quad (6)$$

where R is the radius of the grains, and ν and μ are, respectively,

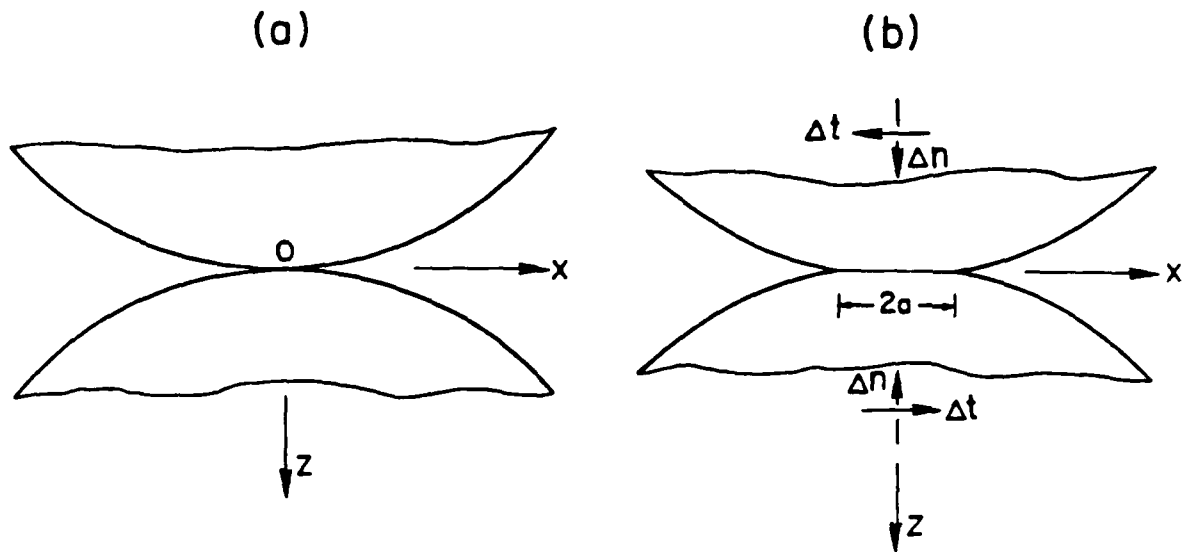


Fig. 6. Elastic spheres in contact.

a) unstressed state,

b) spheres pressed together under normal force, n , applied along the z axis. Circular contact area of radius, a , is formed. Δn and Δt are small (i.e. $\Delta n, \Delta t \ll n$) increments of applied normal and shear stress, respectively, superimposed on n .

the Poisson's ratio and the rigidity (i.e., shear modulus) of the material of the grains. The contact area, A , varies with $n^{2/3}$. The distribution of pressure (fig. 6c) on the contact is

$$\sigma = \frac{3n}{2\pi a^3} (a^2 - r^2)^{1/2} . \quad (7)$$

The relative displacement of the centers of the spheres under the imposition of n , or normal approach is

$$\alpha = 2 \left[\frac{3(1-\nu)n}{8\mu R^{1/2}} \right]^{2/3} . \quad (8)$$

From equations (6) and (8), we obtain for the normal compliance, J_n ,

$$J_n = \frac{d\alpha}{dn} = \frac{1-\nu}{2\mu a} . \quad (9)$$

Mindlin extended the theory to include an additional component of force, t , tangential to the contact surface where $t < fn$. With the application of t , regardless of how small t may be, slip is expected to occur on the contact surface. An infinite traction would otherwise be required along the circumference of the area of contact. Slip begins at the contact circumference and progresses radially inward. The region on which slip occurs (fig. 6c) is an annulus of outer radius, a , and an inner radius, c , given by

$$c = a \left(1 - \frac{t}{fn} \right)^{1/3} , \quad (10)$$

where f is the coefficient of friction of the material of the grains. The distribution of tangential traction on the contact area (fig. 7) is

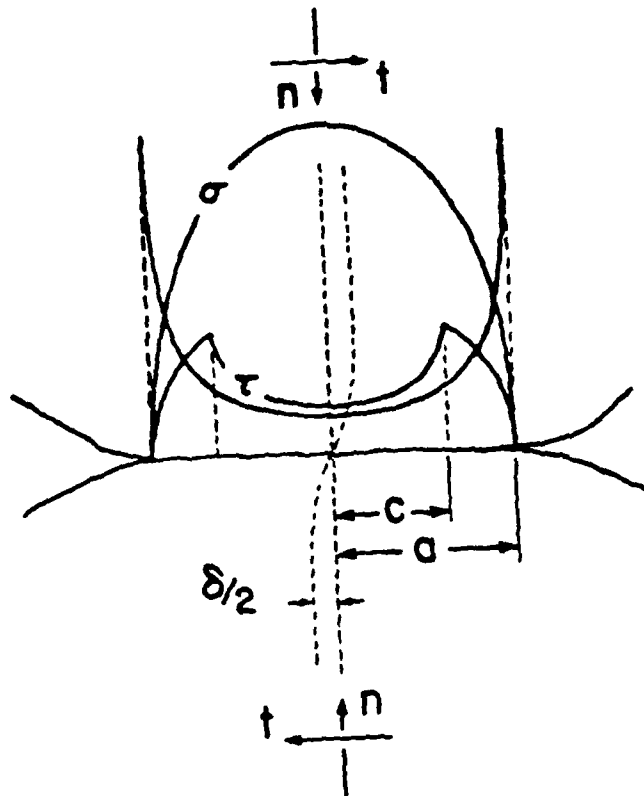


Fig. 6. c) Distribution of normal (σ) and tangential (τ) components of traction on the contact surface.

$$\tau = \begin{cases} \frac{3fn}{2\pi a^3} (a^2 - r^2)^{1/2} , & c \leq r \leq a \\ \frac{3fn}{2\pi a^3} [(a^2 - r^2)^{1/2} - (c^2 - r^2)^{1/2}] , & r \leq c \end{cases} \quad (11)$$

The relative displacement of the centers of the two spheres is

$$\delta = \frac{3fn(2-\nu)}{8\mu a} \left[1 - \left(1 - \frac{t}{fn} \right)^{2/3} \right] . \quad (12)$$

Thus, the tangential compliance is

$$J_t = \frac{d\delta}{dt} = \frac{2-\nu}{4\mu a} \left(1 - \frac{t}{fn} \right)^{1/3} . \quad (13)$$

Mindlin et al. (1951) studied the oscillation of the tangential force between $\pm t^*$ for small amplitudes of loading, i.e. $t \ll fn$. They found that a stable hysteresis cycle is obtained after the first quarter cycle and that the frictional energy loss per cycle due to grain slippage is

$$\phi = \frac{(2-\nu) t^{*3}}{36\mu a fn} \quad (14)$$

The annulus of slip was observed experimentally, and equation 10 was experimentally verified. Johnson (1955) experimentally confirmed the load-displacement relation (equation 10). Energy loss, however, was found to obey equation (14) only for large amplitudes of tangential force. At smaller amplitudes, the energy loss per cycle varied with the square of the amplitude, rather than the cube as predicted by equation (14). Goodman and Brown (1962) elucidated Johnson's findings. And in the discussion following that paper, Johnson revealed that the energy loss dependence on the square of the amplitude had also been observed for oscillating normal force at small amplitudes.

Mindlin and Deresiewicz (1953) further extended the theory to include the addition of a varying force of constant obliquity across a contact surface under the initial normal load, n_0 . The tangential compliance in loading in the stable cycle is

$$J_L = \frac{2-\nu}{4\mu a} \theta + (1-\theta) \left[1 - (1+\theta) \frac{L^*+L}{2(1+\theta L)} \right]^{-1/3} \quad (15)$$

where $L = t/fn_0$, $L^* = t^*/fn_0$, $\theta = f/\beta$, and $\beta = \frac{dt}{dn} \geq f$. The compliance for unloading, J_U , is given by the same expression except that the signs of θ and L are reversed. For small loading, (small L^*) the frictional loss per cycle is

$$\phi = \frac{(2-\nu) t^{*3}}{36\mu a_0 fn_0} (1 - \theta^2) \quad , \quad (16)$$

where a_0 is the contact radius resulting from n_0 .

4. PREDICTED VELOCITIES FOR ORDERED PACKINGS

The dynamic frame moduli of ordered packings of identical smooth elastic spheres may be calculated explicitly. The structural properties of ordered packings of spheres have been formulated by Gratton and Fraser (1935). Early models (Hara, 1935; Iida, 1938, 1939; Gassmann, 1951b) developed dynamic stress-strain relations based on Hertz' contact theory. These models however consistently predict velocities that are too low when tested against experimental results. Furthermore, we know that the tangential stiffness of a contact is of the same order of magnitude as the normal stiffness. Duffy and Mindlin (1958) and Duffy (1959) have since demonstrated how to derive stress-strain relations based on Hertz-Mindlin micromechanics. Directly followed

their approach, we are able to pose explicit expressions for the compressional wave modulus, M_d , and the shear wave modulus, N_d , for simple cubic, hexagonal, close-packed, and face-centered cubic arrays.

Interest focuses on these packings because the hexagonal close-packed (hcp) and face-centered cubic (fcc) arrays constitute the densest packing of identical spheres with $\phi = 0.2595$, while in the simple cubic (sc) array, $\phi = 0.4764$. Smith, Foote, and Busang (1927) have suggested that a random packing may be modeled as a mixture of clusters of hcp and sc microstates.

Duffy and Mindlin (1958) and Duffy (1959) found the fcc and hcp arrays, respectively, to be statically undetermined. That is, the equilibrium equations were not sufficient to determine the stress-strain relations. For these arrays, the relative displacements among the spheres in the lattice are required to simultaneously satisfy the compatibility equations. The compatibility equations involve the contact compliances, they are nonlinear owing to the nonlinearity between the normal contact force and the normal approach in equations (8) and (9). And because of the inelasticity between the tangential force and tangential displacement in equations (12) and (13), they depend on the entire loading history.

Deresiewicz (1958) found the sc packing to be statically determinate. But although the history of loading does not enter into the calculation of the contact forces, the nonlinearity and inelasticity remain in the compliances at each contact.

Two assumptions greatly simplify the equations. 1) If the loading history is isotropic and homothetic, then from symmetry considerations, the initial contact forces are all equal and have no tangential components. From the equilibrium equations and the definition of stress,

the initial contact forces are

$$n_0 = \sqrt{2} R^2 \sigma_0 \quad (17)$$

where σ_0 is the isotropic stress or hydrostatic pressure. Since the loading history is the same, the initial compliances do not vary from contact to contact. ii) If the applied arbitrary stress increments are small compared to n_0 , then the total stress never significantly departs from n_0 . The contact radius becomes

$$a = a_0 = \left[\frac{3(1-\nu)n_0 R}{8\mu} \right]^{1/3} \quad (18)$$

The normal compliance is

$$J_n = \frac{1-\nu}{2\mu a_0} \quad (19)$$

By letting $L^* \rightarrow 0$ in accordance with the small amplitude assumption, we find that

$$J_t = J_L = J_U = \frac{2-\nu}{4\mu a_0} \quad (20)$$

Given these assumptions exact solutions are obtained for the case of an initial isotropic, compressive stress, σ_0 , followed by an arbitrary, yet small, incremental stress. Clearly, these solutions are appropriate for acoustic wave propagation in a granular material under hydrostatic confining pressure.

The set of explicit, continuum, differential constitutive equations takes the general form $dT = C dE$, where T is the stress tensor, E is the strain tensor, and C is the compliance tensor. The equations for the sc packing have the particular form of an isotropic solid. The

independent moduli are two,

$$\begin{aligned} c_{11} &= c_0 \quad , \\ c_{12} &= \frac{\nu}{2(2-\nu)} c_0 \quad , \end{aligned} \tag{21}$$

where $c_0 = \left[\frac{3\mu^2\sigma_0}{2(1-\nu)^2} \right]^{1/3}$. The equations for the hcp array have a symmetry corresponding to a tetragonal crystal with six independent moduli,

$$\begin{aligned} c_{11} &= \frac{1152 - 1848\nu + 725\nu^2}{24(2-\nu)(12-11\nu)} c_0 \quad , \\ c_{12} &= \frac{\nu(120 - 109\nu)}{24(2-\nu)(12-11\nu)} c_0 \quad , \\ c_{13} &= \frac{\nu}{3(2-\nu)} c_0 \quad , \\ c_{33} &= \frac{4(3-2\nu)}{3(2-\nu)} c_0 \quad , \\ c_{44} &= c_{55} = \frac{6-5\nu}{4(2-\nu)} c_0 \quad , \\ c_{66} &= \frac{576 - 948\nu + 417\nu^2}{24(2-\nu)(12-11\nu)} c_0 \quad . \end{aligned} \tag{22}$$

The equations for the fcc array correspond to a cubic crystal. The moduli are

$$\begin{aligned} c_{11} &= 2c_{44} = \frac{4-3\nu}{2-\nu} c_0 \quad , \\ c_{12} &= \frac{\nu}{2(2-\nu)} c_0 \quad . \end{aligned} \tag{23}$$

Results are compiled in Tables 1 and 2.

TABLE 1. Relevant characteristics of the three pertinent ordered packings. The symbol '.' denotes a zero component in the stiffness matrix.

Symbol	Coordination Number	Porosity	Stiffness Matrix
Simple cubic sc	6	0.47	$\begin{pmatrix} C_{11} & & & & & \\ & C_{12} & & & & \\ & & C_{12} & & & \\ & & & C_{11} & & \\ & & & & \frac{1}{2}(C_{11}-C_{12}) & \\ & & & & \frac{1}{2}(C_{11}-C_{12}) & \\ & & & & & \frac{1}{2}(C_{11}-C_{12}) \end{pmatrix}$
Hexagonal Close-packed hcp	12	0.25	$\begin{pmatrix} C_{11} & & & & & \\ & C_{12} & & & & \\ & & C_{13} & & & \\ & & & C_{13} & & \\ & & & & C_{33} & \\ & & & & & C_{44} \\ & & & & & & C_{44} \\ & & & & & & & C_{66} \end{pmatrix}$

TABLE 1 (cont.)

Symbol	Coordination Number	Porosity	Stiffness Matrix
Face-centered	12	0.25	$\begin{pmatrix} C_{11} & & & & & \\ & C_{12} & & & & \\ & & C_{12} & & & \\ & & & C_{11} & & \\ & & & & C_{44} & \\ & & & & & C_{44} \end{pmatrix}$
Cubic			$\begin{pmatrix} \cdot & & & & & \\ & \cdot & & & & \\ & & \cdot & & & \\ & & & \cdot & & \\ & & & & \cdot & \\ & & & & & \cdot \end{pmatrix}$

TABLE 2. Predicted wave moduli, where $C_0 = \left[\frac{3\mu^2\sigma_0}{2(1-\nu)^2} \right]^{1/3}$.

Array	Direction of Propagation	ρ_c	$M_D = \rho_c V^2 = K_D + \frac{4}{3} \mu_D$	$N_D = \rho_c V_s^2 = \mu_D$
sc	isotropic	0.5236 ρ_s	$C_{11} = C_0$	$\frac{1}{2}(C_{11} - C_{12}) = \frac{1-\nu}{2-\nu} C_0$
hcp	[100]	0.7405 ρ_s	$C_{33} = \frac{4(3-2\nu)}{3(2-\nu)} C_0$	$C_{44} = \frac{6-5\nu}{3(2-\nu)} C_0$
fcc	[100]	0.7405 ρ_s	$C_{11} = \frac{4-3\nu}{2-\nu} C_0$	$C_{44} = \frac{4-3\nu}{2(2-\nu)} C_0$

The predictions are unambiguous, and several points are important. Velocities are predicted to be independent of grain size. Velocities depend on the pressure to the 1/6 power. As V_p and V_s for a given packing have the same pressure dependence, V_p/V_s as a function of pressure is a constant. Both V_p and V_s are proportional to the fourth root of the contact area. In fact in general, V_p and V_s are predicted to behave qualitatively the same.

The material has ultimately been modeled as an elastic solid. However, should frictional inelasticity be important, amplitude dependence would be observed in the moduli, velocities, and Q^{-1} , where Q^{-1} is a dimensionless measure of the energy loss per cycle divided by 2π times the maximum energy stored per cycle. Analysis of the frictional dissipation mechanism is deferred to Murphy (1982b).

5. GRAIN SIZE EFFECTS

The apparently strong peak in V_s observed for fine sand at $\phi = 0.45$ observed in the Hamilton and Smith data (fig. 3) finds no support in the careful experiments of Hardin and Richart (1963) or Edil and Luh (1978). By varying grain characteristics in their measurements, Hardin and Richart (1963) found V_s to be independent of grain size, weakly dependent on grain shape, significantly dependent on porosity and dependent on confining pressure to the 1/4 power. Pilbeam and Vaisnys (1973) have made the problem interesting by finding a strong grain size effect and power law pressure dependences with exponents ranging from 1/3 to 1/6. The work of Edil and Luh (1978) generally agrees with Hardin and Richart finding no grain size effect and a weak grain shape effect; however, their empirical

relationship for V_s as a function of porosity and confining pressure is more complicated.

In order to test the theoretical predictions, and to determine once and for all whether or not grain size per se affects velocities, we have measured V_p and V_s in disordered packings of vacuum dry, soda-lime glass beads as a function of grain size. The measurements were made under uniaxial pressures P_a from 0.1 to 35 MPa. The vacuum achieved in the pores was $\sim 5\mu\text{m}$. Glass beads were chosen as the test material because a change in bead size entails minimal inherent changes in other potentially significant grain characteristics, such as grain shape and grain roughness. The measurements are made in carefully compacted samples. The beads are first delicately spooned into the cylindrical pressure vessel. They are then subjected to two preliminary slow, uniaxial pressure cycles in order to obtain reproducible, stabilized packings. In glass beads, the hysteresis cycles stabilize after the initial cycle. An example of a third cycle is given in figure 7. Recalling that the predictions were derived for an isotropic compressive stress, we have been concerned with the uniaxial nature of our applied stress. In figure 7, we compare our example of a pressure cycle with data for similar samples from Domenico (1977). Domenico's data represents an average at each given confining pressure of the loading and unloading cycles. The agreement is satisfactory for the qualitative objectives of our experimental tests. The quantitative discrepancies shall be considered when appropriate in the discussion of the data.

Hereafter, all experimental pressure data given will have been taken from unloading part of the third pressure cycle.

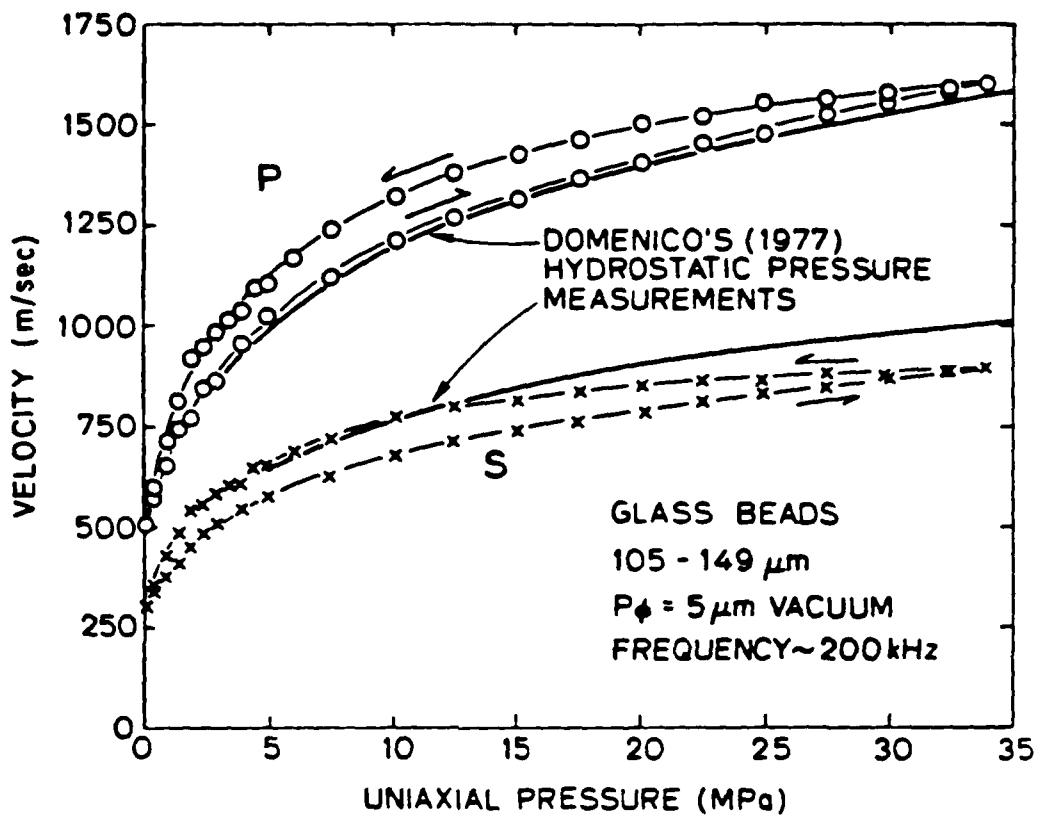


Fig. 7. v_p and v_s vs. uniaxial pressure in vacuum dry glass beads during the third hysteresis cycle. Also plotted is a thicker line which represents a fit to Domenico's (1977) corresponding yet hydrostatic pressure data.

We have tested for strain amplitude dependence in velocities by varying the input voltage which is delivered to the lead zirconate transducers (PZTs). The amplitude was increased at 100 volt intervals from 100 to 1000 volts at $P_a = 0.4, 1.0, \text{ and } 5.0 \text{ MPa}$. No strain amplitude effects were observed. Stoll (1979) has reported the absence of strain amplitude effects in dry and saturated sands below strains of 10^{-6} . Stoll's measurements were made under very low confining pressures. Similar behavior has been observed in sandstones (Winkler et al., 1979; Murphy, 1982a).

Figure 8 gives V_p and V_s against diameter $2R$ divided by sample length, L , at 4 MPa. We observe that if sample length is greater than 100 grain diameters, then the velocities are independent of grain size. Clearly, when $2R/L = 1$, the velocity measured is closer to the speed in a homogeneous block of glass. As $2R/L$ approaches 0.01, the grain packing approaches that of a uniform, disordered granular continuum. In the intermediate range, $0.01 < 2R/L < 1.0$, we may suppose that macroscopic heterogeneities produce high stressed columns of grains in which contact areas are large and dynamic moduli are high.

The theoretical predictions for the glass bead samples in which $\rho_s = 2450 \text{ kg/m}^3$, $\nu = 0.21$, and $\mu = 29.655 \text{ GPa}$ are given in Table 3. In figure 9, we have plotted measured V_p and V_s vs. uniaxial pressure as a function of grain size, along with the theoretical curves. The porosities in the two samples are virtually identical. As the pressure increases from 0.1 to 35 MPa, the porosity in the 149-210 μm sample decreases from 0.392 to 0.372; while porosity in the 74-105 μm samples decreases from 0.387 to 0.370. The two sets of data for the 74-105 μm and 149-174 μm samples represent the largest discrepancy,

TABLE 3

Predicted velocities for soda-lime glass beads, where $\rho_s = 2.45 \times 10^3 \text{ kg/m}^3$, $\nu = 0.21$, and $\mu = 29.655 \text{ Pa}$.

	v_p	v_s	v_p/v_s
sc	$1000 p^{1/6}$	$664.5 p^{1/6}$	1.505
hcp	$1166 p^{1/6}$	$808 p^{1/6}$	1.443
fcc	$1155.4 p^{1/6}$	$817 p^{1/6}$	1.414

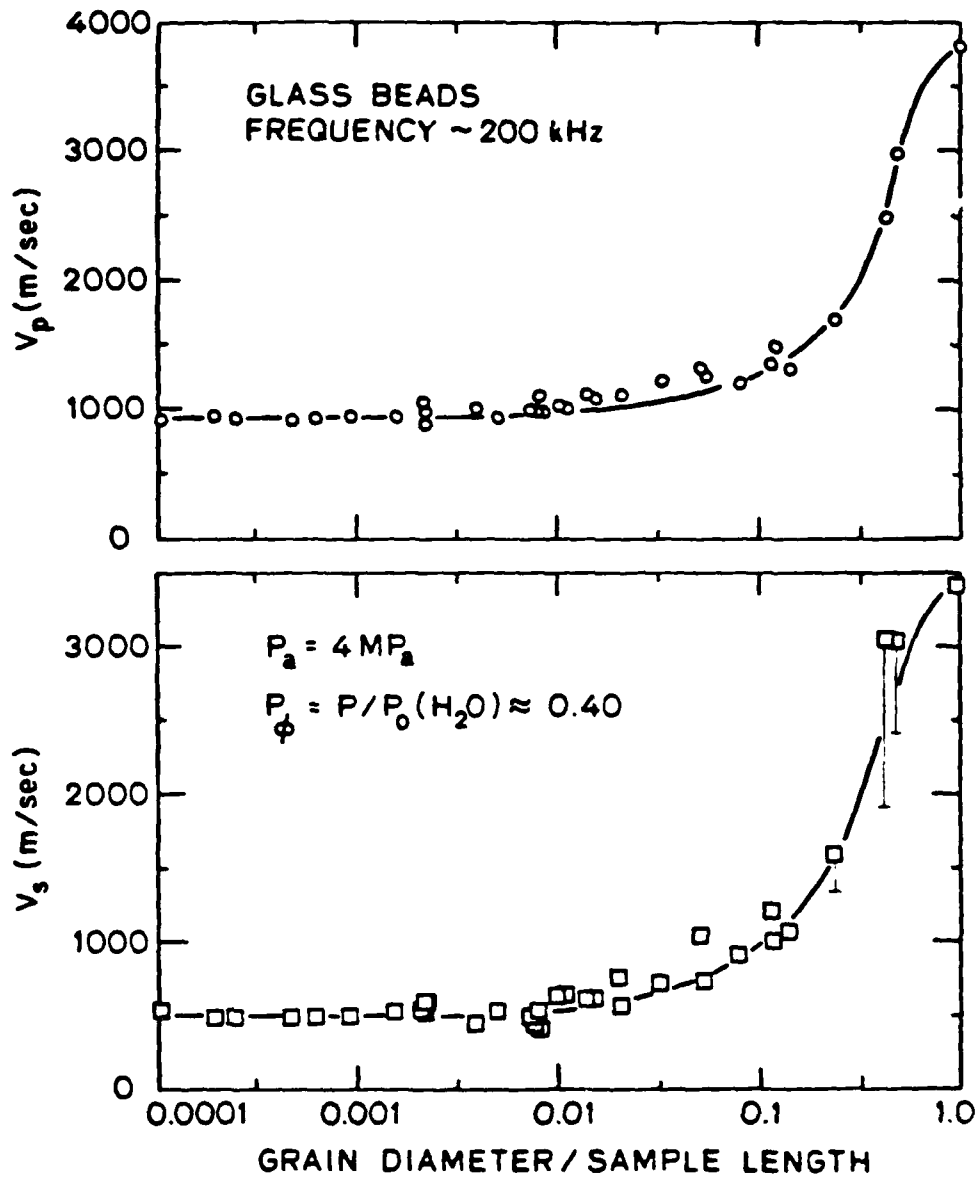


Fig. 8. V_p and V_s vs. grain diameter divided by sample length. Grain diameter divided by sample length is the inverse of the number of grains along the primary wave path.

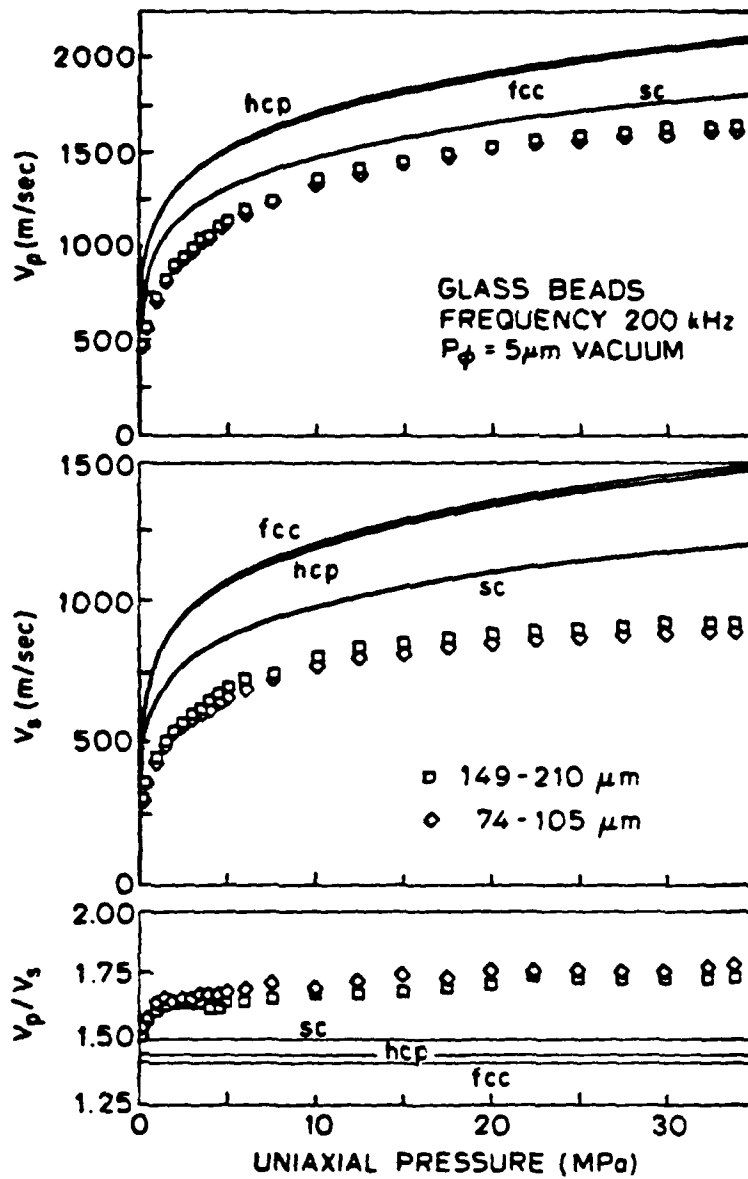


Fig. 9. V_p , V_s , and V_p/V_s vs. uniaxial pressure in vacuum dry samples of different size glass beads. Also plotted are the theoretical predictions from Table 3.

~ 4%, that we have measured in the eight sieve fractions between 62.5 and 250 μm . The larger sieve fractions consistently tend to have higher velocities than the smaller sieve fractions, particularly in shear, but by no more than 4%.

Within experimental tolerance, the model correctly predicts that velocities are indeed independent of grain size. At worst, we find an extremely weak dependence.

However, the velocity dependence on pressure does not conform to a uniform $1/6$ power law. In fact, we observe distinct segments of behavior (figure 10). V_p is best fit by $920 p^{1/6}$ above 10 MPa, but below that pressure it is best described by $750 p^{1/4}$. While V_s is given by $525 p^{1/6}$ at high pressures, and by $450 p^{1/4}$ at low pressures. The transition occurs at lower pressure, 5 MPa, in shear wave velocities. In short, what we are observing is a steeper $1/4$ power law dependence at low pressures, rapidly flattening to a Hertz-Mindlin dependence at intermediate pressures.

If the packing in our disordered samples could be modeled as a mixture of clusters of hcp and sc microstates, as suggested by Smith et al. (1927) the measured velocities would fall between the hcp and sc predictions. Clearly, they do not.

Lastly, V_p/V_s was predicted to be independent of pressure. In figure 9, we find a significant dependence on pressure, particularly below 5 MPa.

6. ADHESION AT GRAIN CONTACTS

The model which has been derived for ordered packings of spheres in Hertz-Mindlin contact has achieved limited success. Improvement may be attempted in two ways: 1) better understanding of individual

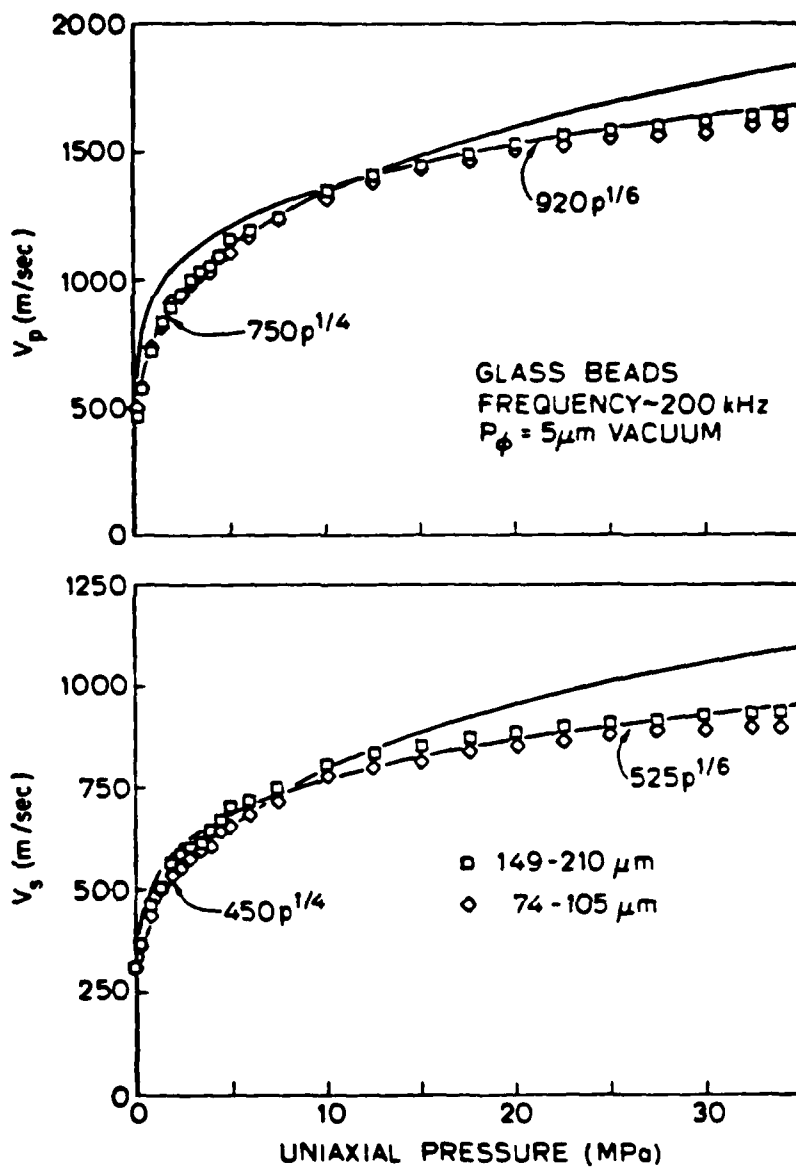


Fig. 10. V_p and V_s data replotted along with best fit power laws.

grain-to-grain contacts and ii) better understanding of disordered packings of grains.

We have thus far treated the grain-to-grain contacts as a purely mechanical interaction responding to a compressive load. A Hertz-Mindlin contact cannot sustain an applied tensile traction. Observations of contacts between spheres and flat plates of low modulus materials have shown that at low applied loads, the Hertz theory (equation 6) predicts contact radii that are consistently too low.

Associated with every surface is a surface energy resulting from the action of surface forces. As two grain surfaces are brought together, there exists an equilibrium separation, z_0 , at which the competing van der Waals forces of attraction and repulsion between atoms and molecules in the two grains are balanced. At a distance less than z_0 the surfaces will repel each other. At distances greater than z_0 they will attract. The force per unit area varies as a function of separation by

$$\sigma_a = -Az^{-3} + Bz^{-6} \quad (24)$$

which graphically has the familiar appearance of figure 11.

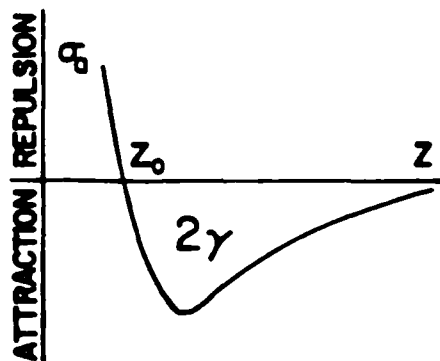


Fig. 11

Repulsion is taken to be positive such that we may speak of heights of energy barriers. Attraction is to be negative, thus we may discuss the depth of energy minima. It is clear that in this construction, a tensile force or force of adhesion must be exerted in order to separate the two grains. The two surfaces each possess a surface energy per unit area, γ , equal in total to the work done in separating the surfaces. γ is given by (Verwey and Overbeek, 1948)

$$2\gamma = \int_{z_0}^{\infty} \sigma_a dz = \frac{A}{6\pi z_0^2} \quad (25)$$

where A is known as the Hamaker constant. The surface energy of silica in a vacuum has been reported to be -0.280 J/m^2 (Brunauer et al., 1956). The Hamaker constant of quartz is roughly $7 \times 10^{-20} \text{ J}$ (Israelachvili and Tabor, 1973). z_0 is then ≈ 1 to 2 \AA , and the maximum adhesive fraction is $\sim 10 \text{ GPa}$, which falls off 2 orders of magnitude at a separation of 5 \AA . The forces of adhesion are large, but their range of action is quite small.

Johnson et al. (1971) have derived an exact expression for the modified Hertz contact area taking into account the surface energy. It is

$$a^3 = a_0^3 \left[1 + \frac{w}{n} \left\{ (2wn+w^2)^{1/2} \right\} \right] \quad (26)$$

where $w = 3\gamma\pi R$ and a_0 is the Hertz contact radius given by equation (6). Several new predictions are immediate. Surface energy generates a larger contact area at a given normal force, especially at small loads, as shown in figure 12. The dependence on normal force is flattened from $n^{1/3}$ to $n^{1/3} + n^{1/2}$.

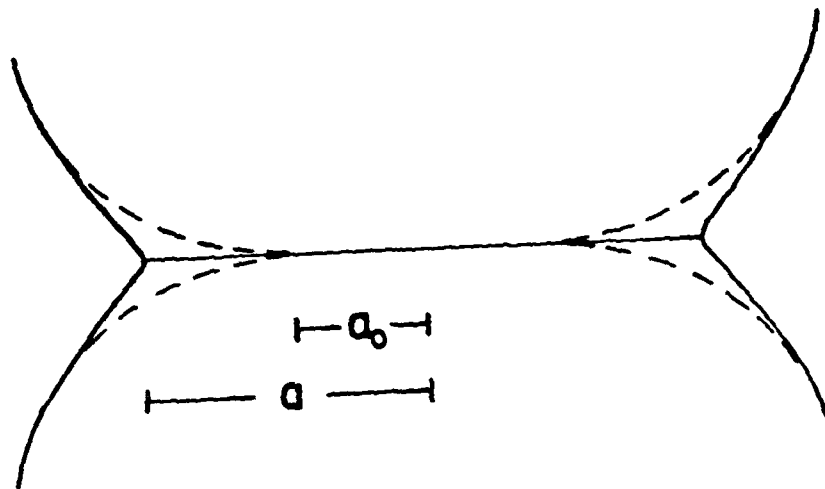


Fig. 12. Increase in the contact radius from a_0 (Hertz) to a (equation 27) due to the force of adhesion.

When $\gamma = 0$, equation (27) reduces to equation (6). At $n = 0$, the contact area remains finite and is given by

$$\hat{a}^3 = \frac{8(1-\nu) R}{3} ; \quad (27)$$

and an applied tensile traction equal to

$$n = -\frac{3}{2} \gamma \pi R \quad (28)$$

is required to separate the spheres. Johnson et al. (1971) have verified these relations experimentally.

Another important point is that the energy loss per cycle under small amplitudes is no longer dominated by friction but by the surface energy which will resist grain slip at the contact edges. During each cycle as contact edges are deformed, hydrogen bonds between surface hydroxyls and molecular water may be broken and energy absorbed (Spencer, 1981). Velocities and Q^{-1} would then be strain independent.

The surface energy of quartz and silica glass is controlled by moisture. Indeed, the surface energy of silica immersed in water drops to 0.139 J/m^2 from 0.280 J/m^2 (Van Voorhis et al., 1957). It is generally thought that the hydration of a fully hydroxylated silica (silanol) surface strongly increases the molecular repulsion forces (Aronson and Princen, 1978; Israelachvili and Adams, 1978; Pashley, 1980; Pashley and Israelachvili, 1981). Diagrammatically, we see in figure 13 that hydration strengthens the short range repulsion forces, dramatically weakens the energy minima, and produces an energy barrier in the electrical double layer (DVLO theory; eg. Sonnatg and Streng, 1972). Kitchner, 1971) has further postulated that a layer of silica gel forms at the silica surface.

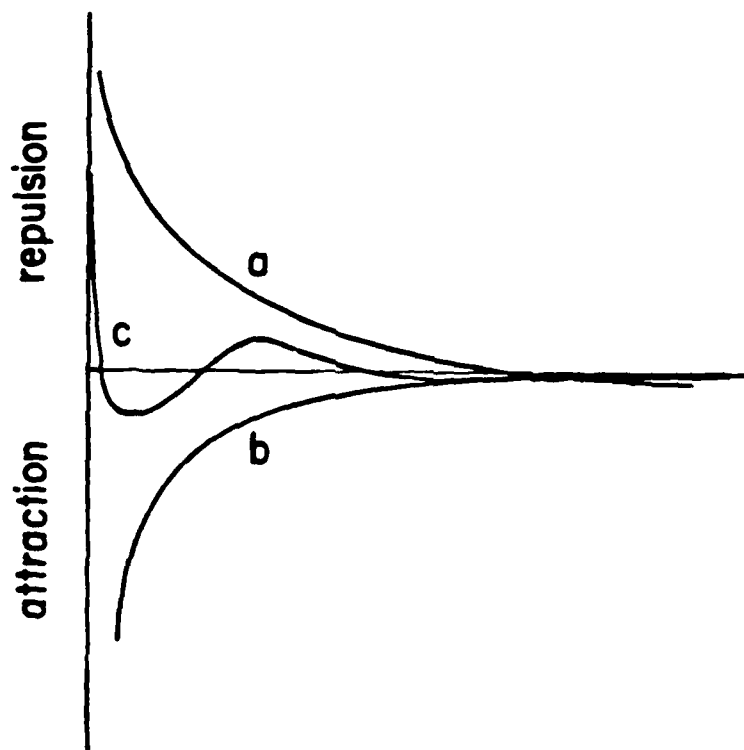


Fig. 13. Sketch of surface forces between wetted grains.

- a) repulsion,
- b) van der Walls attraction, and
- c) resultant of curves a and b.

The reduction in surface energy substantially eliminates the adhesive contribution to the contact compliance. In our uniaxial experiments, we have consistently noted a significant volume expansion in vacuum dry samples when wetted with water. In sands (Hardin and Richart, 1963; Elliott and Wiley, 1975) and sandstones in general, (Pandit and King, 1979; Clark et al., 1980; Spencer, 1981; Murphy, 1982a) a strong defect in the dry frame moduli is observed with a loss of vacuum, or an increase in relative humidity, or bulk wetting. This effect is described in figure 5. Although the effect is relatively weak at 200 kHz, a 15% decline in the V_s of Ottawa sand at 0.1 MPa has been measured in the present experiments with the addition of 0.10 water saturation.

In short, adhesion, though crucial to the dry frame moduli is negligible in the wetted frame moduli. Adhesion cannot help to explain the behavior of V_s in figure 3.

Murphy (1982a) proposed an additional surface mechanism to explain the frame modulus defect. The surface tension of small amounts of water between two quartz grains applies a force of adhesion on the contact given by $n = 2\pi\tilde{\gamma}R$, where $\tilde{\gamma}$ is the surface tension of water. McFarlane and Tabor (1951) have indeed observed such adhesion between a glass sphere and a glass plate as a function of relative humidity. The effect is negligible below a relative humidity of 0.80 and reaches a plateau at 0.85 or 20 monolayers of H_2O . We have observed no such dependence in dynamic moduli, only a monotonic, exponential decrease with increasing relative humidity (Murphy, 1982a; Clark et al., 1980). Although this mechanism is crucial in the construction of sand castles, it appears to be irrelevant to the acoustic properties of granular sediments.

7. GRAIN ROUGHNESS

Grain roughness may or may not be significant in the glass bead samples in which the individual spheres are quite smooth; but it is undoubtedly an important consideration in quartz sand where the relief on the grain surfaces is of the order of $1 \mu\text{m}$ on a $200 \mu\text{m}$ grain. Moreover, the nature of the analysis for micro-roughness suggests a fruitful approach to disordered packing.

Let us assume that a nominally flat surface is rough. It has asperities with spherical summits all of radius, ϵ , which deform elasticity in accordance to equations 6-9. Following Greenwood and Williamson (1966), as the rough surface approaches to a distance h from a truly flat plane, the probability of making contact at any given asperity of height, l is

$$\text{prob } (l > h) = \int_h^{\infty} \phi(l) dl \quad (29)$$

where ϕ is the probability distribution of asperity heights. If one further assumes that the asperities do not interact and defines s to be the standard deviation of asperity heights or roughness, η to be the density of asperities, and \tilde{A} to be the nominal macroscopic contact area we obtain

$$\begin{aligned} m &= \eta \tilde{A} F_0(h/s) \\ A &= m \eta \epsilon s F_1(h/s) \\ n &= \frac{16\mu}{3(1-\nu)} \eta \tilde{A} \epsilon^{1/2} s^{3/2} F_{3/2}(h/s) \end{aligned} \quad (30)$$

where m is the number of contact sites, A is the actual contact area,

and

$$F_k(h/s) = \int_z^{\infty} \left(u - \frac{h}{s}\right)^k \phi^*(u) du \quad . \quad (31)$$

$\phi^*(u)$ is the height distribution scaled such that its standard deviation is 1.

Two particular distributions are of interest. Measured height distributions tend to be Gaussian (Greenwood and Williamson, 1966). However an exponential distribution is a fair approximation to the uppermost 25% of the asperities and gives a simple analytic solution. This solution yields results very close to those obtained numerically for the Gaussian distribution by Greenwood and Williamson (1966).

Given an exponential distribution of heights, i.e. $\phi^*(u) = e^{-u}$, then the functions $F_k(h/s)$ are just $k!e^{-h/s}$. Equation (30) reduces to

$$\begin{aligned} m &= \tilde{\eta} A e^{-h/s} \\ A &= \pi(\tilde{\eta}\epsilon s) \tilde{A} e^{-h/s} \\ n &= \frac{4\mu\pi}{1-\nu} (\tilde{\eta}\epsilon s)^{1/2} (s/\epsilon)^{1/2} A e^{-h/s} \end{aligned} \quad (32)$$

Eliminating the separation (h/s) , we find that both the number of contact sites and the area of contact are exactly proportional to the normal force. Thus, the average size of the contact, and the contact pressure are independent of the load. Of course, a given individual contact grows in area with load, but simultaneously new smaller contacts are being formed. There exists a balance which leaves the average unchanged.

The calculations for a Gaussian distribution show a similar behavior except that the proportionalities, which were exact for the exponential distribution, now vary slowly with load.

In the case of the approach of two rough spheres, the global curvature of the bodies limits the apparent contact area. The asperities can no longer be assumed to be independent, for the force on one contact may change the height of its neighbors. Greenwood and Tripp (1967) have numerically solved this problem for a Gaussian distribution of asperity heights. Hertzian contact theory (equations 6-9) is found to be the high load limit for rough spheres. At low loads, the pressure distribution strongly contrasts with the Hertz predictions. The nominal contact area is an order of magnitude larger, and the maximum pressure is 1/3 smaller. Of course, the actual contact area is much smaller than the Hertzian value. And the pressures on the microcontacts are much higher than Hertzian pressures. They are in fact of the same order as those for nominally flat surfaces, and again are proportional to $\frac{2\mu}{1-\nu} (s/\epsilon)^{1/2}$. The proportionality factor varies slowly with the magnitude of the load.

Some asperities may suffer plastic deformation. The plasticity index, ζ , which combines the material and topographic properties of a surface has been shown to be an accurate criterion for the onset of plasticity (Greenwood and Williamson, 1966). ζ is

$$\zeta = \frac{\mu}{H(1-\nu)} (s/\epsilon)^{1/2} \quad (33)$$

where H is the hardness of the material. $5.15 \times 10^{10} \text{ kg/m}^2$ is the hardness reported by Potters Industries Inc. (1980) for the glass beads. Sharp and rough grains with ζ above 1 will almost certainly

have some plastic deformation, while round and smooth grains with ξ below 0.6 will strain elastically.

The general result however does not rest on the particular constitutive model governing the contacts. The behavior at low loads is not determined by the mechanics of the asperities but rather by the statistics of the surface roughness. If increasing the load creates new contact sites, then $A \propto n$. At high loads where increasing the load simply enhances the size of the existing contacts, the micromechanics takes over, and in the elastic case, $A \propto n^{2/3}$.

Permit one further point for completeness. Surface roughness may inhibit adhesion (Fuller and Tabor, 1974). Consider a dimensionless adhesion parameter, ξ ,

$$\xi = \frac{2\mu(1+\nu) s^{2/3} R^{1/2}}{\gamma E} \quad (34)$$

The denominator is a measure of the adhesive force experienced by a sphere of radius, ϵ . The numerator is a measure of the elastic force needed to push a sphere of radius ϵ to a depth s into a solid of modulus, $2\mu(1+\nu)$. ξ is the ratio of the compressive elastic forces exerted by the higher asperities which are attempting to separate the surfaces and the adhesive forces which are attempting to hold the surfaces together. When the adhesion parameter is small, the adhesion is high. As the surface roughens the adhesion parameter increases. When the asperities are sufficiently high, the surfaces are effectively pried apart and the adhesion falls to a small value.

8. DISORDERED PACKINGS OF UNIFORM SPHERES

In crystallographic arrays, the porosity and coordination number are fixed, microscopically uniform, and known. But in natural and artificial sediments, the packing is disordered. Porosity and coordination are undetermined. They vary microscopically, and their continuum values are averages or probability densities. Porosity can be measured. Coordination number is more difficult to obtain. Most relevant to our interest, porosity and coordination number, especially coordination number, are dependent on pressure.

Without any exaggeration, it is the relation between coordination number and effective pressure which controls the dynamic frame moduli in marine sediments. In this section we continue our analysis of compacted artificial materials, carefully building a solid understanding of the physics. We shall show in Section 11 that the theoretical framework proposed in this section fits a compiled set of in situ data remarkably well.

Virtually no previous work has focused on the effects of disorder on velocities. Gangi (1981) reflects the state-of-the-art.

Brandt (1956) derived a model for the random packing of elastic spheres in Hertzian contact. Coordination number was assumed independent of pressure and fixed at 8.84. V_p was found to vary with $p^{1/6}$.

We find that the change in coordination number with pressure successfully explains our glass bead results. The process involved is similar to that in the case of grain roughness. At low pressures, the increase of contact area due to the creation of new contact sites dominates the pressure dependence, yielding $V = p^{1/4}$. At high pressures, coordination number becomes independent of pressure, and the Hertz-

Mindlin $p^{1/6}$ dependence takes over.

Smith et al. (1927) and Bernal and Mason (1960) have studied the porosity ϕ , coordination number ψ , and their relationship, $\phi = f(\psi)$, in random packings of uniform spheres. Recall that the hcp and fcc packings are the densest possible for uniform spheres with $\phi = 0.2596$ and $\psi = 12$; while, the sc packing is the loosest possible ordered packing with $\phi = 0.4795$ and $\psi = 6$. Random packings have a narrower range of porosities. Random close packing, rcp, yields $\phi = 0.36$. Random loose packing, rlp, has $\phi = 0.40$ (Scott, 1960). Bernal and Mason (1960) were able to measure the distribution of coordination numbers in random packings of uniform spheres. More importantly, they were able to distinguish between those grains which were actually in contact and those which were near to contact. In rcp, the mean actual contacts are 6.4 per grain. While the total coordination, adding actual plus near, is 8.5. The mean actual contacts in rlp are 5.5, and total coordination is 7.1. These results are plotted in figure 14 along with measurements from Smith et al. (1927).

The solid line curve in figure 14 corresponds to the mean total coordination at a given porosity. The porosities measured at 0.1 MPa in our glass bead experiments were roughly 0.40. Measured at 35 MPa, the porosity approached 0.37. The pressure increase decreases porosity, and in figure 13 we move up the solid line curve from 8.2 at 0.40 to 8.8 at 0.37. Yet this is the weak component of the effect. The actual number of contacts at low pressures is far beneath the line, perhaps below 5. The displacements associated with low uniaxial pressure cause the near contacts to progressively come into actual contact. Thus in figure 14, low uniaxial pressures (<10 MPa) drive the rlp

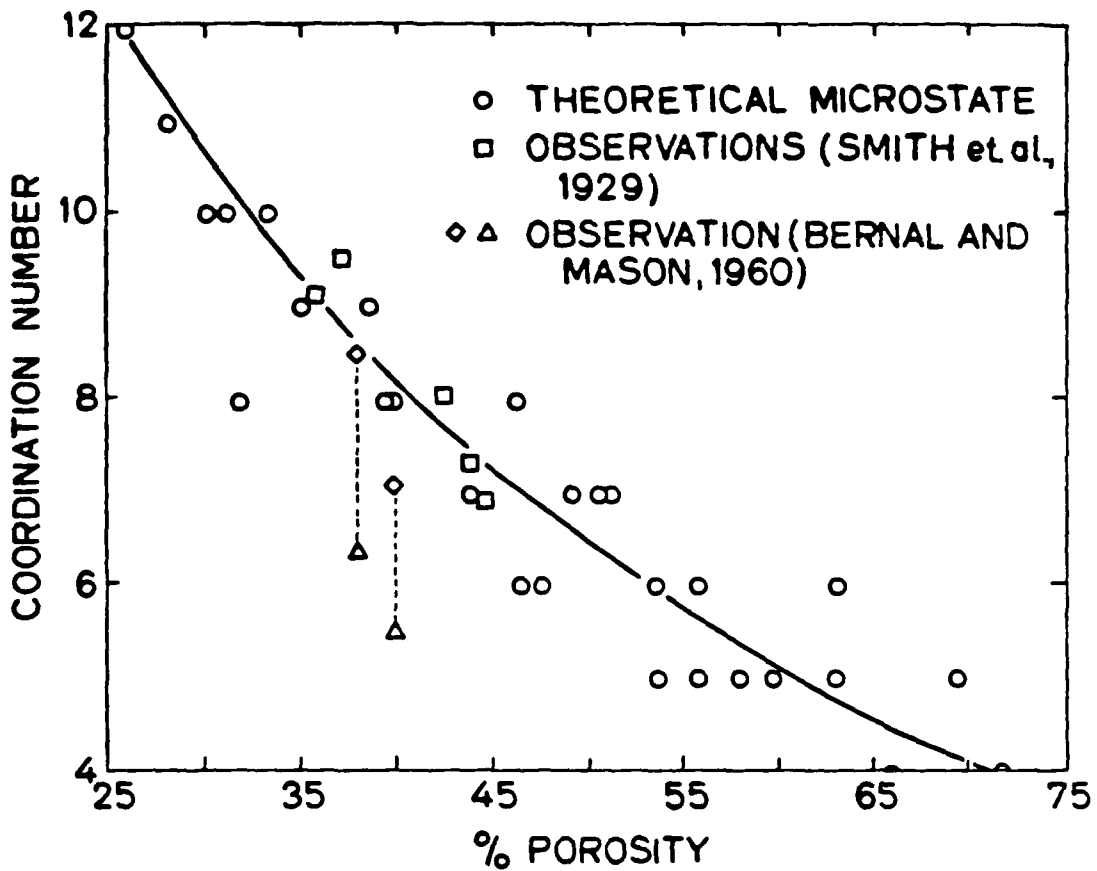


Fig. 14. Coordination vs. porosity. The actual number of contacts in Bernal and Mason's (1960) packings denoted by (Δ). The total number of contacts, actual plus near, are denoted by (\diamond). The theoretical microstates represent twenty-eight possible arrangements of ordered and disordered unit cells.

actual contact number nearly vertically to the solid line. This is the dominant mode of contact area increase at low pressures. By 15 MPa the coordination varies with porosity solely along the solid line.

The argument may be readily formulated in terms of roughness. Consider two layers of spheres, separated by a small distance where the roughness elements assume the radius of the spheres. The centers of the spheres in the "flat" layer are fixed at a depth R below the surface. The centers of the spheres in the approaching plane are distributed in depth between 0 and R according to $\phi(w)$. The governing equations then become equations (30), if we substitute R for ϵ .

In the case of an exponential distribution of sphere heights above the nominal plane, we find that the displacement, α , for two layers of distributed heights is

$$\alpha = 2s \ln \left[\frac{(1-\nu)\eta}{\mu\eta\pi^{1/2} \tilde{A}(s/R)^{1/2}} \right] \quad (35)$$

where s is the standard deviation of heights or roughness, $\eta = 1-\phi$, the density of spheres, and \tilde{A} is the nominal area, say the area of a horizontal section in the sample. The normal compliance of two layers of distributed heights is

$$J_n = \frac{d\alpha}{dn} = \frac{2s}{n} \quad (36)$$

The contact area, A , can be similarly determined. Eliminating the separation, it is clear that A is proportional to n .

An other case of interest is a random or uniform distribution of heights $1/R$ above the nominal plane. Physically, such a distribution corresponds to a constant rate of increase in contact sites per unit

displacement. The displacement, α , is given by

$$\alpha = \left[\frac{15(1-\nu) n}{4\mu\bar{A} \sqrt{2} R^{1/2}} \right]^{2/5}, \quad (37)$$

and the normal compliance is

$$J_n = \frac{d\alpha}{dn} = .68 \left[\frac{1-\nu}{\mu\bar{A} \sqrt{2} R^{1/2}} \right]^{2/5} n^{-3/5} \quad (38)$$

The contact area can be shown to be proportional to $p^{4/5}$.

Defining p to be $\frac{n}{4\eta\bar{A}R^2}$, velocities and contact area may be related to pressure. The results are given in Table 4 along with the corresponding Hertz-Mindlin predictions

TABLE 4

	Exponential Distribution	Random Distribution	Hertz- Mindlin
$V \propto$	$p^{1/2}$	$p^{1/3.3}$	$p^{1/6}$
	$A^{1/2}$	$A^{5/12}$	$A^{1/4}$
	$A \propto p$	$A \propto p^{4/5}$	$A \propto p^{2/3}$

The behavior is strongly determined by the probability distribution chosen. A satisfactory description of a compacted sphere pack would include a $1/4$ dependence at low pressures which implicitly flattens to Hertz-Mindlin behavior at high pressures. The exponential distribution is obviously to disperse for a compacted sphere pack. Neither is the random distribution a satisfactory model. It is however instructive. Again, it implies a constant rate of increase in contact sites per unit displacement. Following the trends in Table 4, some interesting points

may be drawn about the character of a satisfactory model. Obviously, $V \propto p^{1/4}$ falls between the random distribution and the Hertz-Mindlin predictions. The corresponding proportionalities among the other variables calculated from the trends in the table would be $V \propto A^{1/3}$ and $A \propto p^{11/15}$. In terms of the statistical microprocess involved, we may speculate that the rate of increase in contact sites must fall off faster with load than does the displacement.

Recall from the previous section that Greenwood and Tripp (1967) found that a Gaussian distribution of roughness heights on a sphere behaved like an exponential at very low pressures, but at higher pressures approached a Hertz-Mindlin limit. In fact, we find in Section II that in self-loaded, uncompacted, in situ continental shelf sands, the velocities are well described by our model based on the exponential distribution in the first 50 m of depth. Then, from 50 m to 100 m, the velocities follow the predictions based on the random distribution. Presumably, with continuing depth, the velocities would pass through a behavior associated with the $1/4$ power dependence before reaching the Hertz-Mindlin state at some greater depth.

The Gaussian distribution actually corresponds in granular sediments to the radial probability density of nearest neighbors. A physical interpretation of the compaction process is given with the aid of figure 15. The probability of finding a grain center at a radial distance, $2R - \lambda < r < 2R + \lambda$, is represented by a Gaussian distribution. The actual number of contacts per grain is given at the intersection of the cumulative distribution with the vertical line $2R$. At very low pressures, the grains are disperse. The mean is outside the distance, $2R$ (figure 15a). Fewer neighboring grains are in contact now than are

likely to come into contact in the future (with the application of pressure). That is, the likelihood of an increase in the number of contacts resulting from an increment in pressure is very high. The shape of the segment of the Gaussian distribution which intersects $2R$ is well approximated by an exponential distribution. With the application of small loading the packing will tighten. The distribution will narrow and will displace towards the origin. At some small applied pressure, the mean will lie on $2R$ (figure 15b). At this point, the number of grains which are in contact is equivalent to those which are likely to come into contact in the future. Here, the uniform or random distribution is a good approximation. With increased pressure, the mean is now driven inside $2R$ (figure 15c). That is, more grains are currently in contact than are likely to come into contact in the future. The distribution now intersects $2R$ on the down side of the distribution. Here, $V \propto p^{1/4}$. And at some higher pressure still, the distribution is almost entirely within $2R$ (figure 15d). It is now highly unlikely that a grain will gain any new contacts with additional increments of pressure. The sediment is now a Hertz-Mindlin material.

We can summarize this model by saying that the frame moduli in a granular sediment qualitatively evolve with the state of compaction. This model would suggest that the evolution we observe in the laboratory samples is truncated due to pre-compaction.

The model also implies specific predictions about the velocity depth gradients in uncompacted, self-loaded, granular sediments. These predictions differ strongly with standing empirical models. In particular, the standing models predict a fixed pressure dependence with depth. The competing predictions are tested against in situ data in Section II.

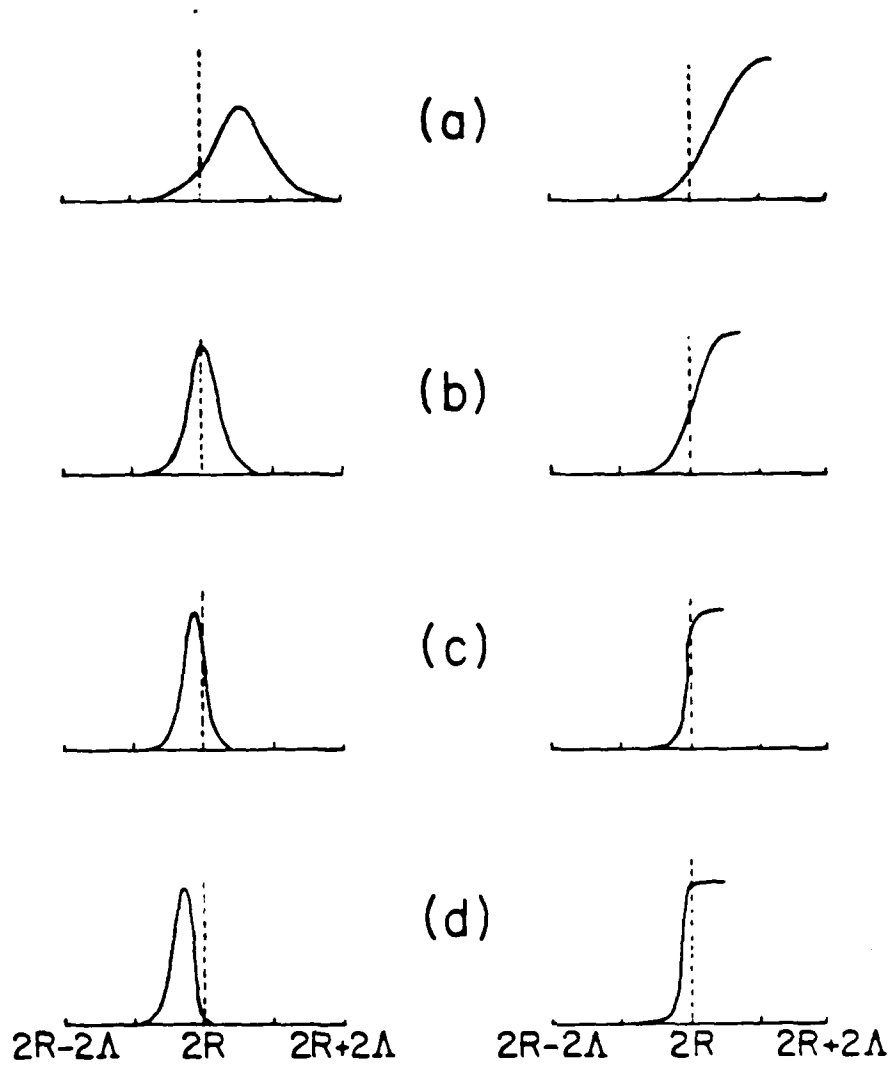


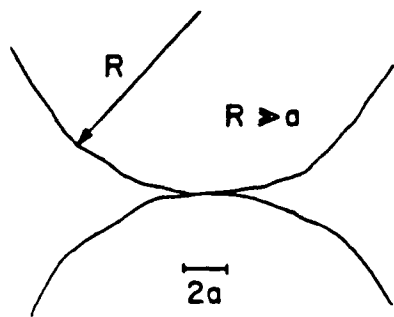
Fig. 15. Schematic micromechanical model of compaction, depicting the transformation of the Gaussian radial distribution with pressure. See text for explanation.

9. EFFECTS OF GRAIN ANGULARITY

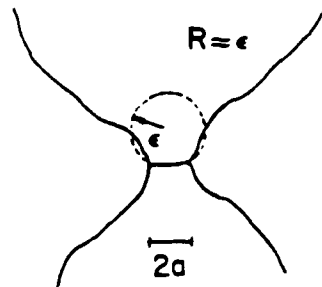
We find that grain angularity produces three distinct effects on velocities: two through the micromechanics of the grain contacts, and the other on the packing. Each effect is separable.

First, recall that a principle assumption in the Hertz-Mindlin contact theory is that the radius of the contact is small compared to the radius of curvature of the grains. When a sharply angular grain comes into contact with another surface (figure 16), this assumption fails. (A similar situation prevails in the case of conformable bodies in contact, which is applicable to sandstones with large secondary quartz overgrowths.) The surfaces in the vicinity of the contact can no longer be modeled as quadric surfaces, and a higher order theory is required. The analysis has been developed for a number of special cases, and approximate solutions have been found by Cattaneo (1947), Deresiewicz (1961), Steurmann (1941, 1943), Lunberg (1939), and Goodman and Keer (1965). Galin (1961) surveys an extensive Russian literature on the subject. The general, relevant conclusion that may be drawn from this work is that the higher order load-displacement relations are stiffer. That is, elastic contact compliances between angular grains are predicted to be stiffer than those between round grains.

Perhaps, another way to visualize this effect is more readily understood. In figure 17, we now focus on a cross-section of the contact gap between grains. In the case of spherical grains, the gap may be thought of as a flat Mavko and Nur (1979) type crack. Near the contact circumference, the contact gap is very compliant. In contrast when two angular grains meet in contact, the geometry of the

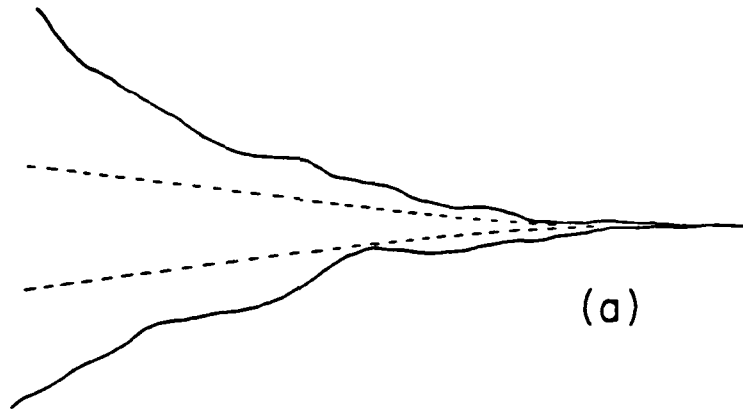


(a)



(b)

Fig. 16. Sketch contrasting the contact between two round grains (a) with that between two angular grains (b).



(a)



(b)

Fig. 17. Sketch contrasting the near-contact gap between two round grains in contact (a) with that between two angular grains in contact (b).

pore is more closely approximated by a Walsh (1965) type spherical or elliptical crack. This configuration is relatively stiff at the contact perimeter.

We have measured V_p and V_s in 149-174 μm , crushed and sieved glass beads as a function of uniaxial pressure. The sample was compacted to a porosity of ~ 0.40 at 0.1 MPa. The results are then compared in figure 18 to those for spherical glass beads. The velocities in the angular grains are consistently 15% higher. The V_p/V_s in the crushed glass is particularly high at 0.1 MPa.

The second effect of angularity on micromechanics is also evident in figure 18. Above 20 MPa, velocities in the crushed grains are nearly independent of pressure. The grains are so sharp; the radius of curvature of the grains, ϵ , at the grain contact is so small that the plasticity criterion in equation (33) has been exceeded. The micromechanics at the contact is plastic because ζ becomes greater than 1 above 15 MPa. At low pressures, V_s is proportional to $p^{1/6}$, while V_p goes as $p^{1/5}$. Apparently, the compaction was sufficient to close most of the near contacts. And at low pressures, the sample seems to behave elastically.

We have also measured V_p and V_s in three, 106-125 μm , quartz sands of differing angularities. The grains in Ottawa sand are round; those in Simplot sand are sub-angular; and Oceanside sand is angular. The results are plotted in figure 19. The porosities vary with pressure from 0.1 to 35 MPa. Those variations in the Ottawa, Simplot, and Oceanside samples are 0.408 to 0.396, 0.412 to 0.398 and 0.415 to 0.397, respectively. We observe virtually no effect of angularity

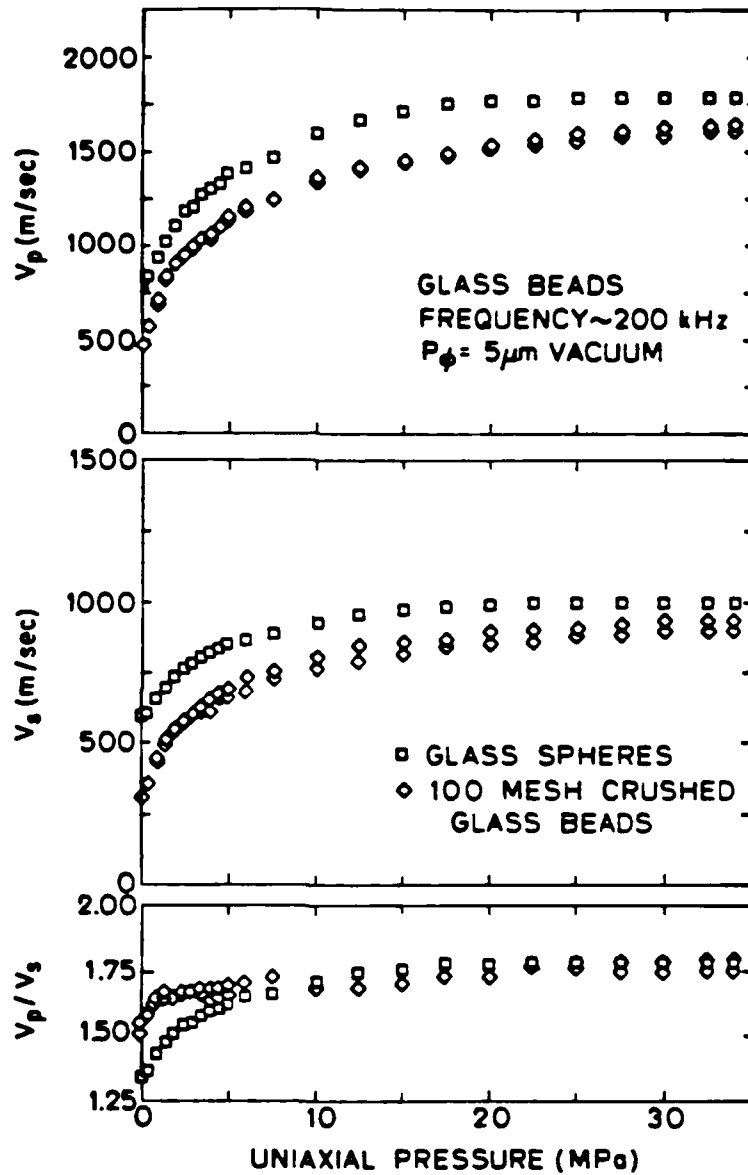


Fig. 18. V_p , V_s , and V_p/V_s vs. uniaxial pressure in 100 mesh crushed and screened glass beads, plotted along with data for spherical glass beads from figure 9.

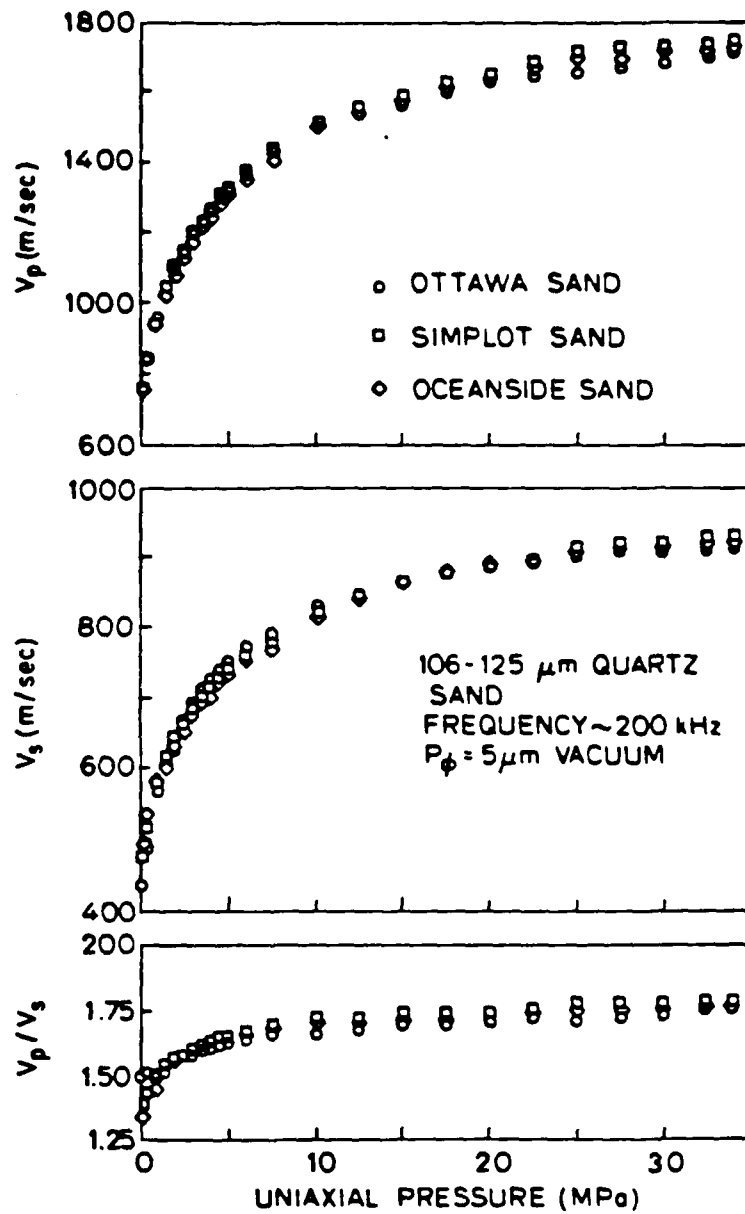


Fig. 19. V_p , V_s , and V_p/V_s vs. uniaxial pressure three vacuum dry sands of differing angularities.

except a relatively pronounced, ~10-15% increase in V_s at very low pressures.

In figure 20, we have replotted the V_p data along with a best fit power law. The expression, $920 p^{1/6}$, is the same as the high pressure fit for the glass beads. The fact that it fits the entire pressure range so well indicates that again compaction had closed most of the near contacts. A better fit is obtained by the combination of $800 p^{1/5}$ and $1000 p^{1/7}$, suggesting that some plastic deformation is occurring at high pressures. The V_s dependence on pressure is very flat, again indicating plasticity.

The third effect of angularity is on the packing, and it is perhaps the most important in natural sediments. Consider an rlp of round grains and another of angular grains as sketched in figure 21. The rlp of round grains may assume a porosity between 0.40 and 0.42; while, the rlp of the angular grains achieves porosities between 0.45 and 0.58 (Brown and Richards, 1966). This result is plotted on a line graph in figure 22. The implications for natural sediments shall be discussed in the next section.

We would also like to suggest that a regular honeycomb of uniform and equant six-point grains would be a good candidate for an ordered packing of angular grains and exact analysis.

10. NATURAL GRAIN SIZE DISTRIBUTIONS AND POROSITY

Up to this point, we have considered packings of grains which have had uniform radii. In this section, we relax this constraint and investigate how natural grain size characteristics affect the frame moduli.

Grain size distributions in natural granular sedimentary materials

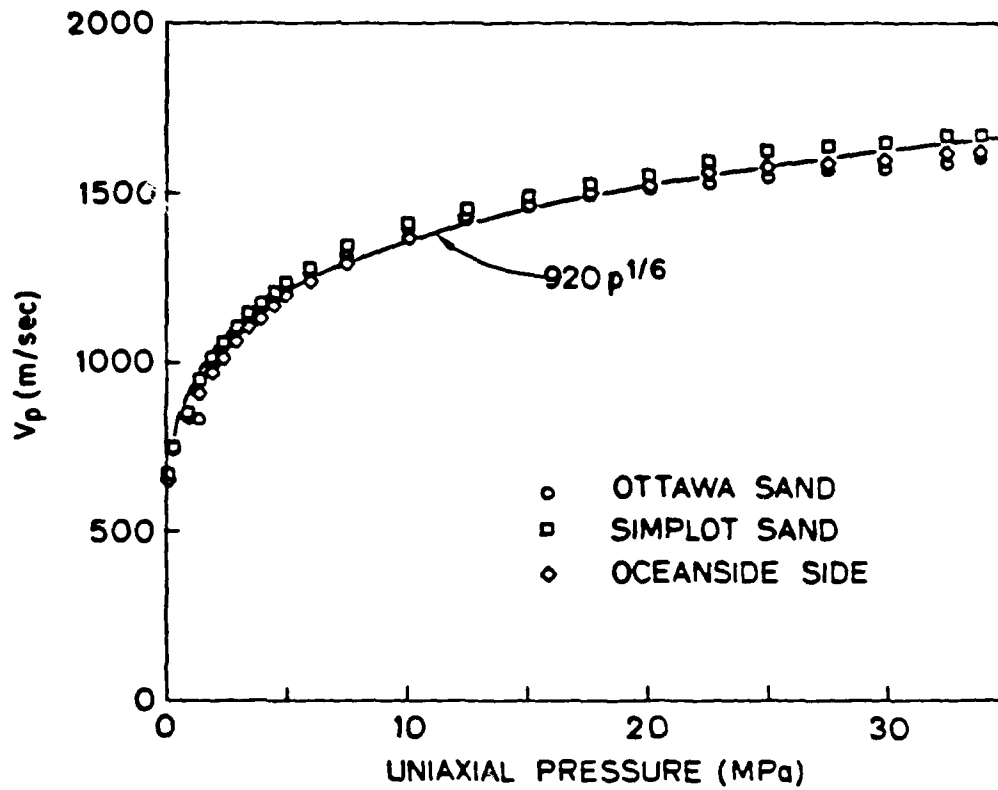
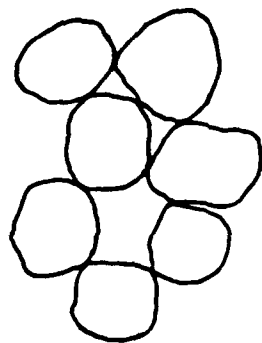


Fig. 20. $920 p^{1/6}$ plotted against the V_p vs. uniaxial pressure data from figure 19.



ROUND



ANGULAR

Fig. 21. Sketch contrasting the random loose packing of round grains with that of angular grains. The packing of angular grains has a higher porosity.

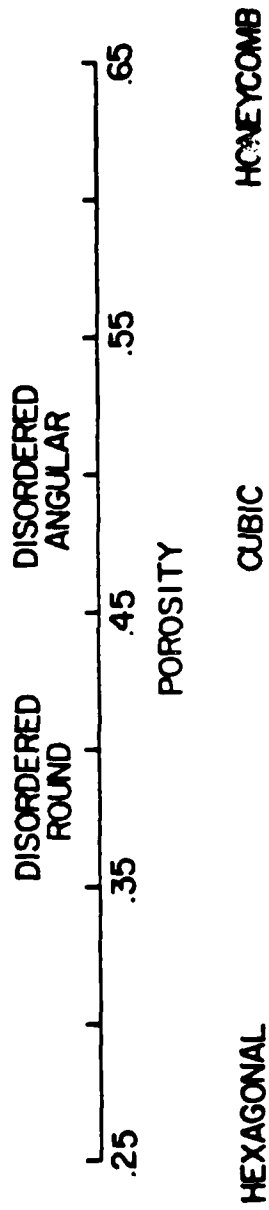


Fig. 22. Porosity for ordered and disordered packings of uniformly sized, yet differently shaped, grains.

are well described as sums of discrete log-normal components (Vischer, 1969). The first moment of the total distribution is the mean, \bar{x} . In phi (negative logarithm to the base 2) units, it is given by

$$\bar{x} = \sum_{i=1}^n f_i x_i \quad (39)$$

where f_i is the frequency in percent for each phi size fraction and x_i is the midpoint of each phi size fraction. The second moment or standard deviation, s , is a measure of the sorting.

$$s = \left(\sum_{i=1}^n f_i (x_i - \bar{x})^2 \right)^{1/2} \quad (40)$$

If the grains are all spherical and surface effects are negligible, porosity declines with a decrease in grain sorting. This is a well-known fact based on the experimental measurements of Westman and Huggill (1930), Furnas (1931), Graton and Fraser (1935), Sohn and Moreland (1968), and Dexter and Tanner (1971). Norman et al. (1971) reached the same conclusion by computer simulation of circle coverings and sphere packs. The mechanism is obvious. The small sphere sizes are able to fill the interstitial pores between the larger grains. If such a model were relevant, the velocities would increase with decreasing sorting because of the increase in the number of contacts per grain.

Grains in natural sediments are not spherical. Indeed, the smaller the grains are, the more angular they become. As grain size diminishes, cleavage, mineralogic habit, and crystallographic properties grow in relative importance. Therefore, implicit in any grain size variation in natural sediments is a change in grain shape.

We have gathered data for porosity in uncompacted sands as a

function of mean grain size and standard deviation from two sources: Pryor (1972) and Beard and Weyl (1973). A map of contours of constant porosity is given in figure 24. Of course, if the grains were all spherical, the contours would be horizontal lines of constant sorting. They are not. Mean grain size controls the porosity in uncompacted sediments with a significant variation due to the sorting (figure 4). Symbolically, we may write that

$$\phi \leftarrow \bar{x} | s \quad (41)$$

where \leftarrow denotes an unspecified function and is read "is determined by".

We have also gathered data on coordination vs. porosity in granular materials. The compilation is plotted in figure 24. It is clear that broadly speaking, coordination number varies logarithmically with $1 - \phi$. Recall that the frame moduli are determined by the grain contact area, and that the contact area is most sensitive to a change in the number of actual contacts per grain, ψ . Thus, we may write that in uncompacted sediments at very shallow effective pressures,

$$V \propto A^{1/2} \leftarrow \psi \leftarrow e^{1-\phi} \quad (42)$$

The proportionality in relation (42) assumes that at very low effective pressures, the limit is well described by our model with an exponential radial distribution function. Relation 43 qualitatively explains the decrease in V_p with porosity in figure 2. The increase in porosity lowers the coordination number. The decline in coordination number reduces the grain contact area causing the frame moduli to soften. Consequently, V_p drops. Relation 42 indicates that a reduction in mean grain size was initially responsible for the entire process.

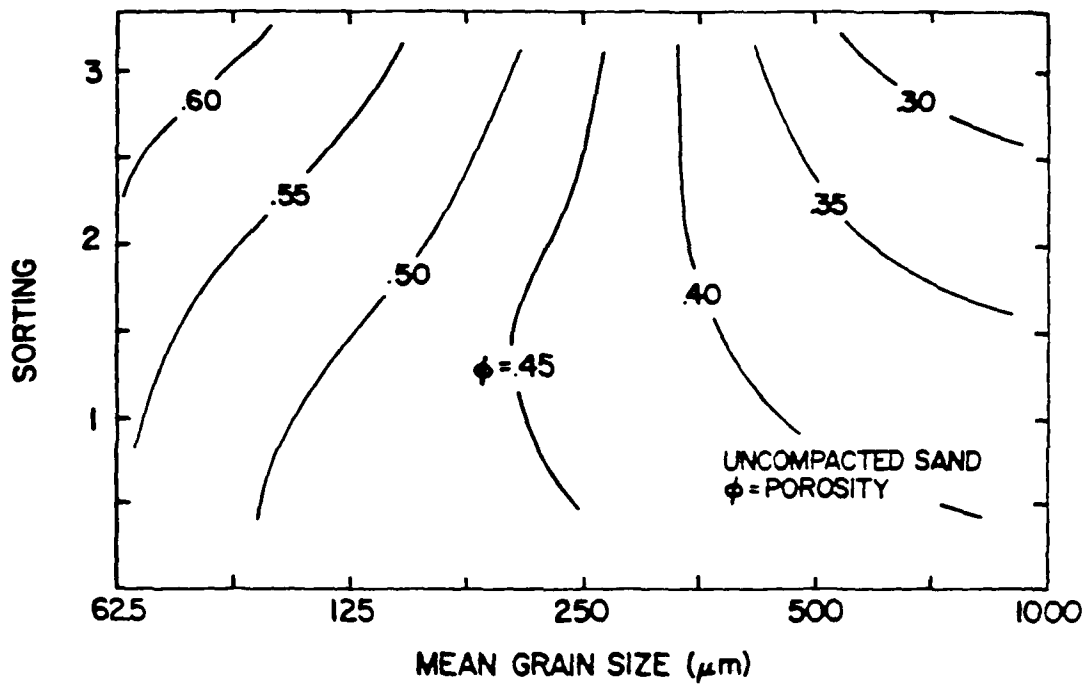


Fig. 23. Porosity as a function of mean grain size and sorting.
 Contours are rough, hand-drawn fits to data from
 Pryor (1972) and Beard and Weyl (1973).

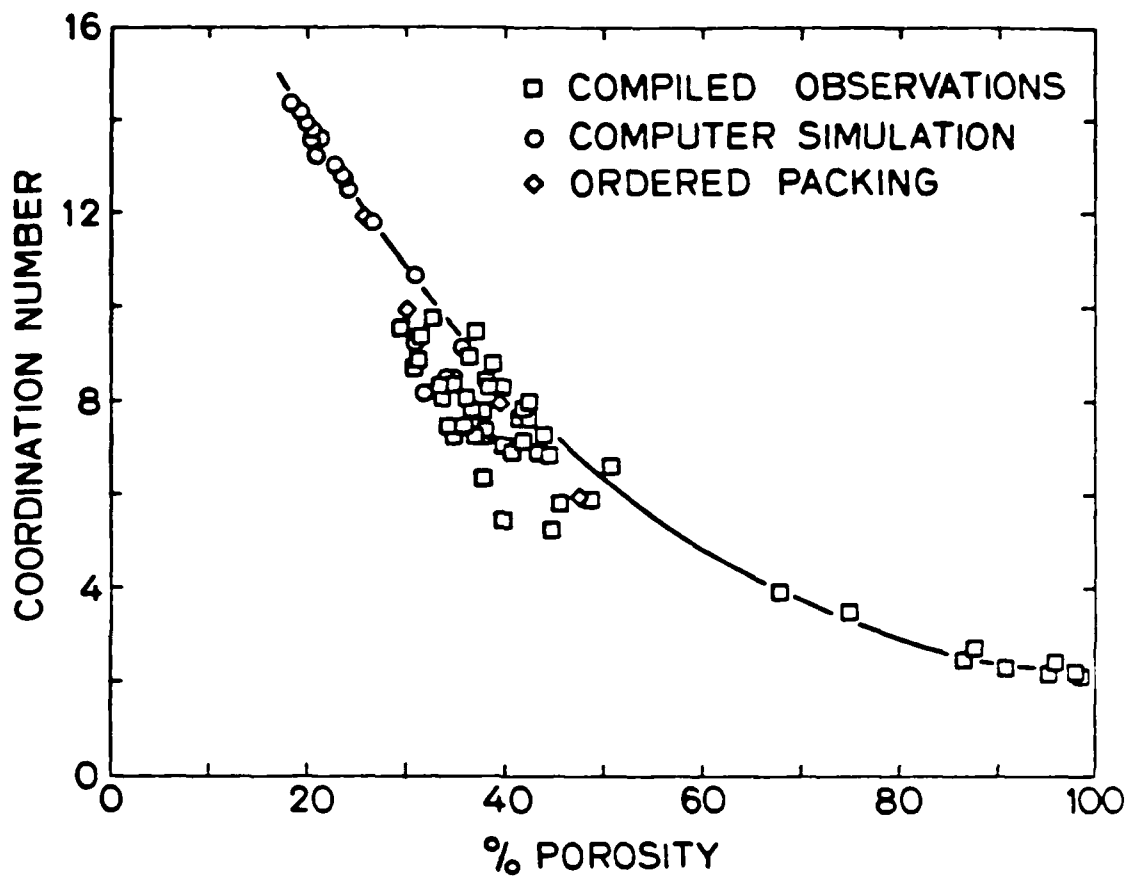


Fig. 24. Coordination number vs. porosity. The computer simulation results for random packing of spheres is from Norman and others (1971). Compiled observations are from Smith et al. (1927), Westman and Hugill (1930), White and Walton (1937), Oda (1977), Meissner et al. (1964), Yanagisawa (1978), and Marsal (1977).

The problem of shear wave velocities in figure 3 may now be resolved. We had sought in compacted sands a micromechanical effect which would significantly distinguish the behavior of the shear frame modulus from that of the bulk frame modulus. The data in figure 2 are considered to be reliable, and the Hamilton (1971, 1974b) and Smith (1974) shear velocity data are problematic. Our experiments have revealed only a small effect due to anularity, -10-15% on V_s . In uncompacted sands, such an effect would be swamped by the effect represented by relation (42). Therefore, without equivocation, we remove the problematic "data" from figure 3, leaving figure 25.

11. VELOCITIES VERSUS DEPTH

Hardin and Richart (1963), Gardner et al. (1964), and Domenico (1977) have measured V_s in compacted sands varying with the 1/4 power of confining pressure. Seed and Idriss (1970), Hardin and Drnevich (1972a), Ohsaki and Iwasaki (1973), and Iwasaki and Tatsuoka (1973), Sherif and Ishibabi (1976), and Yanagisawa (1978) propose empirical equations for in situ sands of the general form

$$\rho V_s = c \cdot \text{fcn}(\phi) \cdot p_c^m \quad (43)$$

where m is constant and close to 1/4. Hamilton (1980) settles on a simple power law for water saturated fine sand, $V_s = 128h^{0.28}$, where h is the depth. He also suggests another similar relationship, $V_s = 104.33h^{0.312}$, as a better fit to the data of Ohta and Goto (1978).

For compressional wave velocity, Hamilton (1978, 1980) proposed $V_p = 1805h^{0.015}$.

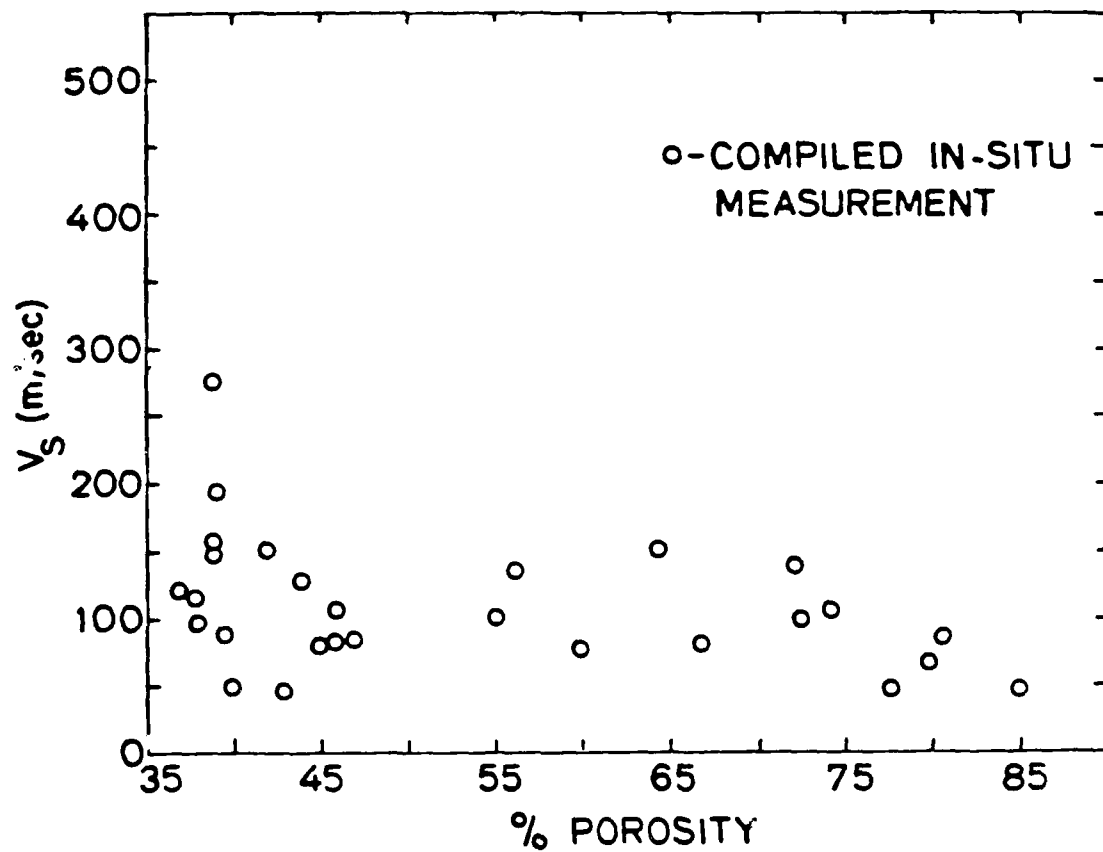


Fig. 25. V_s vs. porosity in in situ sediments.

We have compiled in situ measurements of V_s versus depth in water saturated sands from Barkan (1962), Kudo and Shima (1970), Stokoe and Woods (1972), Stokoe and Richart (1973), Cunny and Fry (1973), Hamilton (1976), Anderson et al. (1978), and Arango et al. (1978). The data are presented in figures 26 and 27.

In figure 26, Hamilton's predictions are plotted against the data. The predictions from our compaction model based on the Gaussian radial distribution function are plotted against the data in figure 27. The three curves presented are for the limiting cases of exponential and random distributions and the "1/4 power" behavior. The wetted shear frame moduli in the respective cases vary as p , $p^{3/5}$, and $p^{1/2}$. We substitute the proportionalities for μ_{WT} in the Biot-Gassman equations (equation 3). Time constraints have as yet precluded quantitative development of the model, and so the coefficients were determined by best fit.

No one curve describes the data accurately. The curve, $75 p^{1/2}$, describes the very shallow, lower velocity data - presumably the most disperse sands - very well. The curve, $160 p^{1/3.3}$, quite accurately describes the upper bound for the higher velocity, very shallow data, as well as most of the data between 50 and 80 m. The curve, $200 p^{1/4}$, satisfactorily describes the data above 80 m. In other words, each curve is successful depending on the state of compaction. Perhaps shear velocity depth profiles rather than just shear velocity may be a useful tool for determining the extent of compact in a granular sediment.

This result strongly suggests that a rigorous development of a compaction model based on a Gaussian distribution function may

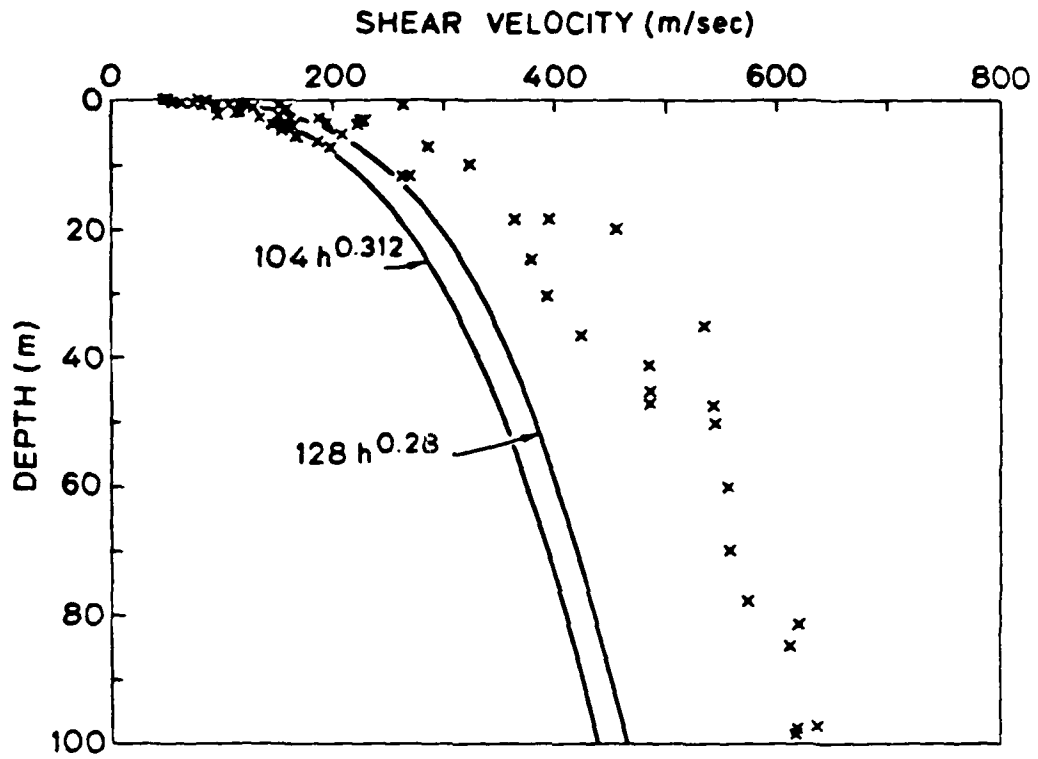


Fig. 26. Hamilton's curves for V_s as a function of depth plotted against compiled in situ data.

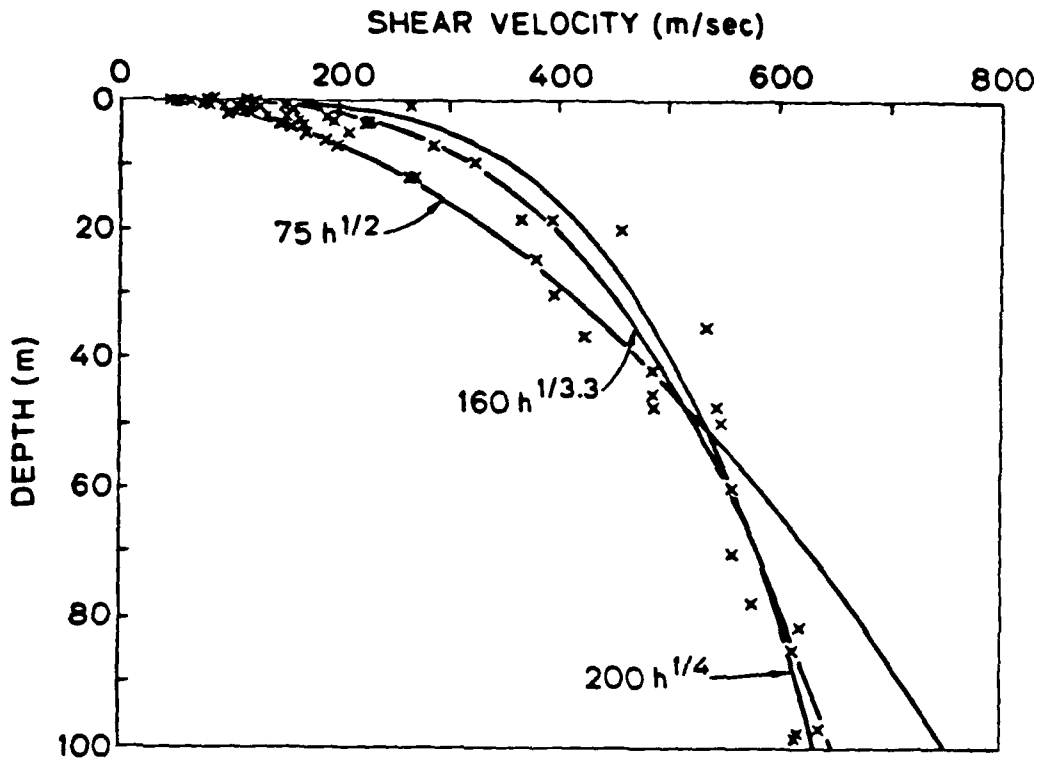


Fig. 27. Three limiting case proportionalities from the compaction model based on a Gaussian radial distribution fit to compiled in situ data.

accurately describe shear velocities in granular sediments.

We expect similar success with V_p . The wetted bulk frame modulus may be similarly determined. Substituting both the bulk and shear proportionalities into the Biot-Gassman equations (equation 2), we can predict the compressional wave dependence on pressure. Unfortunately, we have been unable to gather V_p data for water saturated sands at such shallow depths.

12. CONCLUSIONS

1) Frame moduli in granular sediments are determined by the grain contact area.

2) In the limit of high pressure or strong compaction where the coordination number is independent of pressure, glass beads and quartz sands are well described as a disordered packing of elastic grains in Hertz-Mindlin contact. Velocities vary with a confining pressure to the 1/6 power and contact area to the 2/3 power.

3) Grain contact area in uncompacted materials is dominated by the number of actual contacts per grain. A compaction model is proposed in which the radial distribution of nearest neighbors is Gaussian. The model predicts a strong dependence on the statistics of the packing, and a qualitative evolution of the frame moduli which fits in situ data remarkably well. The high pressure or strong compaction limit is a Hertz-Mindlin material.

4) In vacuum dry materials, adhesion between grain surfaces contracts contacts and significantly increases the area of each contact. Wetting the grains with water eliminates the adhesion. Moduli drop and the material expands measurably. Strain amplitude independence effectively refutes the significance of frictional grain sliding.

5) In uncompacted, disperse, self-loading sediments, velocities vary with the contact area to the $1/2$ power. Contact area is dominated by the actual number of contacts which in turn is logarithmically related to 1 minus the porosity. Thus, compressional and shear wave velocities decrease with increasing porosity.

6) Grain size per se has no effect on frame moduli. However, in natural sediments increased grain angularity accompanies a decrease in mean grain size. Grain angularity in uncompact materials increases the porosity. Therefore, in granular sediments, decreasing grain size generally lowers the frame moduli.

7) Contrarily, grain angularity in compacted materials increase the frame moduli. Grain contacts may be plastic at high pressure.

ACKNOWLEDGEMENTS

Amos Nur is director of the Stanford Rock Physics Program. This paper constitutes the second chapter of a doctoral dissertation. Joel Walls and Peter Gordon were instrumental in the design and construction of the uniaxial pressure vessel. Mary Kovacs sieved sand with remarkable patience, persistence, and good humor. George Parks lead me to the surface chemistry literature. This research was supported by the Office of Naval Research under contract N00014-77-C-0390 with the Marine Geology and Geophysics Program.

WORKS CITED

- Anderson, A.L., and L.D. Hampton, Acoustics of gas bearing sediments, I. Background, J. Acoust. Soc. Am. 67, 1865-1889 (1980).
- Anderson, A.L., and L.D. Hampton, Acoustics of gas bearing sediments, II. Measurements and models, J. Acoust. Soc. Am. 67, 1890-1903 (1980).
- Anderson, D.G., C. Espana, and V.R. Lamore, Estimating in situ shear moduli at competent sites, Proc. Eq. Engr. Soil. Dyn. 1, 181-197 (1978).
- Aronson, M.P. and H.M. Princen, Aqueous films on silica in the presence of cationic surfactants, Colloid Polym. Sci. 256, 140-149, 1978.
- Bea, R.G., Engineering fixed offshore platforms to resist earthquakes, Proc. Eq. Eng. Soil Dyn. III, 1357-1385 (1978).
- Beard, D.C., and P.K. Weyl, Influence of texture on porosity and permeability of unconsolidated sand, Bull. AAGP 57, 349-369 (1973).
- Bernal, J.D. and J. Mason, Coordination of randomly packed spheres, Nature 188, 910-911 (1960).
- Biot, M.A., Theory of propagation of elastic waves in a fluid-saturated porous solid, I. Low frequency range, J. Acoust. Soc. Am. 28, 168-178 (1956).
- Biot, M.A., Theory of propagation of elastic waves in a fluid saturated porous solid, II. High frequency range, J. Acoust. Soc. Am. 28, 179-191 (1956),
- Brandt, H., A study of the speed of sound in a porous granular media, J. Appl. Mech. ASME 22, 497-486 (1955).
- Brandt, H., Factors affecting compressional wave velocity in unconsolidated marine sediments, J. Acoust. Soc. Am. 32, 171-179 (1960).
- Brown, R.J.S., and J. Korringa, On the dependence of the elastic properties of a porous rock on the compressibility of the pore fluid, Geophys. 40, 608-616 (1975).
- Brown, R.L. and J.C. Richards, Principles of Power Mechanics, Chapt. 2, 13-39, Pergamon, Oxford (1966).
- Brunauer, S., D.L. Kantro, and C.H. Weise, The surface energies of amorphous silica and hydrous amorphous silica, Can. J. Chem. 34, 1483-1496 (1956).

- Cataphote Division-Ferro Corporation, World's largest catalog of small glass beads: microscopic glass beads for industrial, scientific, optical, and reflective purposes, Jackson, Miss. (1977)
- Cattaneo, C., Teoria del contatto elastico in seconda approssimazione, *Rc. Mat. Applic.* 6, 504-512 (1947).
- Christensen, R.E., J.A. Frank, and W.H. Geddes, Low-frequency propagation via shallow refracted paths through deep ocean unconsolidated sediments, *J. Acoust. Soc. Am.* 57, 1421-1426 (1975).
- Clark, V.A., B.R. Tittmann, and T.W. Spencer, Effects of volatiles on attenuation (Q^{-1}) and velocity in sedimentary rocks, *J. Geophys. Res.* 35, 5190-5198 (1980).
- Deresiewicz, H. Stress-strain relations for a simple model of a granular medium, *J. Appl. Mech. ASME* 25, 402-405 (1958).
- Deresiewicz, H., A note on second-order Hertz contact, *J. Appl. Mech. ASME* 28, 141-142 (1961).
- Dexter, A.R. and D.W. Tanner, Packing density of ternary mixtures of spheres, *Nature* 230, 177-179 (1971).
- Digby, P.J., The effective elastic moduli of porous granular rocks, *J. Appl. Mech. ASME* 48, 803-808 (1982).
- Domenico, S.N., Elastic properties of unconsolidated porous sand reservoirs, *Geophys.* 42, 1339-1368 (1977).
- Duffy, J., A differential stress-strain relation for the hexagonal close-packed array of elastic spheres, *J. Appl. Mech. ASME* 26, 251-258 (1959).
- Duffy, J. and R.D. Mindlin, Stress-strain relations of a granular medium, *J. Appl. Mech. ASME* 24, 585-593 (1957).
- Edil, T.B. and G.F. Luh, Dynamic modulus and damping relationships for sands, *Proc. Eq. Eng. Soil Dyn. I*, 394-409 (1978).
- Elliott, S.E. and B.F. Wiley, Compressional velocities of partially saturated unconsolidated sands, *Geophys.* 40, 949-954 (1975).
- Fryer, G.J., Compressional-shear wave coupling induced by velocity gradients in marine sediments, *J. Acoust. Soc. Am.* 69, 647-660 (1981).
- Fuller, K.N.G. and D. Tabor, The effect of surface roughness on the adhesion of elastic solids, *Proc. Roy. Soc. A* 345, 327-342 (1975).
- Furnas, C.C., Mathematical relations for beds of broken solids of maximum density, *Indust. Eng. Chem.* 23, 1052-1058 (1931).

- Galin, L.A., Contact Problems in the Theory of Elasticity (English trans.), Appl. Math. Res. Group, North Carolina State, 233 pp. (1961).
- Gangi, A.F., Pressure dependence of the velocity of lunar soil: the velocity/depth variation in the shallow lunar crust, J. Geophys. Res. 86, 9562-9566 (1981).
- Gardner, G.H.F., M.R.F. Gardner, and D.M. Droshak, Effects of pore pressure and saturation on the attenuation of elastic waves in sand, J. Petr. Tech. 16, 189-198 (1964).
- Gassman, F. Ueber die elastizitat poroser median, Vierteljahrsschr. Naturforsch. Ges. Zuerich, Heft I, (1951a).
- Gassman, F., Elastic waves through a packing of spheres, Geophys. 16, 673-685 (1951b).
- Geertsma, J., and D.C. Smit, Some aspects of wave propagation in fluid saturated porous solids, Geophys. 26, 169-181 (1961).
- Goodman, L.E. and L.M. Keer, The contact stress problem for an elastic sphere indenting an elastic cavity, Int. J. Solids Struct. 1, 407-415 (1965).
- Graton, L.C. and H.J. Fraser, Systematic packing of spheres - with particular relation to porosity and permeability, J. Geol. 43, 785-909 (1935).
- Greenwood, J.A. and J.B.P. Williamson, Contact of nominally flat surfaces, Proc. Roy. Soc. A. 97, 300-316 (1966).
- Greenwood, J.A. and J.H. Tripp, The elastic contact of rough spheres, J. Appl. Mech. ASME 89, 153-159 (1967).
- Hamilton, E.L., Sound velocity and related properties of marine sediments, J. Geophys. Res. 75, 4423-4446 (1970).
- Hamilton, E.L., Elastic properties of marine sediments, J. Geophys. Res. 76, 579-604 (1971).
- Hamilton, E.L., Geoacoustic models of the seafloor, in Proc. Symp. Phys. Sound in Mar. Sed. (L.D. Hampton, ed.), 181-221 (1974a)
- Hamilton, E.L., Prediction of deep-sea sediment properties: state-of-the-art, in Proc. Symp. Phys. Engr. Prop. Deep-Sea Sed., (A.L. Inderbitzen, ed.) 1-43 (1974b).
- Hamilton, E.L., Shear-wave velocity versus depth in marine sediments: a review, Geophys. 37, 520-646 (1976a).

- Hamilton, E.L., Variations of density and porosity with depth in deep sea sediments, *J. Sed. Pet.* 46, 28-300 (1976b).
- Hamilton, E.L., Sound velocity-density relations in sea-floor sediments and rocks, *J. Acoust. Soc. Am.* 63, 366-377 (1978).
- Hamilton, E.L., Sound velocity gradients in marine sediments, *J. Acoust. Soc. Am.* 65, 909-922 (1979a).
- Hamilton, E.L., V_p/V_s and Poisson's ratios in marine sediments and rock, *J. Acoust. Soc. Am.* 66, 1093-1101 (1979b).
- Hamilton, E.L., Geoacoustic modeling of the sea floor, *J. Acoust. Soc. Am.* 68, 1313-1340 (1980a).
- Hamilton, E.L., Compressional and shear wave gradients in marine sediments, *J. Acoust. Soc. Am.* 64, Suppl. 1, S141 (abstract) (1980b).
- Hara, G., Theorie der akustischen Schwingungsausbreitung in gekörnten Substanzen und experimentelle Untersuchungen an Kohlepulver, *Elektrische Nachr. Techn.* 12, 191-200 (1935).
- Hardin, B.O., The nature of stress-strain behavior for soils, *Proc. Eq. Engr. Soil Dyn.* I, 3-90 (1978).
- Hardin, B.O. and V.P. Drnevich, Shear modulus and damping in soils, measurements and parameter effects, *J. Soil. Mech. Fdn. Div. ASCE* 98, 603-624 (1972a).
- Hardin, B.O., and V.P. Drnevich, Shear modulus and damping in soils: design equations and curves, *J. Soil Mech. Fdn. Div. ASCE* 98, 667-692 (1972b).
- Hardin, B.O., and F.E. Richart, Elastic wave velocities in granular soils, *J. Soil Mech. Fdn. Div. ASCE* 89, 33-65 (1963).
- Iida, K., The velocity of elastic waves in sand, *Bull. Eq. Res. Inst., Tokyo Univ.* 27, 131-144 (1938).
- Iida, K., Velocity of elastic waves in a granular substance, *Bull. Eq. Res. Inst., Tokyo Univ.* 17, 783-808 (1939).
- Israelachivili, J.N. and G.E. Adams, Measurement of forces between two mica surfaces in aqueous electrolyte solutions in the range 0 to 100 nm, *J. Chem. Soc., Faraday Trans. I*, 74, 975-1001 (1980).
- Israelachivili, J.N. and D. Tabor, Van der Waals forces: Theory and experiment, in Progress in Surface and Membrane Science (J.F. Danielli, M.D. Rosenberg, and D.A. Cadenhead, eds.), v. 7, 1-55, Academic Press, N.Y. (1973).

- Iwasaki, T., and F. Tatsuoka, Dynamic soil properties with emphasis on comparison of laboratory tests and field measurements, Proc. Fifth Conf. Eq. Eng. 1, 2303-2308 (1973).
- Johnson, D.L., Equivalence between fourth sound in liquid He II at low temperatures and the Biot slow wave in consolidated porous media, Appl. Phys. Lett. 37, 1065-1067 (1981).
- Johnson, D.L. and P. Sen, The multiple scattering of acoustic waves with application to the index of refraction of 4th sound, Phys. Rev. B, 24, 2486-2496 (1981).
- Johnson, D.M., A.L. Frisillo, J. Dorman, G.V. Latham and D. Strangway, Compressional wave velocities of a lunar regolith sample in a simulated lunar environment, J. Geophys. Res. 87, 1899-1902 (1982).
- Johnson, K.L., Surface interaction between elastically loaded bodies under tangential forces, Proc. Roy. Soc. A. 230, 531-549 (1955).
- Johnson, K.L., K. Kendall, and A.D. Roberts, Surface energy and the contact of elastic solids, Proc. Roy. Soc. A. 324, 301-313 (1971).
- Kudo, K., and E. Shima, Attenuation of shear waves in soil, Bull. Eq. Res. Inst., Univ. Tokyo, 48, 145-159 (1970).
- Lunberg, G. Elastische Berührung zweier Halbraume, Forsch. Geb. Ingenieurw. 10, 201-211 (1939).
- Marsal, R., Mechanical properties of rockfill, in Embankment - Dam Engineering, 109-208, Wiley, N.Y. (1973).
- Mavko, G.M. and A. Nur, The effect of non-elliptical cracks on the compressibility of rocks, J. Geophys. Res. 83, 4459-4468 (1978).
- McFarlane, J.S. and D. Tabor, Adhesion of solids and the effect of surface films, Proc. Roy. Soc. A. 202, 224-243 (1950).
- Meissner, H.P., A.S. Michaels and R. Kaiser, Crushing strength of zinc oxide agglomerates, I. and E.C. Design Develop. 3, 202-205 (1964).
- Mindlin, R.D., Compliance of elastic bodies in contact, J. Appl. Mech. ASME 16, 259-268 (1949).
- Mindlin, R.D. and H. Deresiewicz, Elastic spheres in contact under varying oblique forces, J. Appl. Mech. ASME 20, 327-344 (1953).

- Mindlin, R.D., W.P. Mason, T.F. Osmer and H. Deresiewicz, Effects of an oscillating tangential force on the contact surfaces of elastic spheres, Proc. First Nat. Cong. Appl. Mech., 203-208 (1956).
- Morse, P.M. and K.V. Ingard, Theoretical Acoustics, McGraw-Hill, N.Y. 927 pp. (1968).
- Murphy, W.F., Effects of partial water saturation on attenuation in Massillon sandstone and Vycor porous glass, J. Acoust. Soc. Am. 71, 6 (in press) (1982a). Also Chapt. III in this volume.
- Murphy, W.F. and A. Nur, On velocities and attenuation as a measure of partial gas saturation on tight sandstones at borehole and ultrasonic frequencies, Geophys. (subm. in July) (1982a). Also Chapt. IV in this volume.
- Murphy, W., and A. Nur, On the acoustic properties of the shallow lunar crust, J. Geophys. Res. (in preparation) (1982b).
- Norman, L.D., and other, Computer simulation of particular systems, U.S. Bureau of Mines Bull. 658, 55p. (1971).
- Oda, M. Co-ordination number and its relation to shear strength of granular material, Sols Fdn. 17, 29-42 (1977).
- Oda, M., J. Konishi, and S. Nemat-Nasser, Some experimentally based fundamental results on the mechanical behavior of granular materials, Geotechnique 30, 479-495 (1980).
- Ohsaki, V. and R. Iwasaki, On dynamic shear moduli and Poisson's ratio of soil deposits, Soils Fdn. 13, 61-73 (1973).
- Ohta, V. and N. Goto, Empirical shear wave velocity equations in terms of characteristic soil indexes, Eq. Engr. Struct. Dyn. 6, 167-187 (1978).
- Pillbeam, C.C. and J.R. Vaisnys, Acoustic velocities and energy losses in granular aggregates, J. Geophys. Res. 78, 810-824 (1973).
- Potters Industries, Inc., Technical quality solid glass spheres for industrial and scientific applications, Hasbrouck Heights, N.J. (1980).
- Pandit, B.I. and M.S. King, The variation of elastic wave velocities and quality factor Q of a sandstone with moisture content, Canad. J. Earth Sci. 16, 2187-2195 (1979).
- Pashley, R.M. and J.N. Israelachvili, A comparison of surface forces and interfacial properties of mica in purified surfactant solutions, Colloid. Surf. 2, 169-187 (1981).

- Pryor, W.A., Reservoir inhomogeneities of some recent sand bodies, Soc. Pet. Eng. J. 253, 229-245 (1972).
- Sherif, M.A. and I. Ishibashi, Dynamic shear moduli for dry sands, J. Geotech. Div. ASCE 102, 1171-1184 (1976).
- Seed, H.B. and I.M. Idriss, Soil moduli and damping factors for dynamic response analyses. EERC 70-10, Eq. Engr. Res. Center, U.C., Berkeley (1970).
- Smith, D.T., Acoustic and mechanical loading of marine sediments, in Proc. Symp. Phys. Sound Mar. Sed. (L.D. Hampton, ed.), 41-61 (1974).
- Smith, W.O., P.D. Foote, and P.F. Busang, Packing of homogeneous spheres, Phys. Rev. 34, 1271-1274 (1927).
- Sohn, H.Y., and C. Moreland, The effect of particle size distribution on packing density, Can. J. Chem. Eng. 46, 162-167 (1968).
- Sonntag, H., and K. Strenge, Coagulation and Stability of Disperse Systems, Wiley, NY, 139 pp. (1970).
- Spencer, J.W., Stress relaxations at low frequencies in fluid-saturated rocks: attenuation and modulus dispersion, J. Geophys. Res. 86, 1803-1812 (1981).
- Steurmann, E., On Hertz's theory of local deformations in compressed elastic bodies, C.R. Acad. Sci. URSS 25, 359-361 (1941).
- Steurmann, E., On the question of local deformations in elastic bodies pressed against one another, C.R. Acad. Sci. URSS 31, 738-741 (1941).
- Steurmann, E., Some special cases of the contact problem, C.R. Acad. Sci. URSS 38, 197-200 (1943).
- Stokoe, K.H., D.G. Anderson, R.J. Hoar, and W.H. Isenhower, Discussion of in situ and laboratory shear velocity and modulus, Proc. Eq. Eng. Soil Dyn. III, 1498-1502 (1978).
- Stokoe, K.H., and F.E. Richart, Shear modulus of soils: in situ and laboratory measurements, Proc. Fifth World Cong. Eq. Engr. 1, 356-359 (1973).
- Stoll, R.D., Experimental studies of attenuation in sediments, J. Acoust. Soc. Am. 66, 1152-1160 (1979).
- Stoll, R.D., Theoretical aspects of sound transmission in sediments, J. Acoust. Soc. Am. 68, 1341-1350 (1980).

- Talwani, P., A. Nur and R.L. Kovach, Compressional and shear wave velocities in granular materials to 2.5 kilobars, *J. Geophys. Res.* 78, 6899-6909 (1973).
- Telford, W.M., L. P. Geldart, R.E. Sheriff, and D.A. Keys, Applied Geophysics, Cambridge Univ., 860 pp. (1976).
- Timoshenko, S. and J.N. Goodier, Theory of Elasticity, McGraw-Hill, N.Y., 372 pp. (1951).
- Tittmann, B.R., M. Abdel-Gawad, and R.M. Housely, Elastic velocity and Q factor measurements on Apollo 12, 14, and 15 rocks, *Proc. Lunar Sci. Conf.* 3, 2565 (1972).
- Tittmann, B.R., L. Alberg, and J. Curnow, Internal friction and velocity measurements, *Proc. Lunar Sci. Conf.* 7, 3123-3132 (1976).
- Tittmann, B.R., L. Alberg, H. Nadler, J. Curnow, T. Smith, and E.R. Cohen, Internal friction quality-factor Q under confining pressure, *Proc. Lunar Sci. Conf.* 8, 1209-1224 (1977).
- Tittmann, B.R., H. Nadler, J.M. Richardson, and L. Ahlberg, Laboratory measurements of P-wave seismic Q on lunar and analog rocks, *Proc. Lunar Sci. Conf.* 9, 3627-3637 (1978).
- Tittmann, B.R., H. Nadler, V. Clark and L. Coombe, Seismic Q and velocity at depth, *Proc. Lunar Sci. Conf.* 10, 2131-2147 (1979).
- Van Voorhis, J.J., R.G. Craig, and F.E. Bartell, Free energy of immersion of compressed powders with different liquids, II. Silica powder, *J. Phys. Chem.* 61, 1513-1519 (1957).
- Verwey, E.J.W., and J. Th. G. Overbeek, Theory of the stability of lyophobic colloids, Elsevier, Amsterdam (1948).
- Vischer, G.S., Grain size distributions and depositional processes, *J. Sed. Pet.* 39, 1074-1106 (1969).
- Walsh, J.W., The effects of cracks on the compressibility of rocks, *J. Geophys. Res.* 70, 381-389 (1965).
- Walton, K., The effective elastic moduli of model sediments, *Geophys. J. R. Astr. Soc.* 43, 293-306 (1975).
- Warren, N., O.L. Anderson, and N. Saga, Applications to lunar geophysical models of the velocity-density properties of lunar rocks, glasses, and artificial lunar glasses, *Proc. Lunar Sci. Conf.* 3, 2587-2598 (1972).
- Warrick, R.E., Seismic investigation of San Francisco Bay mud site, *Bull. SSA* 64, 375-385 (1974).

- Watt, J.P., The elastic properties of composite materials, Rev. Geophys. Space Phys. 14, 541-563 (1976).
- Westman, A.E.R., and Hugill, H.R., The packing of particles, J. Am. Ceramic Soc. 13, 767-779 (1930).
- White, H.E., and S.F. Walton, Particle packing and particle shape, J. Am. Ceramic Soc. 20, 155-166 (1937).
- White, J.E., Seismic Waves: Radiation, Transmission and Attenuation, McGraw-Hill, N.Y., 302 pp. (1965).
- Wilson, R.C., R.E. Warrick, and M.J. Bennett, Seismic velocities of San Francisco Bayshore sediments, Proc. Eq. Eng. Soil Dyn. II, 1007-1023 (1978).
- Woods, R.D., Measurement of dynamic soil properties, Proc. Eq. Engr. Soil Dyn. I, 91-178 (1978).
- Wyllie, M.R.J., A.R. Gregory, and L.W. Gardner, Elastic wave velocities in heterogeneous and porous media, Geophys. 21, 41-70 (1956).
- Wyllie, M.R.L., A.R. Gregory, and G.H.F. Gardner, Elastic wave velocities in heterogeneous and porous media, Geophys. 21, 41-70 (1958).
- Yanagisawa, E., Relation between the dynamic shear modulus and void ratio in granular media, in Proc. Cont. Mech. Stat. Approaches Mech. Granular Mat., (S.C. Cowin and M. Satake, eds.), 64-70 (1978).

ADDITIONAL REFERENCES

- Abramowitz, M., and I.A. Stegun, Handbook of Mathematical Functions, Dover, NY, 1046 pp. (1965).
- Beran, M.J., Statistical Continuum Theories, Wiley, N.Y., 424 pp. (1968).
- Beresford, R.H., Statistical geometry of random heaps of equal hard spheres, Nature 224, 550-553 (1969).
- Bjerrun, L., Geotechnical problems involved in the foundations of structures in the North Sea, Geotechnique 23, 319-358 (1973).
- Brown, C.B., The use of maximum entropy in the characterization of granular media, in Proc. Cont. Mech. Stat. Approaches Mech. Granular Mat. (S.C. Cowin and M. Satake, eds.), 98-109, (1978).

- Burns, G., and A.M. Glazer, Space Groups for Solid State Scientists, Academic, N.Y. 278 pp. (1978).
- de Pater, A.D., and J.J. Kalker (eds.) The Mechanics of Contact Between Deformable Bodies, Delft Univ., 414 pp. (1975).
- Deresiewicz, H., Mechanics of granular matter, *Adv. Appl. Mech.* 5, 233-306 (1958).
- Deresiewicz, H., Bodies in contact with applications to granular media, in R.D. Mindlin and Applied Mechanics (G. Hermann, ed.), Pergamon, N.Y., 105-143 (1974).
- Gardner, G.H.F., and M.H. Harris, Velocity and attenuation of elastic waves in sands, *Trans. Ninth Ann. Log. Symp.* M1-M19 (1968).
- Gray, W.A., The Packing of Solid Particles, Chapman and Hall, Lond., 134 p. (1968).
- Hashim, Z., Theory of composite materials, *Proc. Fifth Symp. Naval Struct. Mech.*, 201-242 (1970).
- Iwasaki, T., F. Tatsucka, and V. Takagi, Shear modulus of sands under cyclic torsional shear loading, *J. Japan Soc. Soil Mech. Fdn. Eng.* 17, 19-35 (1977).
- Jaynes, E.T., Information theory and statistical mechanics, *Phys. Rev.* 106, 620-630 (1957).
- Kendall, K., Sticky solids, *Contemp. Phys.* 21, 277-297 (1980).
- Krinsely, D.H. and J.C. Doornkamp, Atlas of Quartz Sand Surface Textures, Cambridge Univ., 91 pp. (1973).
- Kroner, E., Statistical Continuum Theories, ICMS 92, Springer-Verlag, 157 pp. (1971).
- Ladd, R.S., Specimen preparation and the liquefaction of sands, *J. Geotechn. Eng. Div. ASCE* 100, 1180-1184 (1974).
- Ludwig, W.J., J.E. Nafe and C.L. Drake, Seismic refraction, in The Sea 4, (A.E. Maxwell, ed.), 53-84 (1970).
- McCoy, J.J., Macroscopic response of continua with random microstructures, *Mech. Today* 6, 1-40 (1981).
- Mindlin, R.D., Microstructure in linear elasticity, *Arch. Rat. Mech. Anal.* 16, 51-78 (1964).
- Naar, J. and R.J. Wyal, Structures and properties of unconsolidated aggregates, *Canad. J. Phys.* 40, 818-831 (1962).

- Nafe, J.E. and C.L. Drake, Physical properties of marine sediments, in The Sea 3, (M.N. Hill, ed.), Wiley, N.Y., 794-815 (1963).
- Paterson, N.R., Seismic wave propagation in porous granular media, Geophys. 21, 691-714 (1956).
- Pyke, R., Discussion of measurement of dynamic soil properties, Proc. Eq. Eng. Soil Dyn. III, 1474-1477 (1978).
- Richart, F.E., D.G. Anderson and K.H. Stokoe, Predicting in situ strain-dependent shear moduli of soil, Proc. Sixth World Cong. Eq. Eng. 6, 159-164 (1977).
- Richart, F.E., J.R. Hall, and R.D. Woods, Vibration of Soils and Foundations, Prentice-Hall, Englewood Cliffs, 414 pp. (1970).
- Shirely, D.J., and L.D. Hampton, Shear-wave measurements in laboratory sediments, J. Acoust. Soc. Am. 63, 607-613 (1978).
- Shumway, G., Sound speed and absorption studies of marine sediments by a resonance method, Part I, Geophys. 25, 451-467 (1960). Part II, Geophys. 25, 659-682 (1960).
- Spence, D.A., Self similar solutions to adhesive contact problems with incremental loading, Proc. Roy. Soc. A. 305, 55-80 (1968).
- Spence, D.A., A Wiener-Hopf equation arising in elastic contact problems, Proc. Roy. Soc. A. 305, 81-92 (1968).
- Truell, R. C. Elbaum and B.B. Chick, Ultrasonic methods in solid-state physics, Academic, N.Y., 464 pp. (1969).
- Vaisnys, J.R. and C.C. Pilbeam, Mechanical properties of granular media, Ann. Rev. Earth Sci. 3, 345-360 (1975).
- Vermeulen, P.J. and K.L. Johnson, Contact of non-spherical elastic bodies transmitting tangential forces, J. Appl. Mech. ASME 31, 338-340 (1964).
- Winkelmolen, A.M., Critical remarks on grain parameters, with special emphasis on shape, Sedimentology 29, 255-266 (1982).

Micromechanics of Acoustic Dissipation in
Fully and Partially Water Saturated,
Granular Sedimentary Materials*

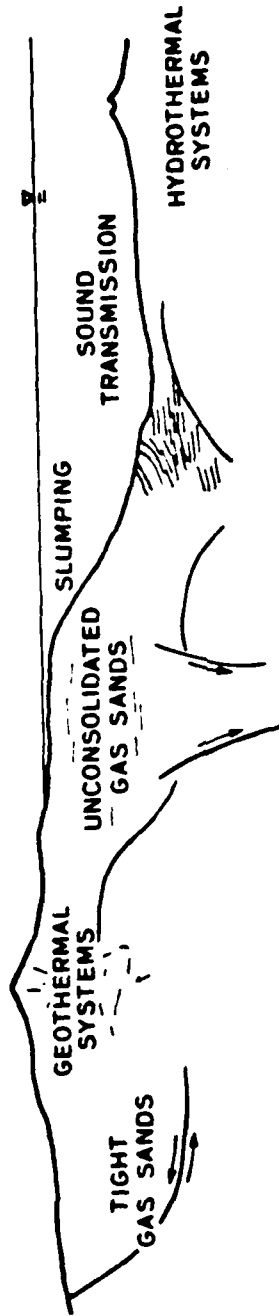
Contents

1. Introduction	209
2. Review of Previously Proposed Mechanisms in Light of Recent Experimental Observations	213
3. Concept of the Model	218
4. Surface Electrochemistry	221
Structure of the Electrical Double Layer	
Surface Energy and Contact Compliance	
Constant Q Energy Loss	
5. Microhydrodynamics	227
Boundary Layer Development	
Squeeze Film Hydrodynamics and Zener Relaxation	
Propagation and Flow in a Compact Pore Neighborhood	
6. General Equations for Acoustic Propagation in Porous Media	241
7. Discussion	246

1. INTRODUCTION

The response to small stress waves is the principle measure used in geophysics to study material bodies in the earth's crust. The class of granular sedimentary materials, which includes sands and sandstones, holds considerable interest in geology and engineering (fig. 1). Several particular problems in the acoustic properties of

*Parts to be submitted to the Journal of Geophysical Research and Journal of the Acoustical Society of America in July or August, 1982.



- 1. MARINE ACOUSTICS
- 2. SEISMIC EXPLORATION
- 3. GEOTECHNICAL PREDICTION
- 4. RESERVOIR ENGINEERING

Fig. 1. Practical applications of geoaoustics.

these materials have been solved recently (Winkler et al., 1979; Spencer, 1981; Murphy, 1982a,b; Murphy and Nur, 1982a). This paper attempts to explain how the granular microstructure and pore water saturation control wave attenuation and velocity dispersion. We are primarily interested in frequency range from 10 to 10^6 Hz.

Our experiments (Murphy, 1982a; Murphy and Nur, 1982a) have shown that in the acoustic frequency range (fig. 2), compressional and shear wave velocities and specific attenuation are strongly dependent on water saturation and frequency. Maurice Biot (1956) has proposed a theory for acoustic wave propagation which has been experimentally corroborated in *simple* porous media such as sintered glass beads (Plona, 1980; Plona and Johnson, 1980). Yet Biot's theory is inconsistent with our observations on sands and sandstones in the acoustic and low ultrasonic frequency ranges. Biot's theory fails because it neglects the *granular* nature of the sedimentary materials.

I wish to propose a model which relates the micromechanics at the grain contacts to linear viscoelastic frame moduli. The frame moduli describe the continuum stiffness and relaxation of the granular frame, and are strongly dependent on frequency and water saturation. When we embed the micromechanical model in general equations for wave propagation in porous media (Biot, 1962; Burridge and Keller, 1981), specific predictions are derived. The predictions test very well against our recent experimental results. Moreover, the theory provides a coherent explanation of the seemingly disparate work of Gregory (1976), Winkler et al. (1979), Pandit and King (1979), Stoll (1979), Plona (1980), Clark et al. (1980), Spencer (1981), Winkler and Nur (1982), and Winkler and Plona (1982).

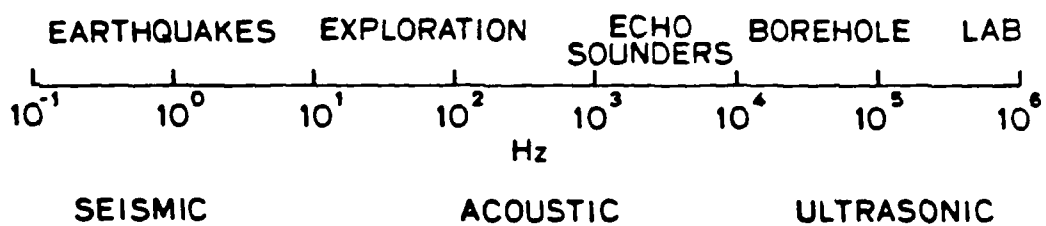


Fig. 2. Spectrum of geoaoustic interest.

The model is by no means fully developed. However, I think that we have laid much of the foundation and correctly identified the specific microprocesses involved.

2. REVIEW OF PREVIOUSLY PROPOSED MECHANISMS IN LIGHT OF RECENT EXPERIMENTAL OBSERVATIONS

Sharp relaxations centered roughly between 1 and 10 kHz (fig. 3) are observed in sandstones (Massillon, Navajo, Schuler-Cotton Valley, and Spirit River), granites (Sierra White and Oklahoma), and Vycor porous glass. Q^{-1} is found to depend strongly on water saturation. Moduli are relaxed below 100 Hz and unrelaxed above 100 kHz (fig. 3). None of the following mechanisms can coherently explain these observations.

Scattering

When the wavelength approaches the size of the grains or pores, scattering will occur (Devaney et al., 1982). The center frequency, f_{ψ} , of scattering by the pores is given by

$$f_{\psi} = \frac{3}{R} \left(\frac{M}{\rho_c} \right)^{1/2} \quad (1)$$

where R is the radius of the grains, ρ_c is the radius of the grains, ρ_c is the composite density, and M is the wave modulus. For our Massillon, Fort Union, Cotton Valley, and Spirit River samples, f_{ψ} is above 5 MHz (fig. 3). A small negative dispersion, indicative of scattering, has been measured in brine saturated Massillon and Boise sandstones at frequencies above 500 kHz (Winkler and Plona, 1982). These particular Massillon and Boise samples had grain diameters of -300 and -200 μm , respectively. Scattering is not important in sandstones below 100 kHz.

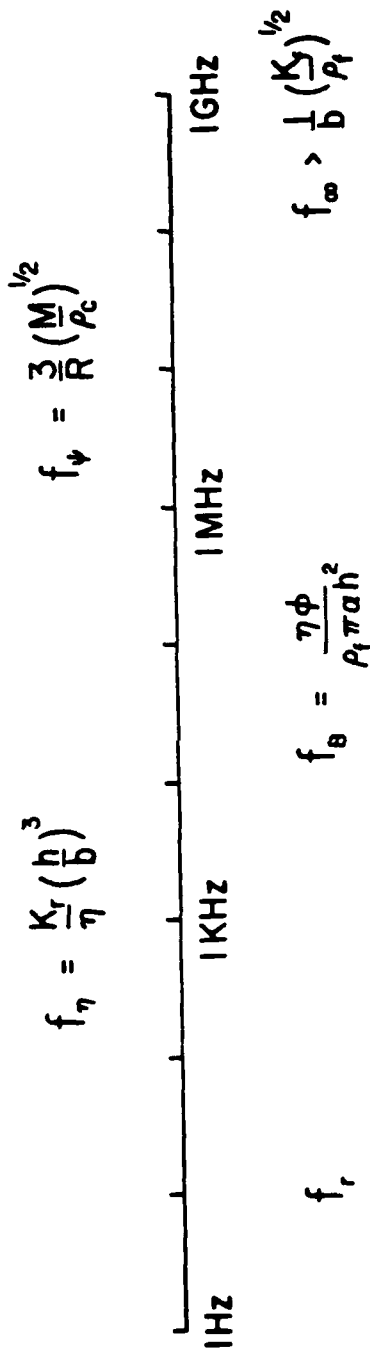


Fig. 3. Specification of critical frequencies for various mechanisms. (See text for explanation.)

Frictional Grain Sliding

Frictional grain sliding is restricted to situations in which strains are greater than 10^{-6} ; they are not important in far-field seismic exploration, echo sounding, or borehole sonic logs (Winkler et al., 1979; Mavko, 1979; Murphy, 1982).

Thermoelasticity

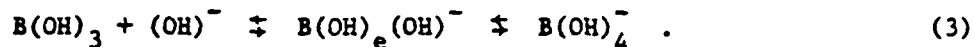
Thermal relaxation has been proposed as an attenuation mechanism by Kjartansson and Nur (1982). The center frequency, f_T , of such a relaxation is given by

$$f_T = \frac{h^2}{D} \quad (2)$$

where h is the half width of the pore and D is the thermal diffusivity of the composite. f_T is roughly 10 kHz for Massillon sandstone. This is indeed very close to the observed 3-5 kHz center frequency (Murphy, 1982a). However, thermal relaxation is diffusion controlled and thus predicted to be quite broad (see fig. 5.4 in Kjartansson, 1979). The observed relaxations in Massillon sandstone (Murphy, 1982a) and Navajo sandstone (Spencer, 1981) are very narrow, nearly single Debye or Zener peaks. The predicted dependence on water saturation is also inconsistent with our observations. Furthermore, Q^{-1} at 1 kHz has been observed to decrease with increasing temperature (Jones, personal communication). This result directly contradicts Kjartansson's model. Thermal relaxation is irrelevant in sands and sandstones at low temperatures and pressures.

Ionic Relaxation Absorption

An important mechanism for low frequency sound absorption in the oceans (Yeager et al., 1973; Fischer and Simmons, 1975; Simmons, 1975; Schulkin and March, 1978) is the two step reaction



Boric acid reacts with hydroxyl ions to form borate ions. This reaction is of interest because we have measured a strong dependence of Q^{-1} on water saturation and frequency in Vycor porous glass (Murphy, 1982a). Vycor consists of 4% boric acid which is concentrated near the pore surface. The center frequency of the ionic relaxation is roughly between 1 to 10 kHz. However, the process is diffusion controlled, and the predicted magnitude of the losses is too small.

Dislocations

Mason (1969, 1971a,b, 1978) has proposed that dislocations move in the grain surfaces as a response to acoustic loading. Dislocations are not activated in quartz at low temperatures and pressures (Griggs, 1969).

Vibrational Relaxation in the Water-Air Mixture

Zuckerwar and Griffin (1981) have measured the absorption of sound in N_2 as a function of relative humidity. The losses are too small to account for those in granular sedimentary materials.

Biot's Solid-Fluid Coupling

Biot's solid-fluid coupling mechanism, which will be discussed in detail in section 4 and 6, implies a sharp peak in Q^{-1} centered at a frequency, f_B , given by

$$f_B = \frac{\eta}{\rho_f h^2} \quad (4)$$

where η is the viscosity of the fluid and ρ_f is the density of the fluid. For Massillon and Navajo sandstones, f_B , is above 100 kHz (fig. 3). The predicted losses in the 1 to 10 kHz range are very small compared to observed losses. f_B is very sensitive to the pore width parameter, h . But, as h goes from $\sim 10 \mu\text{m}$ in Massillon sandstone to less than $1 \mu\text{m}$ in Fort Union sandstone or Sierra White granite, the observed peaks shift hardly, if at all. Nor does this model account for the effects of partial water saturation.

Biot's mechanism may be important in the ultrasonic frequency range in certain materials (Plona, 1980; Winkler and Plona, 1982). "Squirt" (Mavko and Nur, 1979)

Imagine an ordinary laboratory squirt bottle containing some water. Upon squeezing the outside of the bottle, the water discharges as a high Reynold's number jet into an infinite reservoir. This is a process which does not occur during acoustic propagation in sands and sandstones. As we shall later show, Reynolds' numbers are significantly less than 1 in the acoustic frequency range. Moreover, Mavko and Nur (1979) mistakenly formulate the center of the squirt relaxation to be the transition from incompressible to compressible flow in the pore fluid. This choice of frequencies is in fact an infinite frequency, f_∞ . Above f_∞ no flow can occur because the period is too short. The pore fluid behaves as an elastic solid. f_∞ is given by

$$f_\infty > \frac{1}{b} \left(\frac{K_f}{\rho_f} \right)^{1/2} \quad (5)$$

where b is the length of the fluid drop in the contact gap and K_f is the bulk modulus of the fluid. f_∞ approaches 1 GHz in sands and sandstones (fig. 3).

Surface Mechanisms

It has been established beyond doubt that small amounts of water interact with the dry surface of quartz grains, thus reducing the frame moduli and increasing attenuation (Clark et al., 1980; Spencer, 1981; Murphy, 1982a,b; Murphy and Nur, 1982a). However, the physics of the process is still an open question. For example, Spencer (1981) suggests that a surface mechanism controls the sharply peaked relaxation he observes at high water saturations. However, Pandit and King (1979) have shown that Q^{-1} remains independent of frequency as relative humidity increases from 0 to 82%. At a relative humidity of 98%, the data indicates the onset of frequency dependence. 82% relative humidity is equivalent to 5 monolayers of water (Tittmann et al., 1980). The onset of frequency dependence is thus evidently with bulk liquid water and not surface films.

3. THE CONCEPT OF THE MODEL

Sands and sandstones are porous, granular materials. Microstructures vary greatly within the scope of these materials (fig. 4). The resulting differences among their acoustic properties are discussed in Murphy and Nur (1982a). All sands and sandstones however, are distinguished by a common character. They consist of elastic quartz grains in contact, immersed in a viscous pore fluid (fig. 5). The pore fluid in which we are most interested is a binary mixture of water and air. The grains are of course described by bulk and shear moduli, and pore fluid by viscosities and compressibilities.

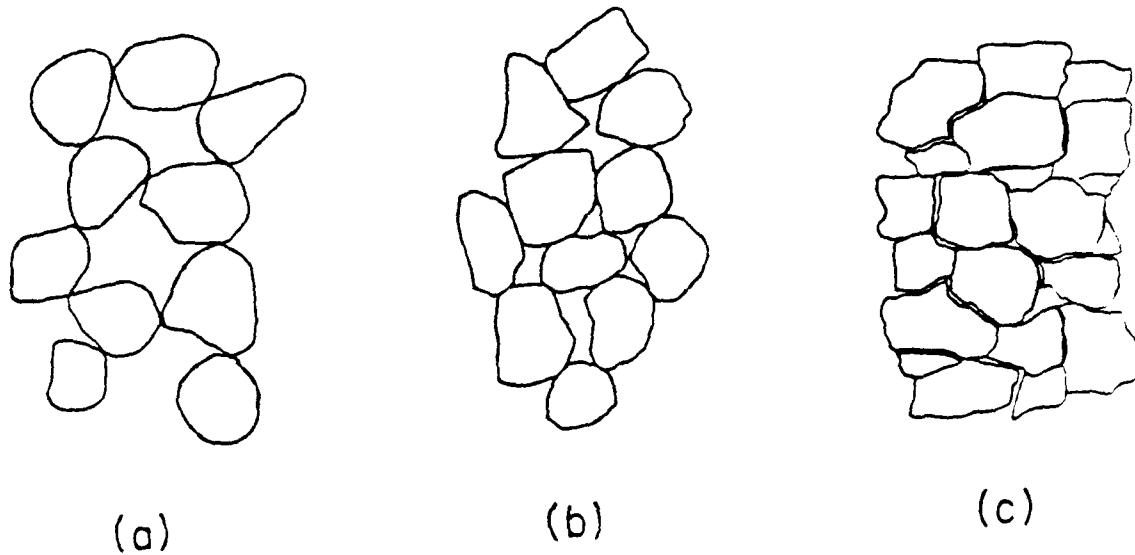


Fig. 4. Sketch of the three extreme types of granular sedimentary materials: (a) unconsolidated sands, (b) high porosity sandstones, and (c) low porosity sandstones.

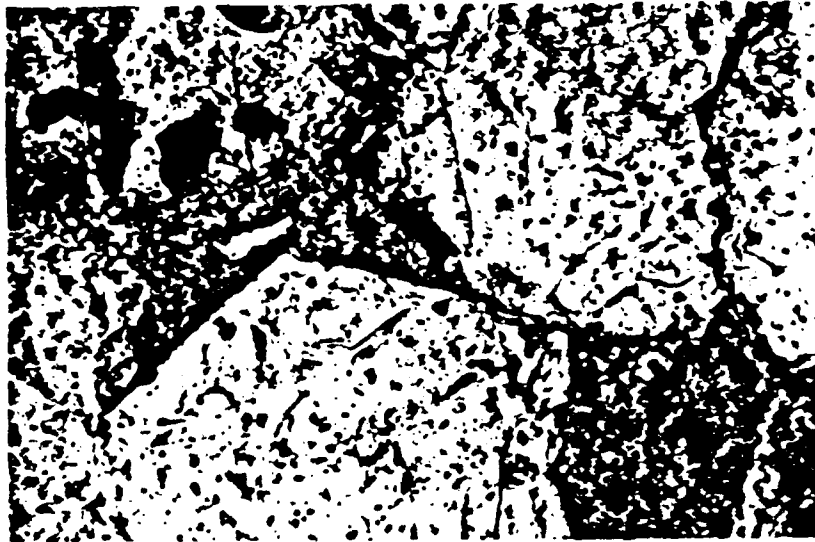
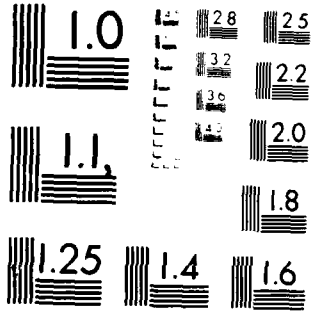


Fig. 5. Photomicrograph of a Massillon sandstone under partially polarized transmitted light. Porosity is shown by the light blue epoxy. Grain size is roughly 150 μm .



MICROCOPY RESOLUTION TEST CHART
NATIONAL BUREAU OF STANDARDS-1963-A

The acoustic behavior however is dominated by the interactions at the contacts. The grain to grain interactions are discussed in Murphy (1982b). The grain/fluid/grain interactions are the cause of attenuation and dispersion. As the grain contacts close and open under oscillatory loading, the water must be squeezed out and sucked back in the thin gaps between grains. These "squeeze films" are coupled to the fluid in the local pore neighborhood. The water also reacts electrochemically with the surface of quartz grains. When exposed to water, the quartz surfaces hydroxylate, and water adsorbs on the hydroxylated or silanol surfaces. An electrical double layer is formed. The double layer may be ~10 nm thick. A layer of silica gel may also be formed.

4. SURFACE ELECTROCHEMISTRY

The three principle effects of moisture or vapor pressure on dry sands and sandstones are the modulus defect, the volume expansion of the granular frame, and the increased constant Q energy losses. Each is a consequence of the electrochemical interactions at the quartz-water interface.

The Structure of the Electrical Double Layer

Consider a freshly broken, clean quartz surface. Such a surface has "dangling bonds". That is to say that silica and oxygen ions lack neighbors on at least one side. These sites are unstable. The surface ions may polarize and relax into a modified structure of lower potential energy. This surface, called the disturbed layer, consists mainly of Si-O-Si bridging or siloxane groups (Parks, 1982). This configuration, for instance, might be the state of a freshly

cleaved quartz surface under a vacuum of 10^{-10} torr at high temperature.

Both dangling bond sites and siloxane groups are chemically reactive. The surface possesses a strong negative charge easily sufficient to drive the ionization of water. Quartz (Gallei and Parks, 1972), amorphous silicas, and glasses hydroxylate upon exposure to water vapor. The hydroxylated surface is dominated by SiOH or silanol groups of various types. The surface retains a reduced yet substantial negative charge. The pore surface of all sands and sandstones are expected to be hydroxylated, probably even those in Tittmann's (1980) experiments (which are subjected to a 10^{-10} torr vacuum and moderate temperatures).

Given a finite vapor pressure or relative humidity, a layer of water adsorbs chemically on the hydroxylated quartz surface. This layer, called the inner Helmholtz layer (fig. 6a) is hydrogen bonded to silanol sites with the bonding strength of 8 to 12 kJ/mole (Parks, 1982). The layer is roughly 1 nm thick. It is structured and possesses low entropy, mobility, and polarizability relative to bulk water.

Increasing vapor pressure deposits a second layer of water, known as the outer Helmholtz layer (fig. 6a). It consists of a surplus of positively charged ions (counterions) and a small deficit of negatively charged ions. The counterions are held by electrostatic attraction. This layer is also about 1 nm in thickness. It is less structured than the inner Helmholtz layer. But it is more structured than the water residing outboard of the Stern double layer (fig. 6a).

Beyond the Stern double layer, we move into the diffuse double layer (fig. 6a). Here, the electrostatic attraction falls off expon-

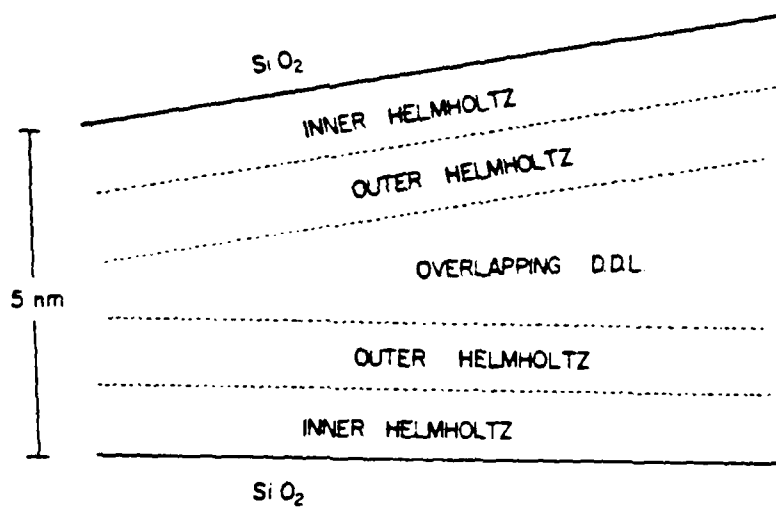
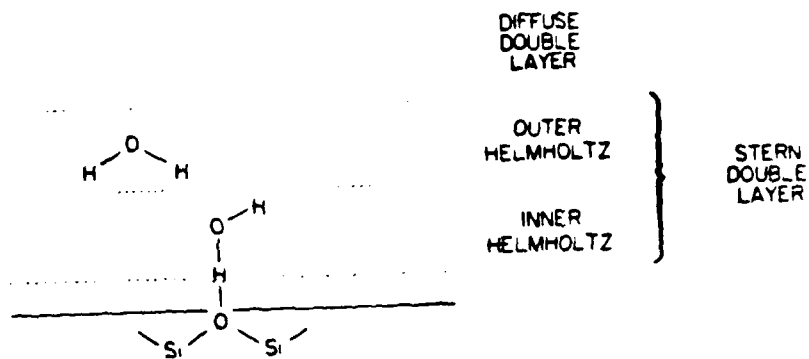


Fig. 6. Sketches of the electrical double layer:
 (a) The structure of the double layer, and
 (b) the interaction between the double layers
 on two adjacent grains.

entially, and the properties in this layer asymptotically approach those of bulk water. The combined thickness of Stern and diffuse double layer is roughly 5 to 10 nm.

Surface Energy and Contact Compliance

Surface free energy, γ , is the work required to produce new surface area. Since deformation by acoustic waves involves changes in surface area, γ is an important factor in contact compliance.

The density and strength of the bonds broken in the fracture principally determine the γ of the freshly cleaved quartz surface (Adamson, 1976). Parks (1982) estimates a γ of as much as 2000 mJm^{-2} . Chemical and electrical interaction of any sort whatsoever will reduce γ relative to the clean surface. Hydroxylation, adsorption, and double layer formation progressively and dramatically reduce γ . This reduction is shown schematically in figure 7.

The reduction in γ causes a proportional decline in the contact and frame moduli (c.f. Amberg and McIntosh, 1952; Spencer, 1981). There are three possible molecular mechanisms. First, the van der Waals attraction between grain surfaces is lowered. The contact area decreases, and the granular frame expands as explained in Murphy (1982b). Second, any hydrogen bonds bridging surface hydroxyls between grains are broken. And third, the intrinsic grain moduli, K_s and μ_s , may be lowered.

Clark et al. (1980), Tittmann et al. (1980), and Spencer (1981) have measured the modulus defect as a function of the composition of the fluid. The results may be understood readily with the aid of the following equations.

The reduction of surface energy by specific or chemical adsorption

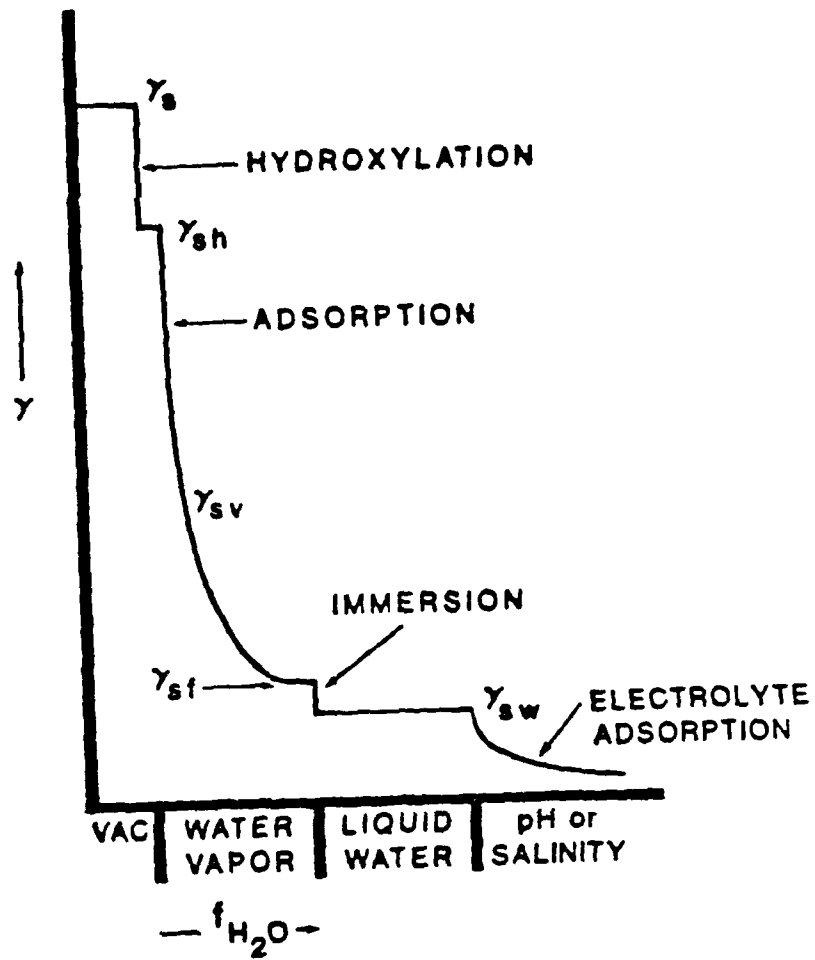


Fig. 7. The surface free energy of quartz as a function of moisture content (after Parks, 1982).

is described by the Gibbs adsorption equation (Hiemcz, 1977)

$$d\gamma = - \sum_i \Gamma_i d\tilde{\mu}_i \quad (7)$$

where Γ_i is the Gibbs excess adsorption density of species i and $\tilde{\mu}_i$ is the chemical potential of species i . The reduction of surface energy by combined chemical and electrical effects is given by

$$d\gamma = -[\sum_i \Gamma_i d\tilde{\mu}_i + \sum_i \Gamma_i d\tilde{\mu}_i] \quad (8)$$

where $\tilde{\mu}_i$ is the electrochemical potential of species i which is related to $\tilde{\mu}_i$ as follows

$$\tilde{\mu}_i = \tilde{\mu}_i + z_i e \psi \quad (9)$$

where ψ is the potential of the charged species in i , z_i is the valence number of the i^{th} charged species, and e is unit positive charge.

Six fluids were tested. Listed in decreasing order of effect observed on the moduli, they are water, ethanol, methane, n-decane, benzene, and hexane. This is also the order of decreasing change in chemical and electrochemical potential.

This model predicts that the addition of an electrolyte to the water would further reduce the frame moduli.

Constant Q Energy Losses

As the contacts oscillate under acoustic loading, the surface near the contacts is deformed. Hydrogen bonds are broken as the film is squeezed away and drawn back to bonding sites. New sites may arise and disappear or the double layers may overlap and separate (fig. 6b). The relaxations are diffusion-controlled. The relaxation times are

broadly distributed because of the variation in mobility across the double layer. The attenuation due to electrochemical surface mechanism is thus constant Q (fig. 8), at least in the frequency range between 10 and 10^6 Hz. The actual relaxation times ought to be predicted from statistical mechanics.

Explanation for the increased loss with increasing moisture or vapor pressure is straightforward. Consider that

$$Q^{-1} \approx \bar{S} \sum_j n_j \phi_b \quad (10)$$

where \bar{S} is the total surface area deformed, j is the number of layers in the double layer at the given vapor pressure, n_j is the number of fluid molecules per layer per unit surface area, and ϕ_b is the energy lost in breaking a hydrogen bond. ϕ_b is a constant. n_j increases (by definition) with increased deposition on the surface. \bar{S} also increases with vapor pressure because the contacts become more compliant.

Several investigators (Born, 1941; Spencer, 1981; Murphy, 1982a) have found that Q^{-1} is frequency independent in dry sandstones. Pandit and King (1979) have shown that Q^{-1} remains independent of frequency up to relative humidities between 80 and 90%. At this vapor pressure, bulk liquid water begins to condense in the smaller contact gaps or capillaries. Frequency dependent Q is associated with the presence of bulk liquid water.

5. MICROHYDRODYNAMICS

When bulk liquid water is present in the contact gaps (fig. 9), oscillatory displacement of the grain surfaces will drive local fluid flow. This process determines the large losses that are dependent on

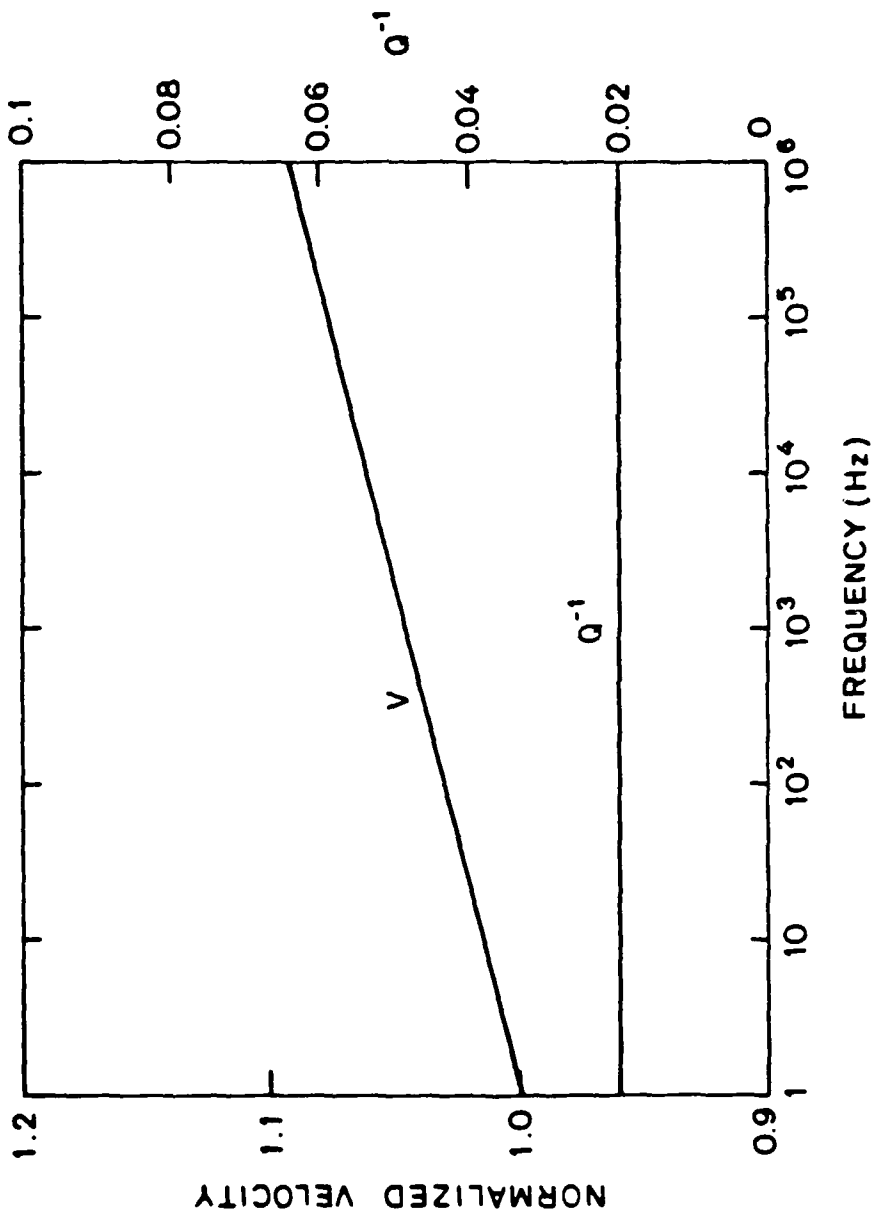


Fig. 8. Phase velocity and Q^{-1} versus frequency at $P/P_0(H_2O) \approx 0.60$ in a dry granular sedimentary material.

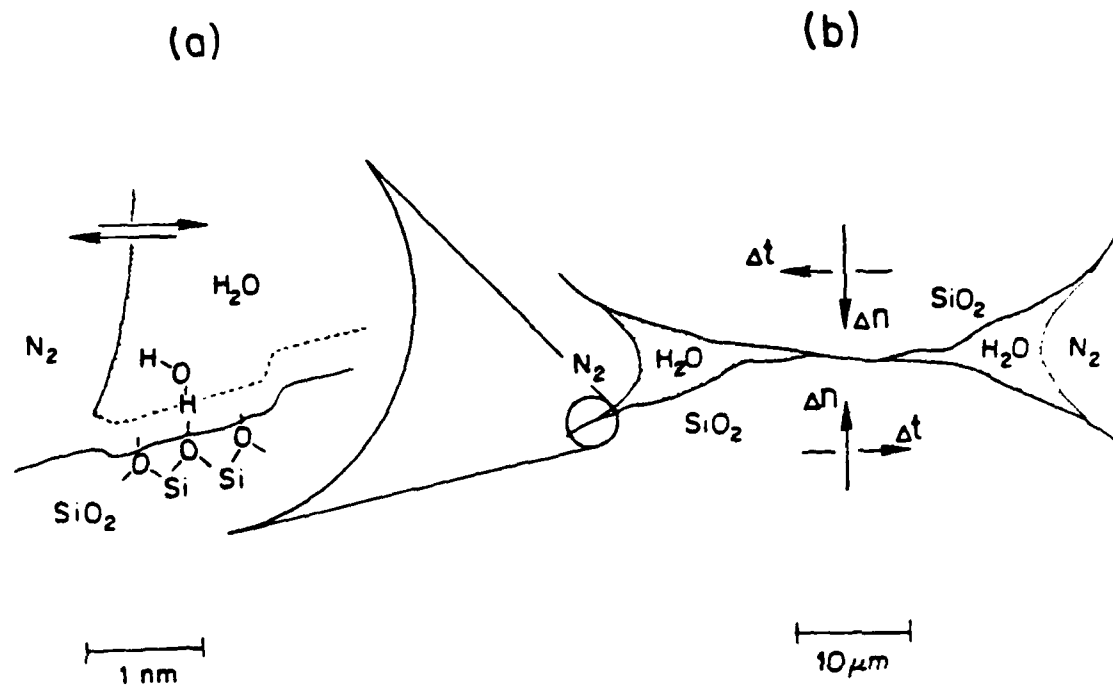


Fig. 9. Two grains in contact in a partially saturated granular sedimentary material.

both water saturation and frequency. Of course, the electrochemical surface mechanism continues to operate. It provides a frequency independent background loss. But in the range from 100 Hz to 100 kHz, local fluid flow dominates. There are three parts to the fluid flow problem: i) boundary layer development, ii) squeeze film elasto-hydrodynamics, and iii) propagation and flow in a compact pore neighborhood.

Boundary Layer Development

In a porous medium under acoustic loading, the pore fluid moves relative to the solid frame (Biot, 1956). Consider a half cycle of an oscillatory displacement of a cylindrical pore in the plane of its axis (fig. 10a). The fluid in contact with the wall adheres to it. A velocity profile develops as viscous tangential stresses diffuse vorticity across the pore width with a diffusivity

$$\nu = \frac{\eta}{\rho_f} \quad (11)$$

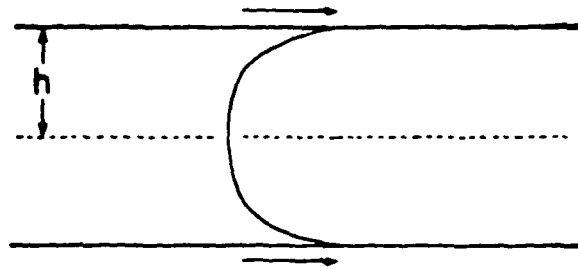
where ν is the kinematic viscosity. Energy is dissipated by the viscous tangential stresses. The depth to which the boundary layer has penetrated before reversal is the skin depth

$$\delta = \left(\frac{\nu}{\omega} \right)^{1/2} \quad (12)$$

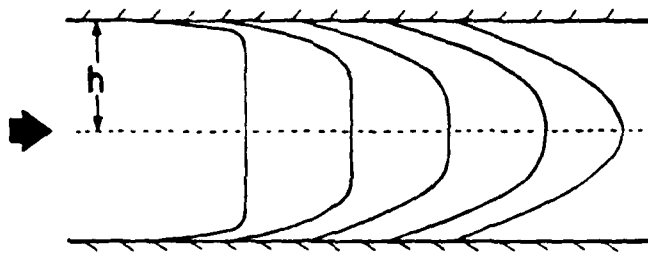
Dissipation is confined to the boundary layer.

When δ reaches h , the flow profile becomes parabolic (i.e. a Poiseuille flow). It is said to be fully developed. At 1 MHz, the flow would be fully developed in pores 3 μm in width. At 10 kHz, flow in 300 μm pores would be fully developed.

Viscous dissipation is defined in general as



(a)



(b)

Fig. 10. Boundary layer development: (a) wall is beginning to move, and the fluid is still; and (b) the wall is fixed, and the fluid is beginning to flow.

$$\phi_v = \text{the rate of energy loss per unit volume per unit time} \quad (13a)$$

$$= \frac{1}{2} \bar{\tau} \cdot \epsilon \quad (13b)$$

$$= \frac{\eta}{2} (\nabla v) + (\nabla v)^T : (\nabla v) + (\nabla v)^T \quad (13c)$$

where ∇ is the del operator and v is the fluid velocity. In this specific solid-fluid coupling model, the dissipation per cycle is a tradeoff between the velocity gradient and the boundary layer thickness. The peak loss occurs at that frequency in which $\delta = h$. This is the micromechanics of Biot's (1956) attenuation mechanism. It is not important at acoustic frequencies in granular sedimentary materials.

However, the basic physics of boundary layer development carries over into another flow model. Consider the flow through a fixed cylindrical pore driven by an oscillatory pressure gradient (fig. 10b). This process is clearly relevant to flow in and out of a contact gap. The rate of energy dissipation per unit area of solid boundary is approximately

$$\frac{1}{2} s (\rho\omega)^{-1} \left| \frac{\partial p}{\partial x} \right|^2 \left(\frac{v}{2\omega} \right)^{1/2} \quad (14)$$

per unit length of tube, where s is the circumference. The energy loss per cycle is proportional to the boundary layer thickness.

Squeeze Film Elastohydrodynamics

The compression of a contact gap (fig. 11) will drive water out of that gap. If the length b is much greater than the width $2h$ and the flow profile is fully developed, the motion of the squeeze film is governed by the Reynold's equation

$$\nabla_p^2 = \frac{3\eta}{2h^3} \frac{\partial h}{\partial t} \quad (15)$$

$$\xi(r,t) = \xi_0(r) + \epsilon e^{i\omega t}$$

→ $\dot{S}(r), \dot{\theta}(r)$

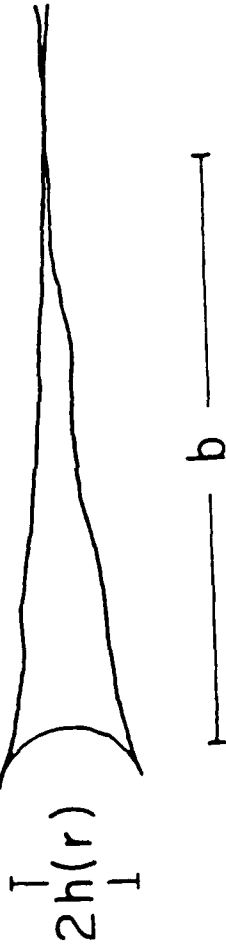


Fig. 11. The gap between two grains in contact.

The rate of closure of the gap $\partial h/\partial t$ is the driving or squeeze term. It is related to the elasticity of the contact gap by

$$\frac{\partial h}{\partial t} = - \frac{b}{M_{\text{gap}}} (i\omega\sigma - \frac{\partial p}{\partial t}) f(\xi) \quad (16)$$

where $i\omega\sigma$ is the acoustic loading, M_{gap} is the modulus of the gap, and $f(\xi)$ is a function of the gap shape.

Phenomenologically, this micromechanism defines a Zener relaxation or standard linear solid (fig. 12). The elastic grains constitute a spring which is in series with a parallel spring (the grain contact) and dashpot (the squeeze film). The characteristic relaxation time, τ , is simply

$$\tau \approx \frac{\eta}{M_{\text{gap}}} \left(\frac{b}{h} \right)^m \quad (17)$$

where the exponent m is dependent on the shape of the gap. As the grain surfaces approach parallelism, m approaches 3. The observed relaxations in sandstones are in the range 10^{-3} to 10^{-4} s. Thus, for $\eta \approx 10^{-3} \text{ Nsm}^{-2}$ and $M_{\text{gap}} \approx 1 \text{ GPa}$, the aspect ratios involved would be in the range 10^{-2} to $10^{-2.5}$. In other words, the gap length is required to be 100 times the half length. This is a very flat gap, but not unreasonable when we consider that the displacements of the gap wall are of the order of nanometers.

For water drops isolated in small constrictions, surface tension may be included in equation 14 by subtracting $2\gamma_w/h$ from the pressure. γ_w is the surface tension of water.

Propagation and Flow in a Compact Pore Neighborhood

The water saturation effects (fig. 13) have yet to be explained. Thus far, we have considered the sites for pore pressure buildup,

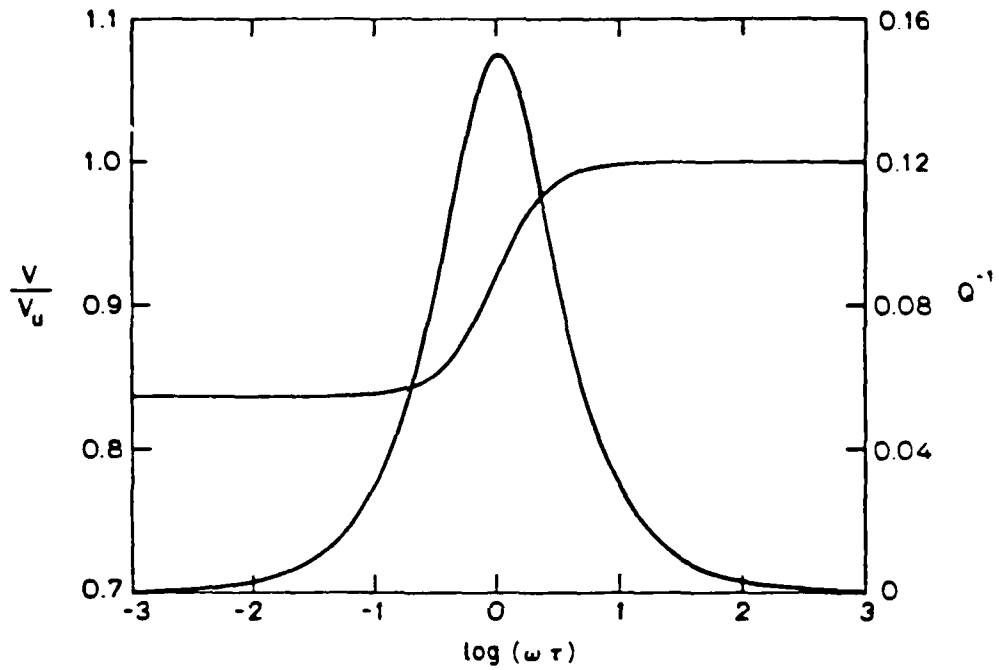
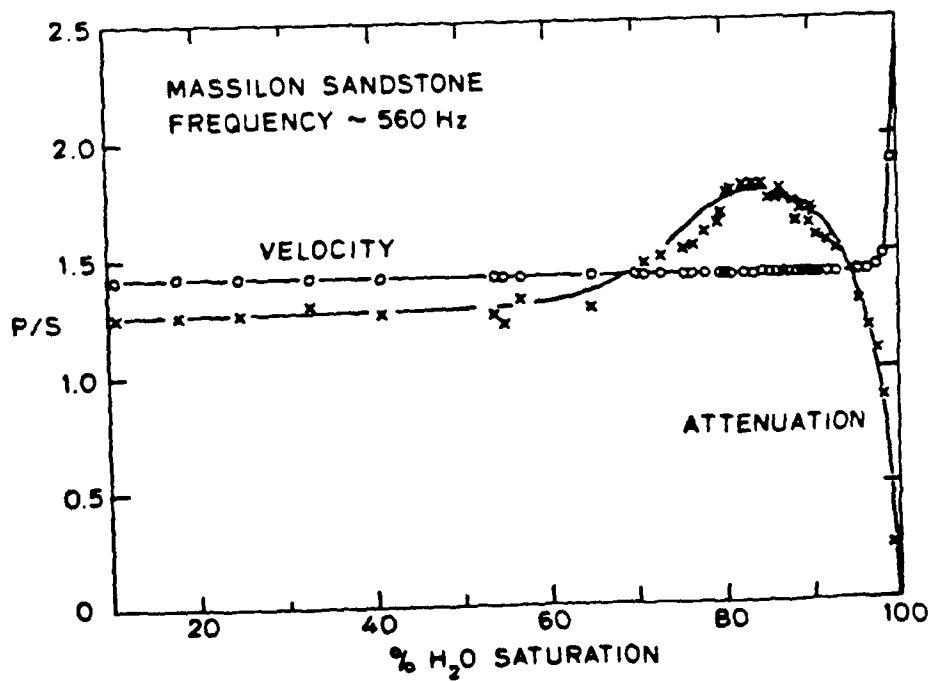
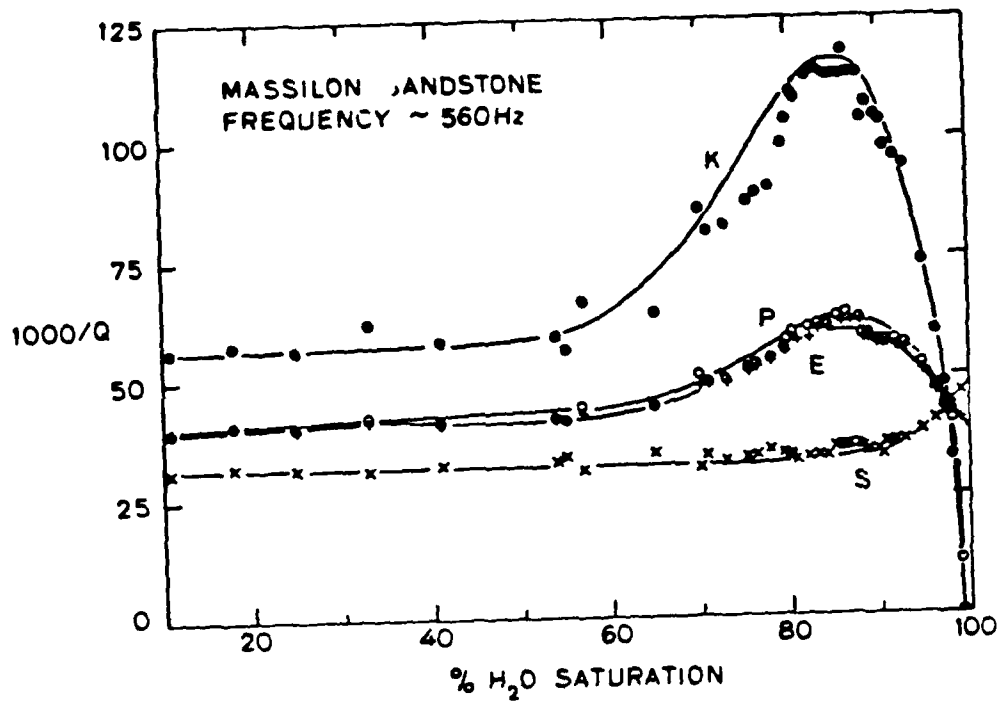


Fig. 12. Phase velocity and Q^{-1} versus frequency in a Zener standard linear solid.



the contact gaps, in terms of discharge into an infinite reservoir at null pore pressure. We have not yet considered the flow in the contiguous pore. In order to understand the effects of water saturation on Q^{-1} , we need to consider flow throughout the local pore neighborhood.

The property which defines the volume flow out the contact gap, or constriction, into the adjacent pore, or cavity, is the admittance. The admittance, β , is defined as the ratio of the volume flow to pressure excess. An effective admittance, β_e , can be defined such that it takes into account the configuration of the pores and gaps in the entire neighborhood (Lighthill, 1975; 1978). Such a device allows us to map complex pore configurations such as those in real sands and sandstones into simple models such as those in figure 14.

If the pore neighborhood is small compared to the wavelength, it is said to be compact. The equations of fluid motion for frequency ω can be expressed as

$$\frac{\partial J}{\partial t} = -\beta_e [\rho_f (B_f + D)]^{-1/2} \frac{\partial p}{\partial x} \left[1 - \left(\frac{v}{i\omega} \right)^{1/2} \frac{s}{S_o} \right] \quad (18)$$

where J is the volume flow, D is the distendibility of the constriction walls, and S_o is the crosssectional area. These motions must satisfy the linearized equations of continuity.

$$\frac{\partial p}{\partial t} = -\beta_e^{-1} [\rho_f (B_f + D)]^{-1/2} \frac{\partial J}{\partial x} \quad (19)$$

The pressure buildup $\partial p / \partial t$ is related to the elasticity of the contact through equation 15. Dissipation is calculated from equation 13.

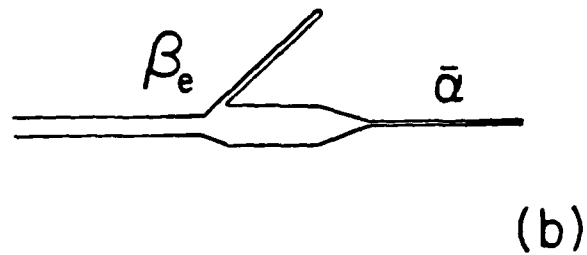
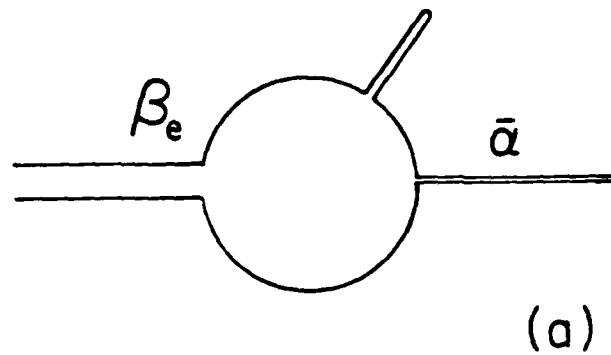


Fig. 14. Models of the local pore neighborhood in (a) high porosity sandstone and (b) low porosity sandstone. The contact gap is the constriction on the left. The cavity in the center is the contiguous pore. The closed end constriction represents connected contact gaps and closed pores. The constriction on the right constitutes the connectivity to the pore network. β_e is the admittance of the contact gap. $\bar{\alpha}$ is Biot's structural factor.

This system of equations provides the foundation to formulate the model rigorously. That task is beyond the scope of this paper.

Consider the pore configuration in figure 14a to be fully water saturated. It is subjected to pure bulk compression as sketched in figure 15. As the entire pore neighborhood is compressed isotropically and the compressibility of the fluid B_f is low, the pore pressure gradient $\partial p/\partial x$ is weak. Volume flow J and the dissipation per cycle Q_k^{-1} is small. The contact gap closure dh/dt cannot occur because the pore pressure buildup $\partial p/\partial t$ cannot relax. The real part of the frame modulus is very high.

On the other hand, pure shear is polarized (fig. 15). Contact gaps having differing azimuths with respect to the polarization may undergo compression or extension. The pore fluid is simultaneously subjected to compression and suction. Pressure gradients $\partial p/dx$ are high. Volume flow J is high and Q_s^{-1} is high. The pore pressure buildup $\partial p/\partial t$ can relax, and gap closure dh/dt proceeds.

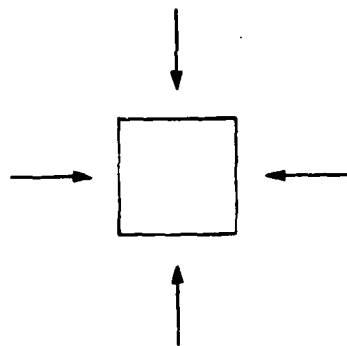
When the pore neighborhoods (fig. 14) are partially saturated the situation is quite different. The high compressibility of the fluid in the cavity allows strong pore pressure gradients to occur, particularly under bulk compression. Volume flow and Q_k^{-1} are high.

We can heuristically summarize the model with the following proportionality

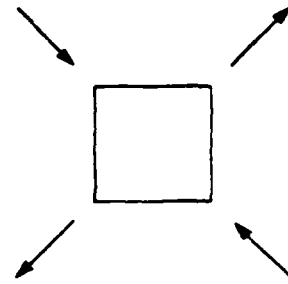
$$Q^{-1} \propto \phi S_w \left(\frac{\delta}{h} \right) \sum_i n_i \left| \left(\frac{\partial p}{\partial x} \right)_i \right|^2 \quad (20)$$

(a) (b) (c)

where the factor (a) merely expresses the volume of viscous fluid per



BULK
COMPRESSION



PURE
SHEAR

Fig. 15. Stress configurations for bulk compression and pure shear.

volume of the composite material, factor (b) represents the boundary layer thickness, and factor (c) is the sum of the number of pore pressure sites times the square of the pore pressure gradient at that site. Factor (c) is controlled by a combination of the aspect ratio of the gaps, the stress configuration, and the compressibility of the fluid in the cavity.

6. GENERAL EQUATIONS FOR ACOUSTIC PROPAGATION IN POROUS MEDIA

Biot (1956) and Morse and Ingard (1968) have studied the macroscopic elastodynamics of a porous, two component system. These theories track the motions and forces in the solid and fluid in two separate equations. The solid frame is perfectly elastic. Granularity is not considered.

Biot (1962) and Burridge and Keller (1981) have proposed a generalized set of equations which can accommodate linear viscoelastic frame moduli. To the best of my knowledge, these equations have not as yet been exploited in the literature. A schematic breakdown of the generalized equations is presented in figure 16. Detailed discussion is beyond the scope of this paper. We wish, however to sketch the theory in order to discuss several predictions.

The equations of motion are for the porous, granular composite

$$\rho_c \ddot{u} + \rho_f \ddot{w} = \text{div } T \quad (21)$$

and for the macroscopic motion of the pore fluid

$$\rho_f \ddot{u} = - \frac{\partial p}{\partial x} + \bar{Y} \dot{w} \quad (22)$$

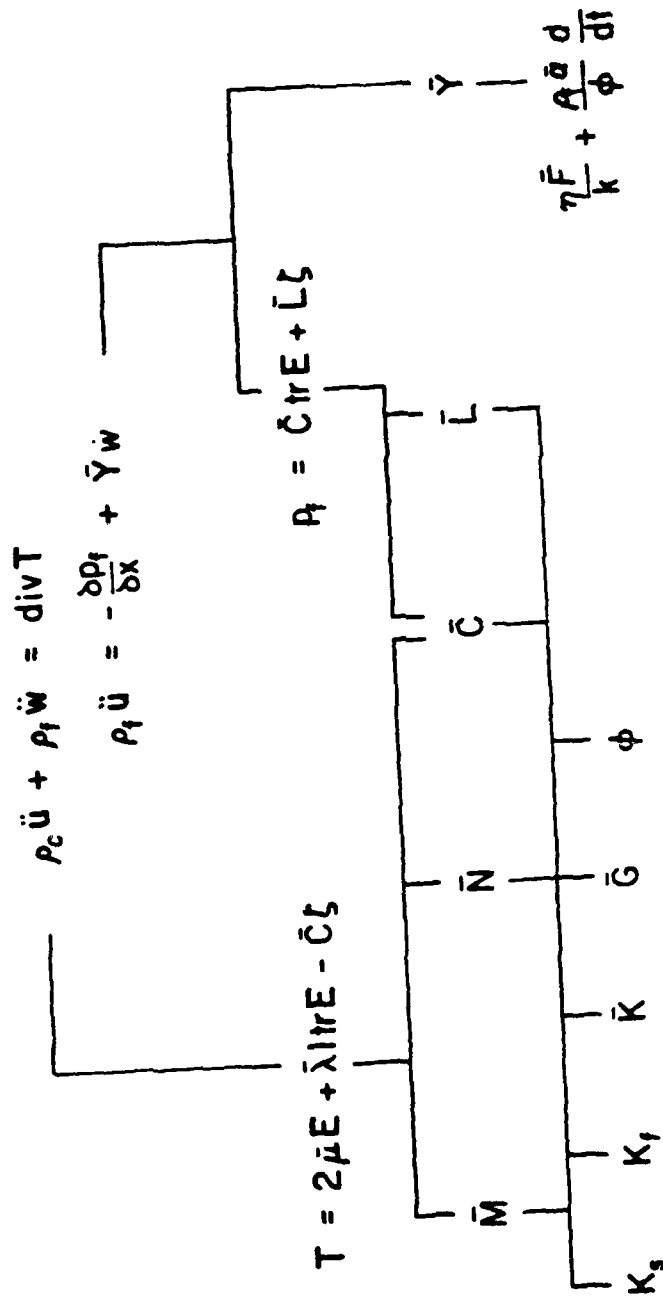


Fig. 16. Outline of the general equations for acoustic propagation in general porous media. (See text for explanation.)

where $\rho_c = (1-\phi) \rho_s + \phi \rho_f$
 $\rho_f = (1-S_w) \rho_g + \phi S_w \rho_w$
 ρ_g = density of the gas
 ρ_w = density of the water
 S_w = water saturation
 ϕ = porosity
 u = displacement of the solid
 $w = u-U$ = relative displacement of the fluid and the solid
 U = displacement of the fluid.

\bar{Y} is the viscodynamic solid-fluid coupling operator.

$$\bar{Y} = \frac{\rho_f \bar{\alpha}}{\phi} \frac{d}{dt} + \frac{\eta \bar{F}}{k} \quad (23)$$

The first term on the right hand side of equation 21 describes the inertial coupling, while the second term describes the dissipation.

p_f is the macroscopic pore pressure

$$p_f = \bar{C} \operatorname{tr} E + \bar{L} \zeta \quad (24)$$

where $\operatorname{tr} E$ is the trace of the stress tensor and ζ is the fluid volume increment per unit pressure, $-\phi \operatorname{div} w$. Equations 21 through 23 govern Biot's solid-fluid coupling, and hereafter shall be neglected.

T is the stress tensor of the composite material

$$T = 2\bar{\mu}E + \bar{\lambda}1 \operatorname{tr} E - \bar{C} \zeta \quad (25)$$

where $\bar{\lambda}$ and $\bar{\mu}$ are the complex Lamé's constants.

The complex moduli \bar{M} , \bar{N} , \bar{C} , and \bar{L} can be given in terms of the intrinsic material properties ϕ , K_s , K_f , \bar{K} , and \bar{G} as

$$\bar{M} = \bar{\lambda} + 2\bar{\mu} + \bar{R} + 2\bar{Q} = \frac{(K_s - \bar{K})^2}{K_s(1-\phi - \frac{\bar{K}}{K_s} + \phi \frac{K_s}{K_f})} + \bar{K} + \frac{4}{3} \bar{\mu}, \quad (26)$$

$$\bar{N} = \bar{\mu} = \bar{G},$$

$$\bar{C} = \frac{\bar{R} + \bar{Q}}{\phi} = \frac{(K_s - \bar{K})}{(1-\phi - \frac{\bar{K}}{K_s} + \phi \frac{K_s}{K_f})} \quad (27)$$

and

$$\bar{L} = \frac{\bar{R}}{\phi} = \frac{K_s}{(1-\phi - \frac{\bar{K}}{K_s} + \phi \frac{K_s}{K_f})} \quad (28)$$

K_s is the bulk modulus of the solid grains. The bulk modulus of the fluid is

$$\frac{1}{K_f} = (1 - S_w) B_g + S_w B_w, \quad (29)$$

where B_g is the compressibility of the gas and B_w is the compressibility of the water.

\bar{K} and \bar{G} are the linear viscoelastic frame moduli, which are determined by the granular micromechanics. The variation of the real part of \bar{K} and \bar{G} as a function of frequency and water saturation is shown in figure 17.

The compressional and shear wave velocities are given by

$$v_p = \left(\frac{\bar{M}}{\rho_c} \right)^{1/2} \quad (31)$$

and

$$v_s = \left(\frac{\bar{N}}{\rho_c} \right)^{1/2},$$

respectively. Specific attenuation is

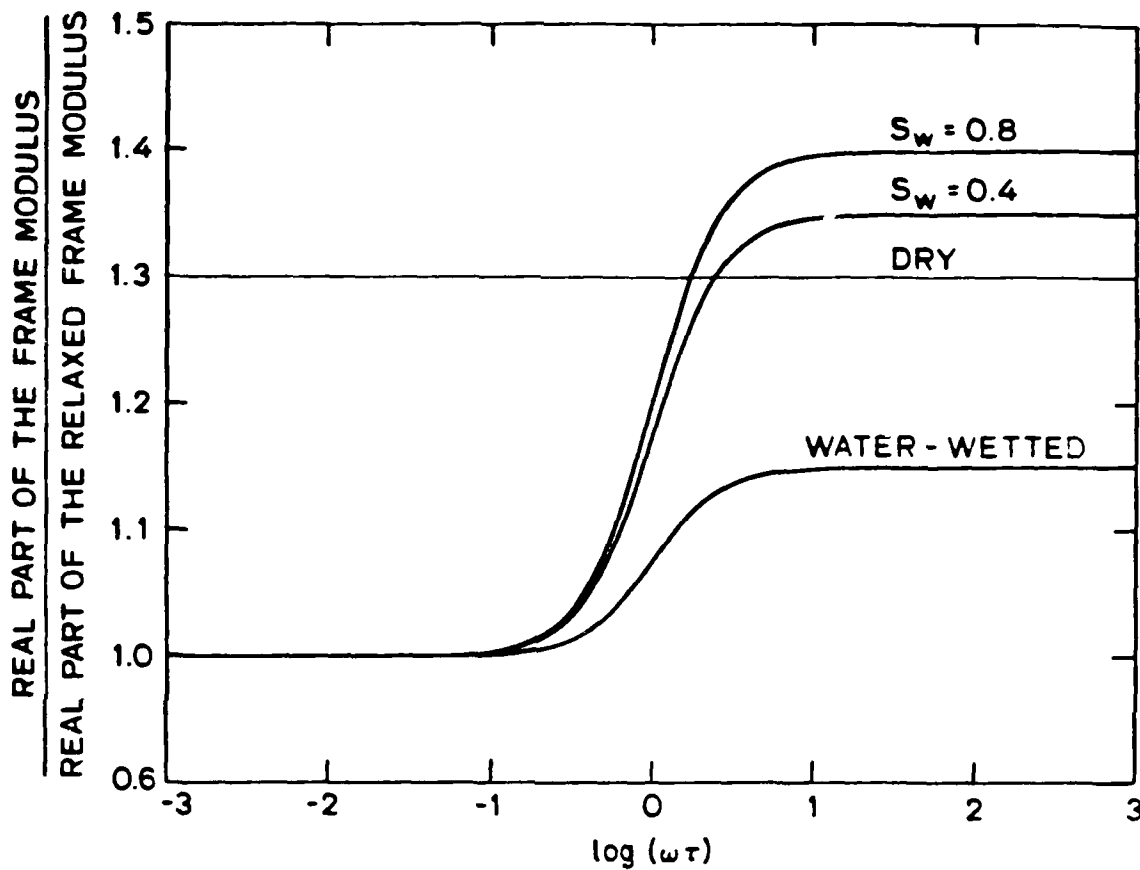


Fig. 17. Theoretical modulus dispersion in sandstones as a function of water saturation. Constant Q loss is suppressed. Water-wetted curve assumes certain degree of capillary condensation.

$$Q_P^{-1} = \frac{\text{Im } \bar{M}}{\text{Re } \bar{M}} \quad (32)$$

and

$$Q_S^{-1} = \frac{\text{Im } \bar{N}}{\text{Re } \bar{N}} \quad (33)$$

7. DISCUSSION

Although the model is not yet complete, I am reasonably confident that most of the major concepts are moving into place.

The velocity equations reduce to the Biot-Gassmann relations at frequencies a decade below the center frequency. This is accomplished as the frequency dependent frame moduli \bar{K} and \bar{G} approach relaxed values K_r and G_r in equations 24, 25, 29, and 30. The center frequency for Massillon sandstone is ~5 kHz. Figure 18 compares the predictions for V_p and V_s vs. S_w with measured values at 550 Hz.

Clark et al. (1980), Tittmann et al. (1980), and Spencer (1981) have added various pore fluids to dry sandstones. The fluids were of varying composition but of similar viscosity. They found that the fluids reduced the real part of the moduli and increased the Q^{-1} in the following order. From

water
ethanol
methanol
n-decane
benzene
hexane

(35)

Clark et al. (1980) and Tittmann et al. (1980) suggest that the process has something to do with the dipole moment. While Spencer (1981)

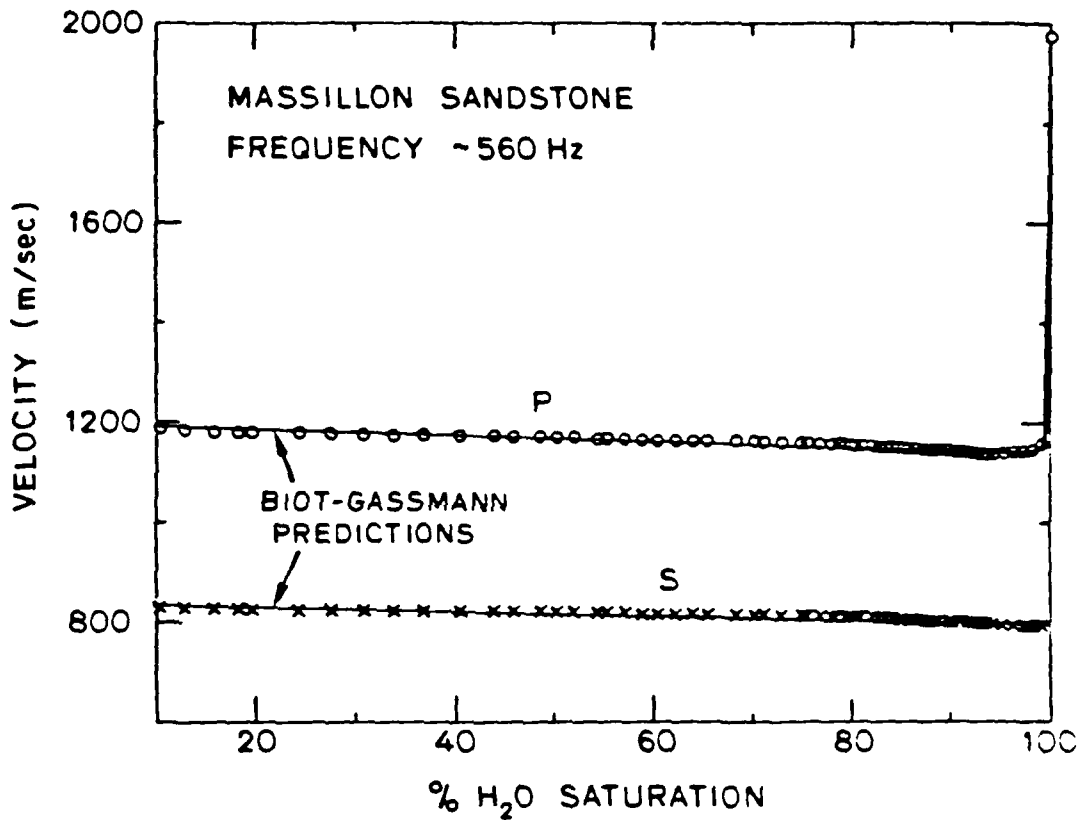


Fig. 18. V_p and V_s vs. % H₂O saturation ($S_w = 1.0 - 0.1$) in Massillon sandstone. Biot-Gassmann predictions plotted against measured values.

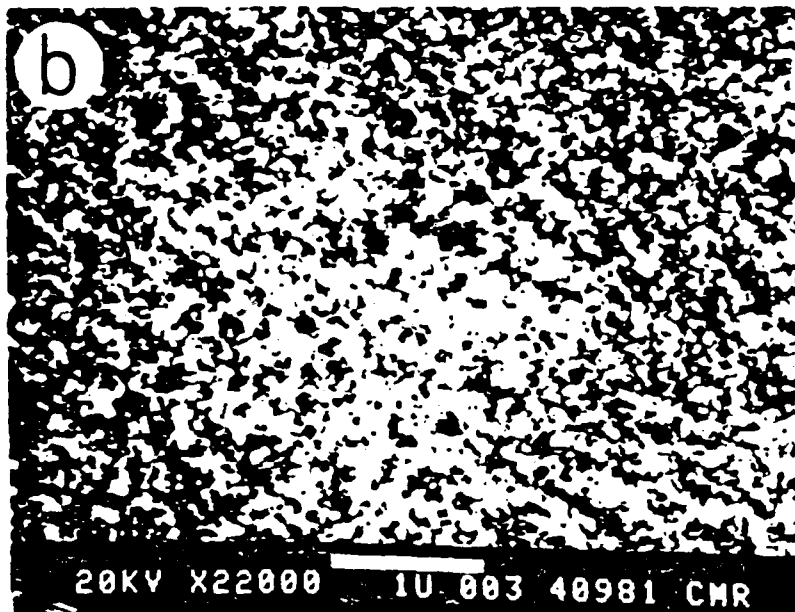
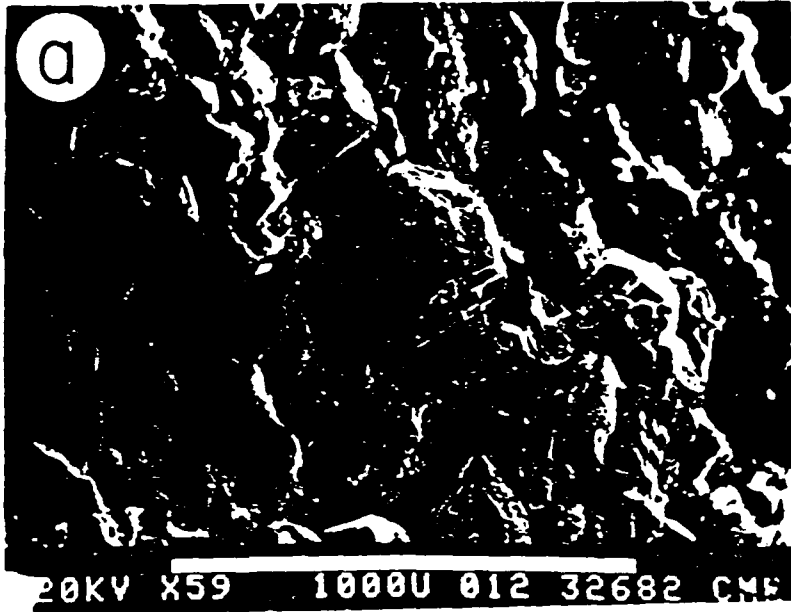
discusses physisorption. Once again, the specific chemical properties of importance are the chemical potential $\bar{\mu}$ and the electrochemical potential $\bar{\mu}_i$. The order in (35) is the order of descending $\int_1 d\bar{\mu}$ and $\int_1 d\bar{\mu}_i$.

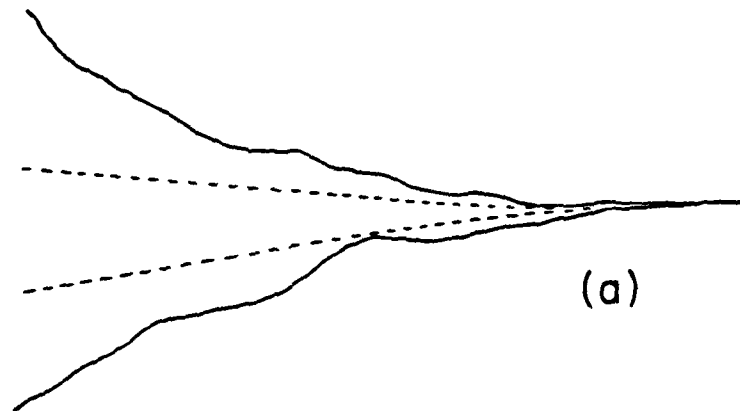
Spencer (1981) further claims that because the observed frequency peaks are depressed in the same order, these peaks must result from the surface effect. Well it is an interesting point, but the conclusion is wrong. From equations 14 and 15, we see that the more compliant the contact, the greater the pore pressure gradient driving the volume flow. Dissipation goes as the square of the pore pressure gradient. The magnitude of the electrochemical effect on contact compliance follows the same descending order as in (35). It stands to reason the height of the peaks due to viscous loss would be depressed correspondingly.

A similar argument can be used to explain the difference between the losses in Massillon sandstone and Vycor porous glass as reported in Murphy (1982a). Although Vycor has a surface area of $\sim 200 \text{ m}^2/\text{gm}^3$ and Massillon has a surface area roughly $10 \text{ m}^2/\text{gm}^3$, the losses in Vycor are consistently 1/6 that in Massillon at all saturations. The difference lies in the compliance of the grain contacts. Vycor has a structure which under a SEM appears similar to sintered glass beads (fig. 19b). Massillon on the other hand has many small aspect ratio near-contact gaps (19a). The basic difference between the contacts is sketched in figure 20. The near contact gaps in the Massillon sandstone provide the sites necessary for pore pressure generation.

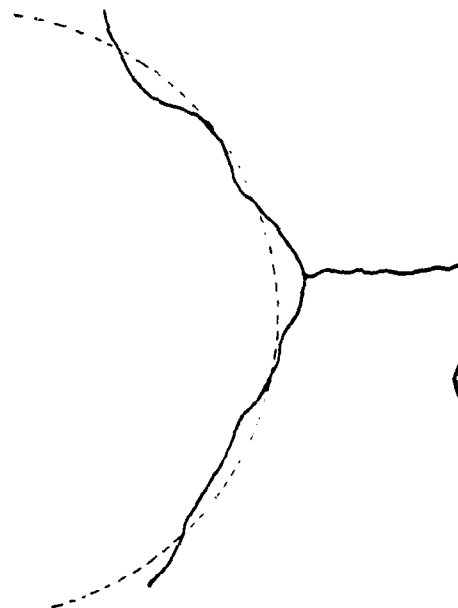
Finally, the effect of temperature may be included in the model by considering the temperature dependence of the viscosity. The

Fig. 19. SEM photomicrograph of (a) Massillon sandstone and (b) Vycor porous glass. The white bar at the base of the photograph is the length scale.





(a)



(b)

Fig. 20. Sketch of the contact gaps in (a) a granular sedimentary material (eg. Massillon sandstone) and (b) Vycor porous glass.

Arrhenius equation predicts that

$$\eta = \eta_0 e^{-\frac{\tilde{E}}{R\theta}} \quad (36)$$

where θ is the temperature, R is the gas constant, η_0 is the viscosity as $\theta \rightarrow 0$, and \tilde{E} is the activation energy of the fluid. The preliminary experimental results of T. Jones (personal communication) are encouraging along this line of reasoning.

ACKNOWLEDGEMENTS

Amos Nur is director of the Stanford Rock Physics Project. This chapter constitutes the fifth chapter of a doctoral dissertation. David Johnson suggested the need for a better microhydrodynamics. Surface electrochemistry was discussed with George Parks. I discuss everything with Ken Winkler. The Stanford Rock Physics Project is sponsored by a consortium of 15 oil companies and S.D.R. The author was supported as a graduate student by the Office of Naval Research under contract N00014-77-C-0390 with the Marine Geology and Geophysics Program.

WORKS CITED

- Adamson, A.W., 1976, Physical Chemistry of Surfaces, Wiley, N.Y., 697 p.
- Amberg, C.H. and McIntosh, R., 1952, A study of adsorption hysteresis by means of length changes of a rod of porous glass, *Canad. J. Chem.* 30, 1012-1032.
- Biot, M.A., 1956, Theory of propagation of elastic waves in a fluid-saturated porous solid,
I. Low frequency range, *J. Acoust. Soc. Am.* 28, 168-178.
II. High frequency range, *J. Acoust. Soc. Am.* 28, 179-191.
- Biot, M.A., 1962, Generalized theory of acoustic propagation in porous dissipative media, *J. Acoust. Soc. Am.* 54, 1254-1264.
- Clark, V.A., Tittmann, B.R. and Spencer, T.W., 1980, Effect of volatiles on attenuation (Q^{-1}) and velocity in sedimentary rocks, *J. Geophys. Res.* 35, 5190-5198.
- Devaney, A.J., Levine, H., and Plona, T.J., 1982, Attenuation due to scattering ultrasonic compressional waves in granular media, in Elastic Wave Scattering and Propagation (V.K. Varadom and V.V. Varadom, eds.), *Ann Arbor Sci.*, Ann Arbor, 131-148.
- Fischer, F.H., and Simmons, V.P., 1975, Discovery of boric acid as the cause of low frequency sound absorption in the ocean, *IEEE Ocean '75*, 21-24.
- Gregory, A.R., 1976, Fluid saturation effects in dynamic elastic properties of sedimentary rocks, *Geophys.* 41, 895-921.
- Griggs, D., 1967, Hydrolytic weakening of quartz and other silicates, *Geophys. J. R. Soc.* 14, 19-31.
- Hiemenz, P.C., 1977, Principles of Colloid and Surface Chemistry, Dekker, NY, 516 p.
- Kjartansson, E., and Nur, A., 1982, Attenuation due to thermal relaxation in porous rocks, *Geophys.* (in press).
- Lighthill, M.J., 1978, Waves in Fluids, Cambridge Univ. Press, 504 p.
- Lighthill, M.J., 1975, Mathematical Biofluidynamics, SIAM, Phila., 281 p.
- Mavko, G.M., 1979, Frictional attenuation: an inherent amplitude dependence, *J. Geophys. Res.* 84, 4769-4775.
- Mavko, G.M., and Nur, A., 1979, Wave attenuation in partially saturated rocks, *Geophys.* 44, 161-178.

- Mason, W.P., 1969, Internal friction mechanism that produces an attenuation in the earth's crust proportional to frequency, *J. Geophys. Res.* 74, 4963-4966.
- Mason, W.P., 1971a, Internal friction at low frequencies due to dislocations: Applications to metals and rock mechanics, in Physical Acoustics: Principles and Methods (W.P. Mason and R.N. Thurston, eds.) 8, 347-371.
- Mason, W.P., 1971b, Internal friction in moon and earth rocks, *Nature* 234, 461-463.
- Morse, P.M., and Ingard, K.V., 1968, Theoretical Acoustics, McGraw-Hill, NY, 927 p.
- Murphy, W.F., 1982a, Effects of partial water saturation on attenuation in Massillon sandstone and Vycor porous glass, *J. Acoust. Soc. Am.* 71, 6 (in press). Also Chapt. III in this volume.
- Murphy, W.F., 1982b, Micromechanics of acoustic dissipation in fully and partially water saturated granular sedimentary materials, *J. Geophys. Res.*, subm. July. Also Chapter V in this volume.
- Murphy, W.F. and Nur, A., 1982a, On velocities and attenuation as a measure of partial gas saturation in tight sandstones at borehole and ultrasonic frequencies, *Geophys.*, subm. July. Also Chapter IV in this volume.
- O'Connell, R.J., and B. Budanisky, 1977, Viscoelastic properties of fluid-saturated cracked solid, *J. Geophys. Res.* 82, 5119-5736.
- Parks, G.A., 1982, The surface and interfacial free energies of quartz, *J. Geophys. Res.*, to be submitted.
- Pandit, B.I., and King, M.S., 1979, The variation of elastic wave velocities and quality factor Q of a sandstone with moisture content, *Canad. J. Earth Sci.* 16, 2187-2195.
- Schulkin, M., and Marsh, W.H., 1978, Low-frequency sound absorption in the ocean, *J. Acoust. Soc. Am.* 63, 43-48.
- Simmons, V.P., 1975, Investigation of the 1 kHz sound absorption in sea water, Ph.D. Dissertation (Univ. Calif. San Diego).
- Spencer, J.W., 1981, Stress relaxations at low frequencies in fluid-saturated rocks: Attenuation and modulus dispersion, *J. Geophys. Res.* 86, 1803-1812.
- Stoll, R.D., 1979, Experimental studies of attenuation in sediments, *J. Acoust. Soc. Am.* 66, 1152-1160.
- Tittmann, B.R., Clark, V.A., Richardson, J.M. and Spencer, T.W., 1980, Possible mechanisms for seismic attenuation in rocks containing small amounts of volatiles, *J. Geophys. Res.* 85, 5199-5208.

- Winkler, K.W., Nur, A. and Gladwin, M., 1979, Frictional sliding and seismic attenuation in rocks, *Nature* 227, 528-531.
- Winkler, K.W. and Nur, A., 1982, Seismic attenuation: Effects of pore fluids and frictional sliding, *Geophys.* 47, 1-15.
- Winkler, K.W., and T. J. Plona, 1982, Technique for measuring ultrasonic velocity and attenuation spectra in rocks under pressure, *J. Geophys. Res.*, submitted.
- Yeaker, E., Fischer, F.H., Miceli, J. and Bressel, R., 1973, Origin of the low frequency sound absorption in sea water, *J. Acoust. Soc. Am.* 53, 1705-1707.
- Zuckerwar, A.J., and Griffin, W.A., 1981, Effect of water vapor on sound absorption in nitrogen at low frequency/pressure ratios, *J. Acoust. Soc. Am.* 69, 150-154.

ADDITIONAL REFERENCES

- Batchelor, G.K., 1976, Developments in microhydrodynamics, in Theoretical and Applied Mechanics (W.T. Koiter, ed.), North Holland, Amsterdam, 33-55.
- Brennan, B.J., and Smylie, D.E., 1981, Linear viscoelasticity and dispersion in seismic wave propagation, *Rev. Geophys. Space Phys.* 19, 233-246.
- Coleman, B.D., and Noll, W., 1961, Foundations of linear viscoelasticity, *Rev. Mod. Phys.* 33, 239-249.
- de Jong, B.H.W.S., and Brown, G.E., 1980, Polymerization of silicate and aluminate tetrahedra in glasses, melts and aqueous solutions, II. The network modifying effects of Mg^{2+} , K^+ , Na^+ , Li^+ , OH^- , F^- , Cl^- , H_2O , CO_2 and H_3O^+ on silicate polymers, *Geochim. Cosmochim. Acta* 44, 1627-1642.
- Dutta, N.C., and Ode, H., 1979, Attenuation and dispersion of compressional waves in fluid-filled porous rocks with partial gas saturation (White model), Part I. Biot theory, *Geophys.* 44, 1777-1788. Part II. Results, *Geophys.* 44, 1789-1805.
- Dutta, N.C. and Sherif, A.J., 1979, On White's model of attenuation in rocks with partial gas saturation, *Geophys.* 44, 1806-1812.
- Ferry, J.D., 1970, *Viscoelastic properties of polymers*, Wiley, NY, 671 p.
- Gurtin, M.E., and E. Sternberg, 1962, On the linear theory of viscoelasticity, *Arch. Rat. Mech. Anal.* 11, 291-356.
- Moore, D.F., 1965, A review of squeeze films, *Wear* 8, 245-263.

- Moore, D.F., 1975, Principles and Applications of Tribology, Pergamon, Oxford, 388 p.
- Moore, D.F., 1972, The Friction and Lubrication of Elastomers, Pergamon, Oxford, 288 p.
- McDonald, D.A., 1974, Blood Flow in Arteries, Arnold, London, 496 p.
- Pedley, T.J., 1980, The Fluid Mechanics of Large Blood Vessels, Cambridge Univ. Press, 446 p.
- Pinkus, B., and Sternlicht, O., 1961, Theory of Hydrodynamic Lubrication, McGraw-Hill, NY 465 p.
- Strick, E., 1981, Application of the general anelastic model to water saturated rock, Geophys., submitted.
- Wormsley, J.R., 1955, Oscillatory motion of a viscous liquid in a thin-walled elastic tube, I. The linear approximation for long waves, Phil. Mag. 46, 199-221.
- Wormsley, J.R., 1957, Oscillatory flow in arteries: the constrained elastic tube as a model of arterial flow and pulse transmission, Phys. Med. Biol. 2, 178-187.
- Yates, D.J.C., 1954, The expansion of porous glass on the adsorption of non-polar gases, Proc. Roy. Soc. London, 224, 526-544.

LMED
8